CELL GEOMETRIC CONSTRAINTS REGULATE NUCLEAR & CHROMATIN PLASTICITY VIA ACTOMYOSIN CONTRACTILITY

EKTA MAKHIJA

(MSc. (Physics) IIT Kanpur, India)

A THESIS SUBMITTED

FOR THE DEGREE OF DOCTOR OF PHILOSOPHY

MECHANOBIOLOGY INSTITUTE

NATIONAL UNIVERSITY OF SINGAPORE

2015

DECLARATION

I hereby declare that this thesis is my original work and it has been written by me in its entirety. I have duly acknowledged all the sources of information which have been used in the thesis.

This thesis has also not been submitted for any degree in any university previously.

Ekta Makhija

20 July 2015

ACKNOWLEDGEMENTS

It is a genuine pleasure to express my deep sense of thanks and gratitude to my supervisor, Prof. Shiva, who always had the time and enthusiasm to discuss my experiments and results. He showed me how to be a good scientist, pushed me to discover my own potential, and taught me how to perform multi-tasking and collaborations. He supervised me with the perfect balance of letting me explore things on my own while not letting me feel completely lost at the same time. He also provided me with the perfect lab environment which offered intellectual stimulation and a friendly work culture. I am truly thankful, happy and proud to be his student.

I thank my thesis committee members Prof. Michael Sheetz and Prof. Alexander Bershadsky for their inputs throughout my PhD. I thank MBI for making my PhD extremely smooth by providing me with good research scholarship, excellent state-of-the-art scientific instruments, safe and intellectually stimulating research environment and supremely helpful staff of microscopy, nanofabrication, wet-lab, protein expression, and IT core research facilities. I also thank MBI admin staffs Carol and AiLeng who were very helpful with all graduate matters.

I thank my lab-mates, colleagues and friends Abhishek, Shefali, Shova, Venky, Soumya, Nisha, Nikhil, Qingsen, Yejun, Mallika, KeeChua, Kathirvel, Aninda, Kamal, RK, Prasuna, Shifali, Bibhas, Karthik, Payel, Shi Yuan, Karthik, Saradha, Chris, Mrinal, Feroz, Dipanjan, Aneesh, Xiaowei, Rishita, Stuti, Surabhi, Ranjit, Shruti, and Devika for various scientific and philosophical discussions.

I thank my parents and in-laws for letting me pursue my dreams and for their constant love, support, and encouragement throughout my PhD. I thank my husband, Utkarsh, for his patience, love, support, for relocating to Singapore, for sharing the housework, and for listening to my scientific and non-scientific lab problems.

-Ekta

TABLE OF CONTENTS

ABSTRACT vi

LIST OF PUBLICATIONS vii

LIST OF FIGURES viii

LIST OF ABBREVIATIONS x

CHAPTER 1: INTRODUCTION 1

1.1 Why Study the Effect of Cell Geometry on Nucleus and Chromatin? 2

1.2 Physical Signal Transduction from Cell Periphery to Nucleus 5

1.3 Mechanical Force Sensing by Chromatin 7

1.4 Overview of this Thesis 9

CHAPTER 2: MECHANICAL CORRELATION BETWEEN CELL TRACTION FORCES AND NUCLEAR AND HETEROCHROMATIN DYNAMICS 16

2.1 Micropillar Deflections Relate to Actomyosin Forces 22

2.2 Dynamic Correlations between Micropillar and Nuclear Displacements 25

2.3 Force Transduction from Apical Stress Fibers to Heterochromatin Foci 28

CHAPTER 3: ACTOMYOSIN CONTRACTILITY REGULATES NUCLEAR AND CHROMATIN PLASTICITY 34

3.1 Reduced Matrix Constraints Enhance Nuclear Plasticity 40

3.2 Actin, Myosin and Formin Regulate Matrix Assisted Nuclear Plasticity 44

3.3 Nesprin and Microtubules Affect Amplitude of Nuclear Area Fluctuations 48

3.4 LaminA/C Levels Inversely Regulate Nuclear Plasticity 52

3.5 Plastic Nuclei have Increased Chromatin Dynamics 55

CHAPTER 4: CELL GEOMETRIC CONSTRAINTS MODULATE CHROMATIN COMPACTION STATES 65

4.1 Core Histone Anisotropy Measures Chromatin Compaction 71

4.2 Time Lapse FAI to Study Chromatin Dynamics 72

4.3 Time Lapse FAI Reveals Distinct Dynamics between Heterochromatin and Euchromatin Assembly 77

4.4 FAI Captures Changes in Chromatin Dynamics in Distinct Cellular Differentiation States 78

4.5 Cell Geometric Constraints Affect Chromatin Dynamics 80

4.6 Simultaneous Anisotropy of Transcription Cofactor and Core Histone 82

CHAPTER 5: CONCLUSION AND DISCUSSION 88

BIBLIOGRAPHY 93

ABSTRACT

Extracellular mechanical signals (EMS) can regulate nuclear morphology and chromatin dynamics via the physical link from focal adhesions to chromatin via the cytoskeleton, linker proteins on the nuclear envelope and the nuclear lamina. However, how such force transmission from cytoskeleton to the nucleus is regulated by different EMS and their effect on nuclear and chromatin dynamics is not well understood. In the first project, using micropillar substrates and correlation analysis techniques, we measured the time scale at which nuclear and chromatin dynamics respond to traction forces at cell periphery in unperturbed cells. In the second project, using nuclear envelope fluctuations and heterochromatin dynamics as readout, we characterized how cytoskeletal forces alter depending on the EMS provided by micropatterned substrates. In the third project, we developed a technique to quantify chromatin dynamics and used it to study the effect of cytoskeletal perturbations on chromatin dynamics and binding of transcription regulators. Taken together, this work provides a quantitative understanding of the coupling between cellular mechanotransduction and nuclear and chromatin plasticity.

LIST OF PUBLICATIONS

- ***The regulation of dynamic mechanical coupling between actin cytoskeleton and nucleus by matrix geometry***
  Li Q, Kumar A, **Ekta Makhija** and G. V. Shivashankar
  Biomaterials, 2014. 35(3): p. 961-9.

- ***Probing Chromatin Structure and Dynamics Using Fluorescence Anisotropy Imaging***
  Ekta Makhija, K. Venkatesan Iyer, Shefali Talwar and G. V. Shivashankar
  Handbook of Imaging in Biological Mechanics (Edited by Corey P. Neu, Guy M. Genin, 10/2014: chapter 31: pages 391-400; CRC Press., ISBN: 9781466588134)

- ***Micropillar displacements by cell traction forces are mechanically correlated with nuclear dynamics***
  Li Q*, **Makhija E***, Hameed FM and Shivashankar GV
  Biochem Biophys Res Commun, 2015. 461(2): p. 372-7.
  * Equal Contributors

- ***Nuclear Plasticity and Telomere Dynamics are Regulated by Extracellular Matrix Constraints***
  Ekta Makhija, D. S. Jokhun and G. V. Shivashankar
  (Under Review in PNAS)

- ***Role of Cell Geometry on Nuclear Mechanics, Chromosome Reorganization, and Gene Expression***
  Yejun Wang*, **Ekta Makhija***, Karthik Damodaran and G. V. Shivashankar
  Molecular and Cellular Mechanobiology (Edited by Shu Chien, Adam Engler, and Peter Wang) (In preparation 2015)
  * Equal Contributors

LIST OF FIGURES

Figure 1.1: Effect of EMS on Physical Properties of Cells.

Figure 1.2: Physical Link from Cell Periphery to Nucleus and Chromatin.

Figure 2.1: Method of Micropillar Preparation and Cell Seeding.

Figure 2.2: Imaging and Tracking of Micropillars.

Figure 2.3: Measurement of Micropillar Displacements.

Figure 2.4: Pillar Displacement and Traction Force.

Figure 2.5: Autocorrelation and Cross-Correlation of Micropillars and Nucleus.

Figure 2.6: Angle between Nucleus Trajectory and Pillar Deflection.

Figure 2.7: Direct Transduction of Forces to Heterochromatin by ASF.

Figure 3.1: Effect of Cell Geometry on Nuclear Morphology.

Figure 3.2: Effect of Cell Geometry on Nuclear Plasticity.

Figure 3.3: Role of Actin in Cell Geometry Mediated Nuclear Plasticity.

Figure 3.4: Role of Myosin in Cell Geometry Mediated Nuclear Plasticity.

Figure 3.5: Role of Formin in Cell Geometry Mediated Nuclear Plasticity.

Figure 3.6: Actin-Myosin-Formin Asters Apply Force on the Nucleus.

Figure 3.7: Role of Nesprin in Cell Geometry Mediated Nuclear Plasticity.

Figure 3.8: Role of Microtubules in Cell Geometry Mediated Nuclear Plasticity.

Figure 3.9: Role of LaminA/C in Cell Geometry Mediated Nuclear Plasticity.

Figure 3.10: Model for Cytoskeletal and Nucleoskeletal Regulation of Nuclear Plasticity.

Figure 3.11: Effect of Cell Geometry on Chromatin Dynamics.

Figure 3.12: Role of Actin Polymerization in Chromatin Dynamics.

Figure 3.13: Effect of Cell Geometry Mediated Actomyosin Forces on Chromatin Dynamics.

Figure 3.14: Effect of Cell Geometry Mediated Actomyosin Forces on Correlation between Heterochromatin Foci.

Figure 3.15: Reversible Nature of Actomyosin Mediated Nuclear and Chromatin Plasticity.

Figure 4.1: Principle of Fluorescence Polarization Anisotropy.

Figure 4.2: Relation between intensity and anisotropy.

Figure 4.3: Image Pearson correlation coefficient (PCC) to measure dynamics.

Figure 4.4: Interpretation of anisotropy PCC.

Figure 4.5: Anisotropy PCC depends on imaging conditions.

Figure 4.6: Anisotropy PCC measures chromatin dynamics.

Figure 4.7: Anisotropy PCC shows that euchromatin is more dynamic than heterochromatin.

Figure 4.8: Chromatin dynamics of stem cells vs differentiated cells.

Figure 4.9: Effect of cell shape on chromatin dynamics.

Figure 4.10: MKL translocation to the nucleus.

Figure 4.11: Relation between MKL binding and chromatin compaction.

Figure 4.12: Effect of cell geometry on dynamics of MKL binding foci.

LIST OF ABBREVIATIONS

ASF	Apical Stress Fiber
CI	Constrained Isotropic (500μm^2 circle)
DN-KASH	Dominant Negative Klarsicht ANC-1 Syne Homology
EMS	Extracellular Mechanical Signals
ES	Embryonic Stem
FAI	Fluorescence Anisotropy Imaging
FITC	Fluorescein Isothiocyanate
FRAP	Fluorescence Recovery after Photobleaching
FRET	Forster Resonance Energy Transfer
FWHM	Full Width at Half Maximum
GFP	Green Fluorescent Protein
HDAC	Histone Deacetylase
HP1	Heterochromatin Protein 1
INM	Inner Nuclear Membrane
KASH	Klarsicht ANC-1 Syne Homology
LBR	Lamin B Receptor
LINC	Linker of Nucleoskeleton and Cytoskeleton
LP	Large Polarized (1800μm^2 1:5 rectangle)
MACFs	Microtubule-Actin Crosslinking Factors
MEF	Mouse Embryonic Fibroblast
MKL	Megakaryoblastic Leukemia Factor
MSC	Mesenchymal Stem Cells
MSD	Mean Square Displacement
MTOC	Microtubule-Organizing Centre
NA	Numerical Aperture

NF-κB	Nuclear Factor Kappa-light-chain-enhancer of activated B cells
NLS	Nuclear Localization Signal
ONM	Outer Nuclear Membrane
PCC	Pearson Correlation Coefficient
PDMS	Poly Dimethyl Siloxane
PMEF	Primary Mouse Embryonic Fibroblasts
PNAF	Projected Nuclear Area Fluctuations
RFP	Red Fluorescent Protein
RGD	Arginylglycylaspartic Acid
RT-PCR	Reverse Transcription Polymerase Chain Reaction
SMIFH2	Small Molecule Inhibitor of Formin Homology 2 Domains
SUN	Sad1p, UNC-84
TAZ	Tafazzin
YAP	Yes-Associated Protein

CHAPTER 1: INTRODUCTION

1.1 Why Study the Effect of Cell Geometry on Nucleus and Chromatin?

The interaction between cells and their environment plays an important role in regulating cell behavior and various cellular functions such as division, differentiation and migration. Extracellular chemical signals such as cytokines, growth factors and hormones typically engage receptor molecules on cell surface, which have a ligand binding domain and an effector domain that brings about the cellular response by initiating various intracellular signaling pathways [1]. The cellular response to such chemical signals has been well studied and established. However, studies on extracellular mechanical signals (EMS) such as rigidity or geometry of the substrate and shear or normal forces from the surrounding medium and their effect on cell behavior, collectively termed as mechanobiology, have only begun in the last two decades [2-9].

Exposure to such EMS for several weeks results in changes in gene expression profile and differentiation patterns. Mesenchymal stem cells (MSCs) cultured for few weeks on soft substrates become neurogenic, on rigid substrates become osteogenic and on substrate of intermediate rigidity become myogenic [8]. MSCs cultured for a week on geometries such as rectangles or stars, which exhibit enhanced actomyosin contractility, become osteogenic, while those cultured on squares or flowers become adipogenic [10]. MSCs exposed to fluid shear stress for a week also exhibit osteoblastic phenotype [11]. However, changes in gene expression can be detected as early as a few hours of exposure to mechanical signals. Within three hours of culturing on fibronectin micropatterns of large polarized (LP) geometry (1800μm^2 1:5 rectangle), fibroblasts exhibit an upregulation of genes related to actin cytoskeleton, cell migration, cell-substrate and cell adhesion, while those

cultured on constrained isotropic (CI) geometry (500μm^2 circle) exhibit upregulation of genes related to cell division, cell death and negative regulation of cell-matrix adhesion [12].

Several studies aimed at understanding such mechanotransduction have shown that physical properties of cells such as its shape, strength of focal adhesions, cytoskeletal organization and nuclear morphology are altered upon exposure to EMS (Figure 1.1). For example, endothelial cell shape changes from polygonal to ellipsoidal upon exposure to fluid shear stress and orient themselves in the direction of fluid flow [13]. The integrin-cytoskeletal links become stronger when cells are cultured on rigid matrix [5]. Actin stress fibers are induced in human vascular endothelial cells in response to shear stress [14]. Cell morphology and stress fiber organization becomes more polarized with increase in substrate rigidity [15, 16]. The nuclear morphology follows cell morphology, becoming more rounded on soft substrates and more flattened on rigid substrates [17, 18]. Nuclei are more elongated and flattened in cells cultured on polarized geometries such as rectangles compared to more isotropic geometries such as squares or circles [19].

In addition to these physical changes in the cell, various signaling pathways related to transcription factors have also been observed to be sensitive to EMS. Armadillo, which is a transcription coactivator for the transcription factor twist, translocates to the nucleus in drosophila embryos upon application of unilateral compression [20]. Activity of serum response factor and nuclear accumulation of its cofactor Megakaryoblastic Leukemia Factor (MKL) is enhanced in cells with stretched and polarized geometries [12] and upon application of force [21]. The p65 subunit of the transcription factor Nuclear

Factor Kappa-light-chain-enhancer of activated B cells (NF-κB) shuttles to the nucleus upon application of fluid shear force in endothelial and bone cells [22]. The transcriptional coactivator Yes-Associated Protein (YAP) has higher nuclear localization in cells cultured on rigid substrates [23].

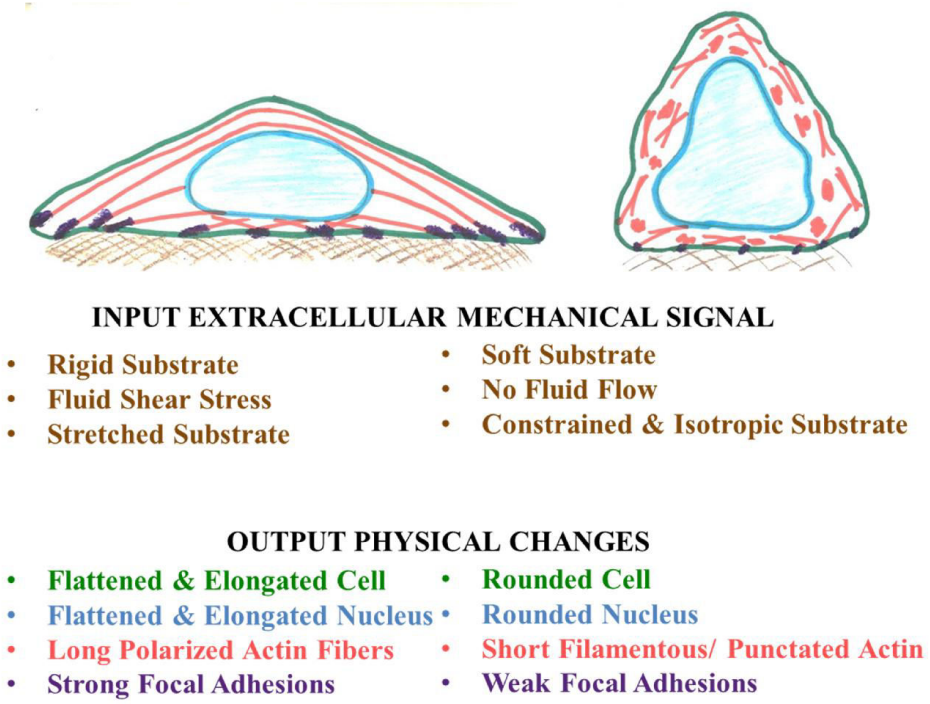

Figure 1.1: Effect of EMS on Physical Properties of Cells.

However, the physical and chemical cellular responses to EMS may not be mutually exclusive as nuclear shuttling of various transcription factors has been shown to depend on their interaction with focal adhesions and the cytoskeleton. MKL shuttling to the nucleus is dependent on the state of actin polymerization [24]. It binds to G-actin in the cytoplasm, which conceals its nuclear localization signal. When extracellular signals trigger actin polymerization, MKL shuttles to the nucleus with the help of importins [25]. Mechanical activation of the NF-κB pathway gets perturbed in cells which lack the focal adhesion kinase [26]. Similarly, the YAP/TAZ activity and its

nuclear shuttling require cytoskeletal tension; latrunculin-A perturbation lowers its nuclear localization [23]. Additionally, the spatial localization of the enzyme histone deacetylase is regulated by actomyosin contractility; myosin inhibition by blebbistatin results in its nuclear shuttling.

With this overview of the physico-chemical changes that occur in response to EMS, we aimed at understanding the process of mechanotransduction at three levels - the nucleus, the chromatin and the transcriptional regulator, by posing the following questions:

1. How do mechanical signals transduce to the ***nucleus*** and how do they affect nuclear morphology and dynamics?
2. Can ***chromatin*** "feel" the mechanical signals – are chromatin compaction and dynamics affected by mechanical signals?
3. What is the effect of mechanical signals on the binding of a ***transcriptional regulator*** like MKL?

1.2 Physical Signal Transduction from Cell Periphery to Nucleus

The nucleus and chromatin are physically coupled to the cell periphery via cytoskeleton, which primarily comprises of actin, microtubules and intermediate filaments. Actin, along with myosin and some cross-linking proteins, forms tensile filaments that originate at the focal adhesions and has been implicated in force transduction to the nucleus [27]. Microtubules originate as filaments from the microtubule-organizing centre and form a network around the nucleus [28]. Vimentin, which is a type III intermediate filament, forms a scaffold in the cytoplasm, which is highly dense around the nucleus [29]. These cytoskeletal structures are physically linked to the nucleus

via transmembrane proteins on the outer nuclear membrane (ONM) – nesprin-1 and nesprin-2 bind to actin, nesprin-3 binds to plectin, which binds to intermediate filaments and nesprin-4 binds to microtubule motors [30]. These proteins on the ONM have a Klarsicht ANC-1 Syne Homology (KASH) domain, which interacts with the Sad1p, UNC-84 (SUN) domain of transmembrane proteins on the inner nuclear membrane (INM) (Figure 1.2).

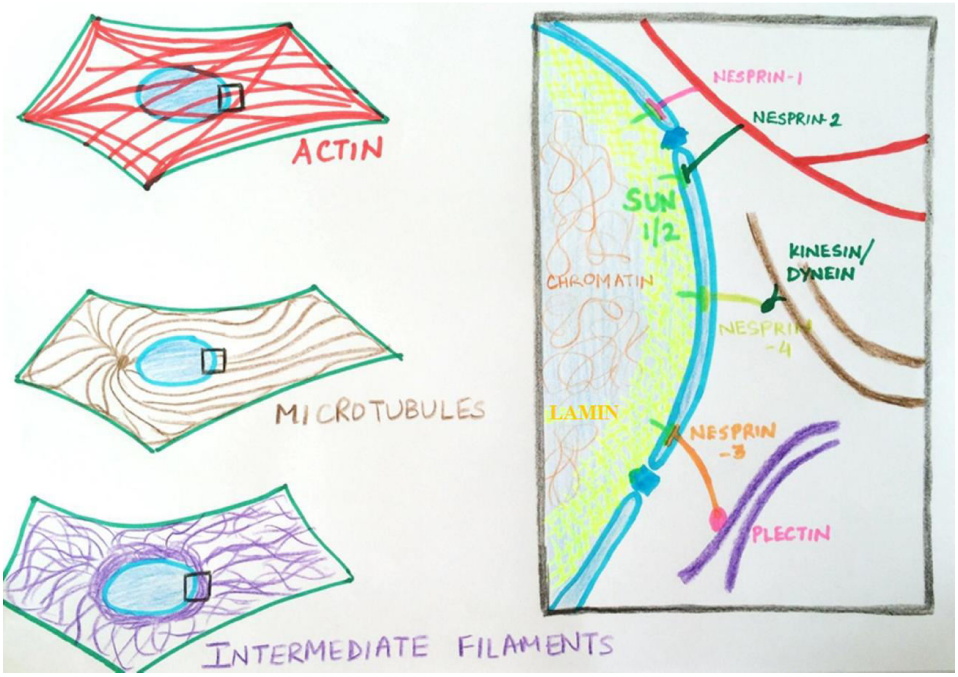

Figure 1.2: Physical Link from Cell Periphery to Nucleus and Chromatin.

Mechanical signals from the extracellular matrix can travel as stress waves through this physical link between focal adhesions and the nucleus. Such transmission occurs at time scale of a few milliseconds [31-33]. Additionally, active forces from the physical cytoskeletal link maintain the nucleus under prestress which governs its morphology. Any perturbation of the components of this physical cytoskeletal link from focal adhesions to nucleus inhibits propagation of mechanical signals and affects nuclear morphology as well as

subsequent functional responses such as transcription and differentiation. Actin perturbation by cytochalasin-D or myosin inhibition by blebbistatin results in decreased nuclear projected area. On the other hand, microtubule perturbation results in increased nuclear projected area, suggesting that while actomyosin fibers apply tensile load, microtubules apply a compressive load on the nucleus [34, 35]. Myosin inhibition or expression of dominant negative Klarsicht ANC-1 Syne Homology (DN-KASH) domains eliminates the modulation of nuclear shape by substrate rigidity [18]. Myosin inhibition also blocks elasticity-mediated lineage specification [8]. Knockdown of nesprin-3, which is a linker between intermediate filaments and the nucleus, alters shear-flow mediated mechanotransduction in human aortic endothelial cells [36].

1.3 Mechanical Force Sensing by Chromatin

In addition to the cytoskeletal physical link from focal adhesions to the nucleus, there also exists a physical link from INM to the chromatin. Various transmembrane proteins on the INM bind to lamins and emerin [37]. Lamin B receptors (LBR) and LaminA/C further tether heterochromatin to nuclear periphery via interaction with Heterochromatin Protein 1 (HP1) [38-40]. These links, along with cytoskeletal links from focal adhesions to the ONM, facilitate the transduction of physical signals from cell periphery to chromatin, thereby providing permissivity to alter chromatin structure and function in response to EMS. Upon application of fluid shear stress, subnuclear structures labelled with fibrillarin-GFP in HeLa, human umbilical vein endothelial, and osteosarcoma cells exhibit dynamics that scales with the amplitude of shear stress [41]. Local extracellular force application using RGD-coated magnetic bead resulted in direct dissociation of a major multi-protein complex in the

cajal body, a prominent subnuclear structure [42]. Such protein dissociation in the subnuclear structure upon extracellular force was not observed when the physical cytoskeletal to chromatin link was perturbed by disruption of actin, myosin or laminA/C. Mechanical stimulation of cells via magnetic particles adhered to plasma membrane resulted in chromatin remodeling as measured using fluorescence anisotropy of H2B-EGFP [21]. Such force dependent chromatin remodeling was abolished upon actin or myosin perturbation by cytochalasin-D and blebbistatin respectively.

Perturbations of the physical link from focal adhesions to the chromatin also results in altered dynamics of various chromatin binding proteins. Fluorescence recovery after photobleaching (FRAP) experiments reveal enhanced dynamics of core histones and HP1α in embryonic stem cells compared to primary fibroblasts, which can be explained by the absence of physical links between cell periphery to nucleus and chromatin in stem cells [43, 44]. Perturbation of focal adhesion protein vinculin or actin or KASH domain protein also results in enhanced dynamics of core histone proteins [34]. Altering actomyosin contractility via cytochalasin-D or blebbistatin treatments enhances cytoplasmic to nuclear shuttling of the chromatin remodeling enzyme histone deacetylase 3 (HDAC3) resulting in lower acetylation levels [12]. Such alteration in the dynamics of histones and chromatin remodeling enzymes would assist in structural changes required for regulating gene expression in response to mechanical signaling.

1.4 Overview of this Thesis

Mechanical Correlation Between Cell Traction Forces and Nuclear and Heterochromatin Dynamics

This project probes the inherent time scale at which the nucleus and subnuclear structures respond to the traction forces generated at the focal adhesions. To measure these time scales, correlation was calculated between displacement of tips of micropillar arrays on which the cells were adhered and the displacement of nucleus centroid and heterochromatin foci.

Micropillar arrays coated with fibronectin when used as a substrate for culturing cells, allow the measurement of forces generated by cells [45]. The displacement of the micropillar tips is directly proportional to the magnitude of the force. In this project, fibroblasts expressing H2B-EGFP and lifeact-RFP were cultured on micropillar arrays and simultaneous imaging was performed in bright field for micropillars and in fluorescence for actin and nucleus. Pillars under cells typically showed higher mean displacements (~0.1μm) than control pillars (~0.04μm). A measurement of mean micropillar displacement for each pillar showed that the pillars at the cell periphery exhibited maximum displacement. Inhibition of myosin significantly reduced the amplitude of these displacements, validating that the experimental set-up could indeed capture the effect of traction forces on micropillar displacements. Autocorrelation curves for pillar, nucleus and heterochromatin displacement showed similar decorrelation time scales of ~40s, which is close to the time scale of fibroblast cell contraction [46]. Cross-correlation analysis of front and rear end pillar displacement with the nuclear displacement showed

instantaneous (less than 1s) negative and positive correlation, respectively. A measurement of the angle between pillar trajectory and nuclear trajectory also showed that while the nucleus moves forward, most pillars on the front edge move rearward and most pillars on the rear edge move towards the front. Myosin inhibition removed such spatial correlation between pillar and nucleus displacements. These results suggest a highly coordinated contractile process mediated by elastic cytoskeletal links to test local microenvironment during cell migration.

As a next step, the spatiotemporal coupling between these elastic actomyosin links and the nucleus and heterochromatin was studied. In cells constrained on polarized geometry, perinuclear actin was observed to form parallel apical stress fibers, which connect focal adhesions on opposite ends and exert active compressive force on the apical surface of the nucleus. As a result of this compressive load, the nucleus formed indents at sites where it is pressed by the stress fibers. The stress fibers were observed to move transversely over the nucleus at ~0.3μm/min, simultaneously moving the indents which form on the nucleus. Interestingly, the heterochromatin nodes within the nucleus, which are regions of dense chromatin, were also observed to move along with the apical actin stress fibers. Taken together, this work provides direct evidence for instantaneous force transmission from focal adhesion to nucleus and chromatin via apical actin stress fibers.

Actomyosin Contractility Regulates Nuclear and Chromatin Plasticity

This project explores the role of actomyosin contractility in regulating nuclear and chromatin plasticity. We altered actomyosin contractility via micropatterned substrates and pharmacological reagents and measured

resulting fluctuations of nuclear area and dynamics of functional chromatin structures.

Firstly, cells were cultured on microfabricated fibronectin patterns of two extreme geometries –LP and CI. Previous work in the lab has shown that cytoskeletal organization [19] and gene expression profiles [12] are highly distinct in these two geometries. Consistent with these studies, it was observed that the LP cells were flat and had long apical actin stress fibers while CI cells were dome shaped and had short filaments and punctated structures of actin. In LP cells, the projected nuclear area did not vary with time, while in CI cells it showed periodic fluctuations. Treatment with various pharmacological inhibitors showed that the amplitude of projected nuclear area fluctuations (PNAF) was dependent on the state of actin polymerization. Experiments with small molecule inhibitors revealed that myosin and formin were also necessary for these fluctuations. However, direct physical links between actin and nucleus, either via nesprin or via microtubules were not necessary for the PNAF. Hence, the active force for generating nuclear fluctuations comes from the dynamic actin-myosin-formin asters that exist in intermediate polymerization state of actin. Next, laminA/C expression levels were measured in LP and CI cells, since laminA/C levels have been linked to nuclear rigidity [47].Quantitative RT-PCR experiments revealed 80% reduction in laminA/C levels in CI cells compared to LP cells. Consistently, laminA/C overexpression in CI cells reduced the PNAF while laminA/C knockout cells on LP patterns displayed enhanced fluctuations. In summary, both active forces from the cytoskeleton and nuclear rigidity from the laminA/C together regulate the PNAF.

To understand if the PNAF have an effect on chromatin dynamics, heterochromatin foci were tracked in time series of confocal H2B-EGFP images and their trajectories in LP and CI cells were compared. The foci were much more dynamic in CI cells as visualized and quantified using line kymographs, XY trajectories and mean squared displacement (MSD) vs time plots. Blebbistatin treatment in CI cells decreased the dynamics, while cytochalasin-D treatment in LP cells enhanced the dynamics. To assess if the heterochromatin foci trajectories of a nucleus were correlated in either cell geometry, vectorial Pearson correlation coefficient between 3D trajectories of all heterochromatin foci pairs was calculated, generating a correlation matrix for individual nuclei. The heterochromatin foci trajectories were much more correlated in LP cells (mean correlation = 0.57) than CI cells (mean correlation = 0.15). The correlations showed apical-basal grouping, i.e. foci in either group were more correlated with other foci in the same group than with the other group. Overall, the correlations decreased upon cytochalasin-D treatment in LP cells and enhanced upon blebbistatin treatment in CI cells. This dependence of heterochromatin trajectory correlations on actomyosin suggests that active cytoskeletal forces may be able to regulate the rheological properties of chromatin. Interestingly, the actomyosin mediated PNAF as well as heterochromatin foci dynamics and correlations were reversible, implying the existence of structural memory in chromatin organization.

Cell Geometric Constraints Modulate Chromatin Compaction States

This project aims at a direct visualization of chromatin compaction and transcription factor binding in the nucleus, which would provide a better understanding of how EMS regulate gene expression. We measured

spatiotemporal dynamics of chromatin compaction and transcription cofactor binding in live cells cultured on fibronectin micropatterned substrates using fluorescence anisotropy imaging (FAI) of fluorescently tagged core histone proteins and transcription cofactor MKL.

Fluorescence anisotropy measures the rotational mobility of fluorophore-bound proteins by quantifying the depolarization in the emitted light [48]. Rotational mobility of H2B-EGFP represents local chromatin compaction state - a compact local packaging would decrease the rotational mobility of core histones in the nucleosome and vice versa [49]. As a first step, to develop a quantitative technique for analyzing the dynamics of chromatin compaction, Pearson correlation coefficient (PCC) between anisotropy images was computed as a function of time lag between images. Fitting the PCC vs time lag curve with an exponential decay function gave three quantities – the noise (η), the time scale of chromatin compaction dynamics (τ) and a measure of the total dynamic fraction of the chromatin (α). Comparing anisotropy and intensity PCC vs time lag curves for fixed and live cells confirmed that anisotropy is more sensitive than intensity in capturing the difference in chromatin dynamics. Anisotropy PCC could capture local chromatin dynamics in 3.5x3.5 μm^2 regions at heterochromatin and euchromatin sites. Euchromatin regions had significantly higher noise (η=0.5) and drop rate (α/τ=0.035 min^{-1}) than heterochromatin (η=0.2, α/τ=0.025 min^{-1}), implying a rapid loss of structural information and faster polymer relaxation time scales. Anisotropy PCC could also capture differential chromatin dynamics in distinct differentiation states. Embryonic stem (ES) cells exhibited significantly higher drop rates (α/τ=0.12 min^{-1}) than primary mouse embryonic fibroblasts

(PMEFs) (α/τ=0.06 min^{-1}), suggesting that chromatin is more dynamic in stem cells. Although the global chromatin dynamics is faster in ES cells, local anisotropy PCC analysis by dividing the nucleus into 1.6x1.6 μm^2 regions revealed that the spatial heterogeneity is higher in PMEFs.

Next, to study the effect of cell geometry on chromatin dynamics, the anisotropy PCC vs time lag curves were compared for cells cultured on either LP or CI fibronectin micropatterned substrates. CI cells exhibited significantly faster chromatin dynamics (α/τ=0.03 min^{-1}) and larger dynamic fraction of chromatin (α=0.4) than LP cells (α/τ=0.02 min^{-1}, α=0.2). Actin depolymerization in LP cells increased chromatin dynamics (by 21%) and dynamic fraction (by 21%) while actin stabilization in CI cells decreased the dynamics (by 11%) and dynamic fraction (by 59%), suggesting that actin polymerization regulates chromatin dynamics.

Next, fluorescence anisotropy was used to visualize spatiotemporal binding of MKL. MKL, which is a transcription cofactor for serum response factor, binds to G-actin in the cytoplasm and shuttles to the nucleus when G-actin polymerizes to F-actin [24]. Consistent with previous reports [50], both serum stimulation and cytochalasin-D treatment induced nuclear shuttling of MKL within 15 minutes. To investigate the coupling between MKL binding and chromatin compaction, the fluorescence anisotropy of MKL mCherry was measured in the nucleus and compared with H2B-EGFP anisotropy. Regions of high MKL anisotropy showed inverse correlation with H2B anisotropy, suggesting that MKL binds in regions of decompact chromatin. 2D spatial tracking of high anisotropy foci of MKL-mCherry and H2B-EGFP revealed higher dynamics of MKL foci in LP cells while dynamics of H2B foci were

higher in CI cells. In summary, using FAI and correlation analysis, the chromatin compaction pattern was observed to be more dynamic in CI cells while the activity of transcription cofactor MKL was higher in LP cells.

CHAPTER 2: MECHANICAL CORRELATION BETWEEN CELL TRACTION FORCES AND NUCLEAR AND HETEROCHROMATIN DYNAMICS

INTRODUCTION

Cells sense EMS such as matrix rigidity [8], substrate geometry [10, 12], and mechanical forces [51] to modulate their gene expression profiles. The signal transduction from cell matrix interface to nucleus and chromatin occurs via both physical and chemical links [52, 53]. The physical link originates at the focal adhesions, which are connected to the cytoskeleton, which in turn is connected to linker proteins on the nuclear envelope, which are further connected to the lamin meshwork and the chromatin [54-58]. The chemical links comprise of the signaling intermediates and transcription regulatory molecules which get activated or shuttle to the nucleus upon receiving signals from extracellular matrix [21]. While the chemical signaling occurs mostly via diffusion, at millisecond to second time scales, the physical signals travel much faster, at microsecond timescales as elastic waves through the cytoskeleton [33, 59]. In response to EMS, the cytoskeletal links reorganize, thereby altering forces on the nucleus, which in turn modulate its morphology and chromatin remodeling [41, 60]. However, the inherent time scale of this coupling between forces at the cell periphery and the dynamics of the nucleus and chromatin has not been explored.

In this project, we measure the coupling between forces at cell periphery and nuclear and chromatin movement. To measure the forces at cell periphery, we culture cells on micropillar substrates and measure deflection of pillar tips, which is an indicator of magnitude and direction of traction forces. Simultaneously, nuclear and hetereochromatin centroid displacements are captured using similar particle tracking algorithms. To get an estimate of the

time scales of coupling between cell periphery and nucleus, auto and cross-correlation analysis is done for pillar deflections and nuclear and heterochromatin movements. Our results are suggestive of a strong viscoelastic coupling that mediates differential force transmission to the nucleus. Additionally, to see the direct effect of the physical cytoskeletal links on chromatin remodeling, we carried out simultaneous time-lapse imaging of actin stress fibers and chromatin in cells cultured on fibronectin micropatterns. We constrained cells on rectangular fibronectin micropatterns to form long parallel apical stress fibers which link to focal adhesions. We observed that these fibers can transduce forces to heterochromatin foci inside the nucleus.

MATERIALS AND METHODS

Cell Culture, Transfection and Drug Treatment: H2B-EGFP NIH3T3 fibroblasts and PMEFs were cultured in low glucose Dulbecco's Modified Eagle Medium supplemented with 10% Fetal Bovine Serum and 1% Penicillin-Streptomycin at 37°C and 5% CO2 in humid conditions. All cell culture reagents were from Gibco, Life Technologies.

Transfections were carried out with lifeact mRFP using jetPRIME (Polyplus transfection).

For myosin inhibition, cells were treated with 25μM Blebbistatin (Sigma) for 2h.

Micropillar Preparation, Fibronectin Stamping and Cell Seeding: Poly Dimethyl Siloxane (PDMS) micropillars were prepared from PDMS Elastomer Kit (SYLGARD 184, DOW Corning). The curing agent and

precursor were mixed homogenously in the ratio 1:10, degassed in dessicator for 30 minutes to remove air bubbles and then poured onto the micropillar array mould in a silicon wafer followed by curing at 80°C for 2 h (Figure 2.1). The micropillars so formed were 2 μm in diameter, 5 μm in height with pillar centre to centre distance of 3 μm as confirmed by electron microscopy imaging.

30 μl of 100 μg/ml fibronectin solution was deposited on a flat PDMS block substrate for 10 min. The solution was then removed and the block dried for 5 min. The stamp was then inverted over the UV treated micropillars for 5 min. The stamp was then removed and the PDMS micropillars washed with PBS and further treated with 1 ml of 2 mg/ml Pluronic F-127 (Sigma) for 2 h to passivate non-fibronectin coated regions.

Cells were trypsinized (Gibco, Life Technologies) and seeded on fibronectin (Sigma) coated PDMS micropillar arrays and allowed to spread for 12 h. The PDMS micropillars were then placed upside down on glass bottom petridish (Ibidi) with a 60 μm thick PDMS membrane placed at the edges of PDMS pillar block as spacer. This inverted setup has dual advantages. First, it provides direct access to the high numerical aperture (NA) objective with short working distance. Second, it prevents the imaging artifacts caused by interference of fluorescence beam passing through the micropillars.

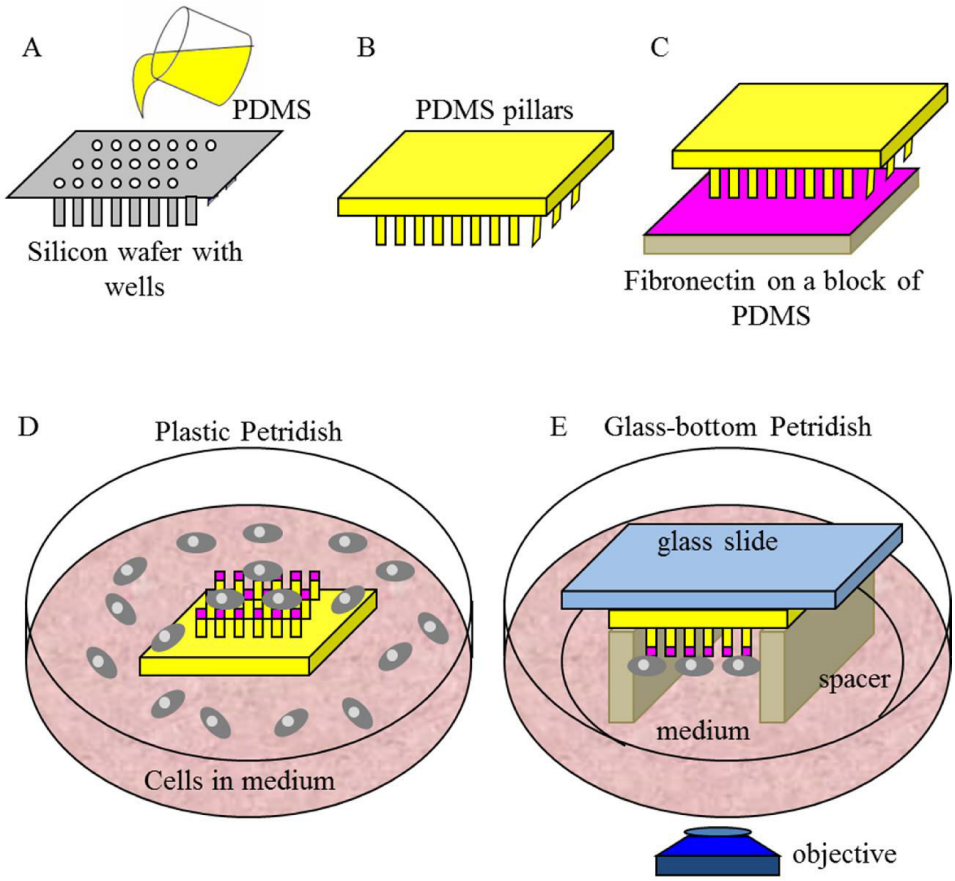

Figure 2.1: Method of Micropillar Preparation and Cell Seeding. (A) PDMS mixed with cross linking agent (10:1) is poured over the silicon wafer. **(B)** PDMS pillars after drying at 80C for 2 hours. **(C)** Pillars are inverted over fibronectin on a block of PDMS. **(D)** Pillars are kept facing up on a plastic bottom petridish, medium containing cells is poured over it and the cells are allowed to adhere on the pillars for 24 hours. **(E)** The pillars with cells are stuck on a glass slide and inverted over two thin PDMS spacers on a glass bottom dish for imaging. 2 ml of cell culture medium is added.

Live Imaging: All images were captured using inverted confocal microscope (Perkin Elmer Spinning Disk, 60X, 1.2 NA objective) at 1 frame every 3–7 s for at least 3 min.

Tracking of Pillars, Nucleus, Heterochromatin foci and Actin Stress Fibers: The deflections of the pillar tips and the nucleus were calculated using custom code written in *MATLAB*. The tips of the pillars show up as bright spots in the bright field images. To calculate the position of the pillar tips,

bright field pillar images were thresholded and centroid was calculated for each time point. The images were corrected for XY drift using the mean displacement of pillars in the control region. A representative image of micropillars, H2B-EGFP labelled cell nucleus and lifeact-mRFP labelled F-actin is shown in Figure 2.2A. The tracking of heterochromatin foci and actin stress fibers was done manually in *ImageJ*.

Fitting of Ideal Lattice to the Micropillar Array: An ideal square lattice for original pillar position was generated by calculating the distance between adjacent pillars in the control region. The lattice was then best fit to the cell region by translation and rotation so as to minimize the deflection of pillars in the control region (Figure 2.2B, C).

Correlation Analysis: The time series were analyzed for autocorrelation and cross correlation using custom written code in *MATLAB*. The autocorrelations of the displacement (magnitude) of the pillar, the nucleus, and heterochromatin foci were calculated and plotted to arrive at their typical timescales. Further, the cross correlations between displacements (component along direction of nucleus movement) of individual micropillars at different regions under the cell were plotted with respect to the displacements (component along direction of nucleus movement) of nucleus and heterochromatin foci.

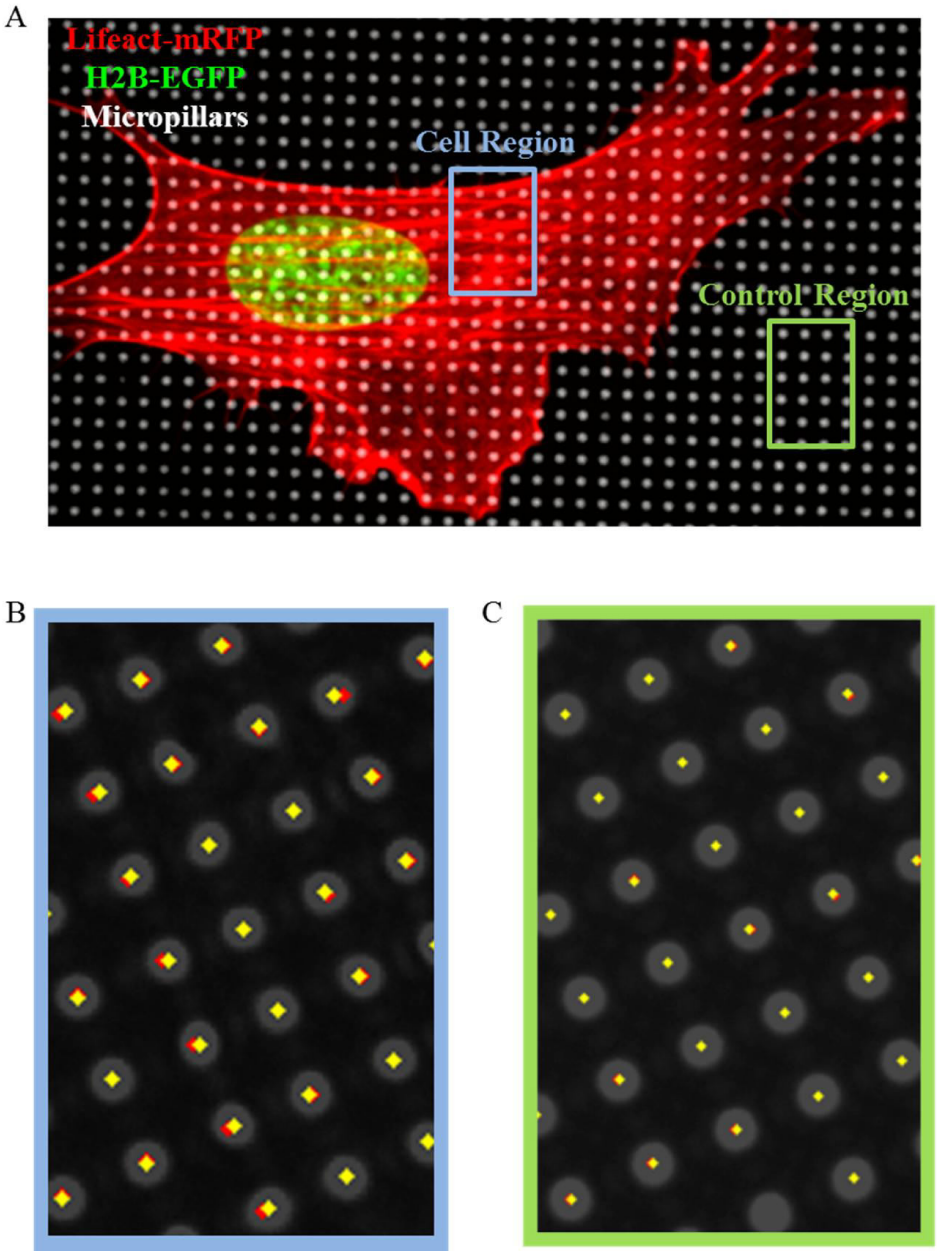

Figure 2.2: Imaging and Tracking of Micropillars. (A) Typical image of a lifeact-mRFP and H2B-EGFP labelled cell spread over pillars. **(B,C)** Pillar centroids (yellow) and original pillar positions (red) calculated using MATLAB for pillars in cell region (B) and control region (C).

RESULTS

2.1 Micropillar Deflections Relate to Actomyosin Forces. NIH3T3 fibroblast cells stably expressing H2B-EGFP were allowed to spread for 12 h

on force sensitive micropillar arrays. Simultaneous time-lapse imaging under bright field for pillars and EGFP fluorescence for chromatin was carried out. The imaging setup consisted of the cells plated on micropillars placed upside down on glass bottom dishes, with 60 μm thick PDMS spacers at the edges (Figure 2.1). This inverted setup has dual advantages. First, it provides direct access to the high NA objective with short working distance. Second, it prevents the imaging artifacts caused by interference of the fluorescence beam passing through the micropillars. A representative image of micropillars, H2B-EGFP labeled cell nucleus and lifeact-RFP labeled F-actin is shown in Figure 2.2A. The centroids of all micropillars under the cell (cell region) and those away from it (control region) were tracked over time using custom written code in MATLAB (Figure 2.2B,C). Typical XY trajectories for the pillar centroids (Figure 2.3A), distance (from mean position) vs time curves (Figure 2.3B), fluctuations in the radial position (Figure 2.3C) and histogram of pillar displacements (Figure 2.3D) showed up to three times larger displacements in the cell region compared to the control region.

The original position of pillars under the cell was calculated by fitting a square lattice (distance between pillars calculated using control region) to minimize the deflections of pillars outside the cell (Figure 2.2B,C). The distance between the original position and the mean observed position of each pillar was measured as the pillar deflection and was used to calculate the magnitude of force on each pillar (Figure 2.4). The maximum pillar deflections were of the order of few hundred nm, corresponding to forces of order of few nN (consistent with previous reports). Myosin inhibition using blebbistatin reduced the magnitude of pillar deflections in the cell region, suggesting that

the pillar deflections are caused by cell traction forces generated by actomyosin (Figure 2.3A,B, Figure 2.4).

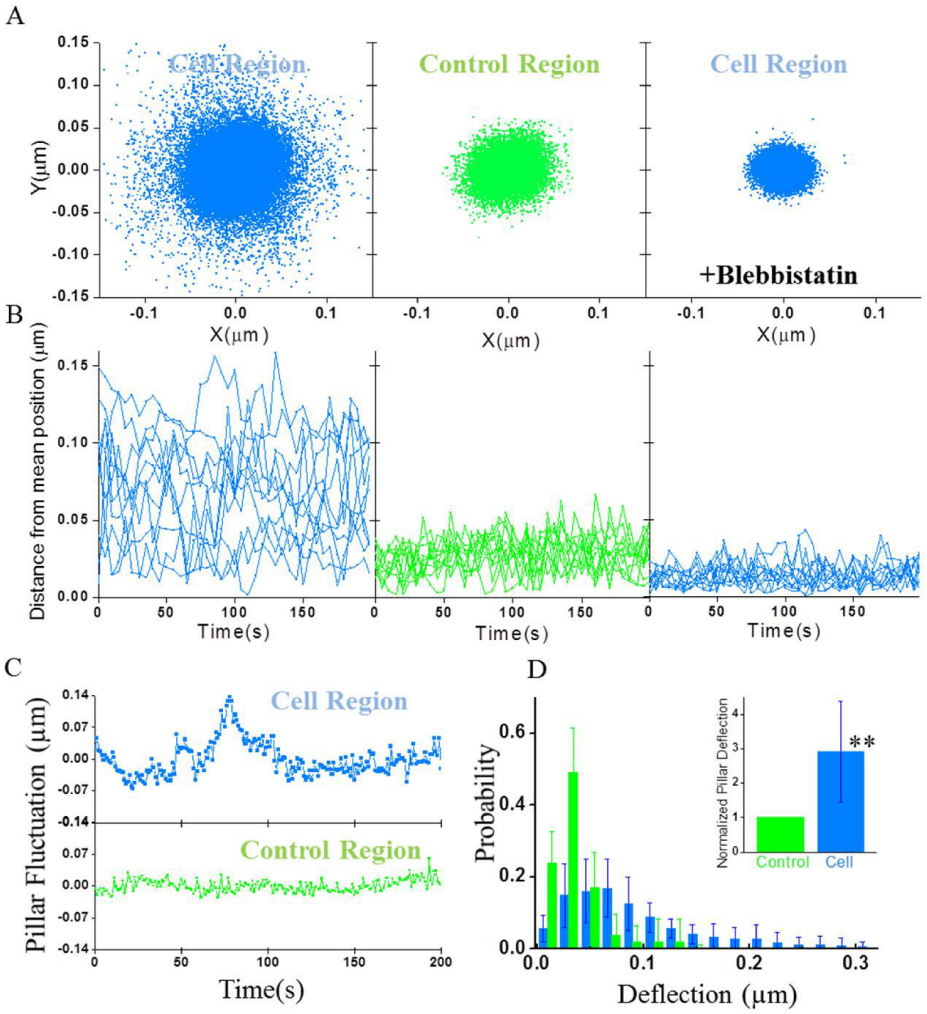

Figure 2.3: Measurement of Micropillar Displacements. (A) XY trajectory of typical pillars in cell region, control region and cell region after blebbistatin treatment. **(B)** Distance (r) from mean pillar position as a function of time for typical pillars in cell region, control region and cell region after blebbistatin treatment. **(C)** Fluctuations in pillar radial position ($r(t) - r_{mean}$) as a function of time for typical pillars in control and cell regions. **(D)** Normalized histogram for pillar deflections in control and cell regions.

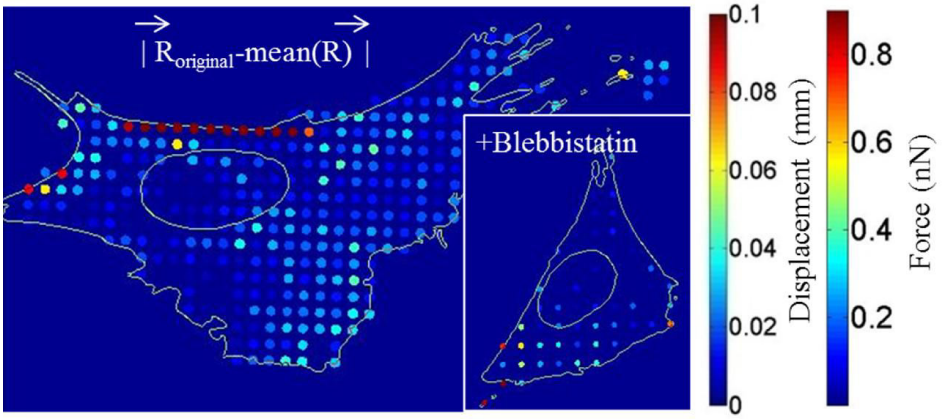

Figure 2.4: Pillar Displacement and Traction Force. Color coded pillar displacement from mean pillar position in a control and blebbistatin treated cell. Second color map on the right is for force (F), calculated from displacement using the formula $F = (3/4\pi E \frac{r^4}{L^3})\Delta x$.

2.2 Dynamic Correlations between Micropillar and Nuclear Displacements. To understand the response time scales of the nucleus upon mechanical stimulation from the extracellular matrix, we probed the dynamic correlation between micropillars and nuclear displacements. Autocorrelation analysis for micropillars and nucleus provides a direct measure of the underlying active cellular processes driving their displacements. Autocorrelation function was plotted for the magnitude of displacement of individual pillars in the control and cell regions (Figure 2.5A). The pillar displacements in the cell region exhibited a decorrelation time scale of ~40 s. As expected, the autocorrelation curves for the pillars in control region dropped sharply. We then evaluated the autocorrelation function for the nucleus and heterochromatin foci displacement magnitudes and noticed similar time scales (Figure 2.5B). The similar decorrelation time scales of ~ a minute suggest that actomyosin contraction drives both pillar and nucleus movement.

Cross-correlation analysis provides a measure of the lag time scale between pillar and nucleus displacements. We carried out cross-correlation analysis between front and rear edge pillar displacements and the movement of the nucleus and heterochromatin foci (component along direction of nucleus movement) to investigate the spatiotemporal nature of the coupling. We observed that the correlation for micropillar in different regions of the cell were distinct. Pillars at the leading edge showed a negative correlation with the movement of the nucleus while those at the rear edge showed a positive correlation (Figure 2.5C). These results showed a minimal time lag (less than 1s) in the cross correlation between pillar and nuclear movements. Further, calculation of the angle between pillar deflection and nucleus movement (Figure 2.6) showed that pillars in the front edge deflect back towards the nucleus (angle ~ 180°) while those at the rear edge deflect forward towards the nucleus (angle ~ 0°). Upon myosin inhibition with blebbistatin treatment, this distinct correlation is partially lost (Figure 2.6 inset). This result confirms the 'nucleo-centric' traction force profile of fibroblasts and suggests viscoelastic coupling with less than a second lag time between focal adhesions and nucleus.

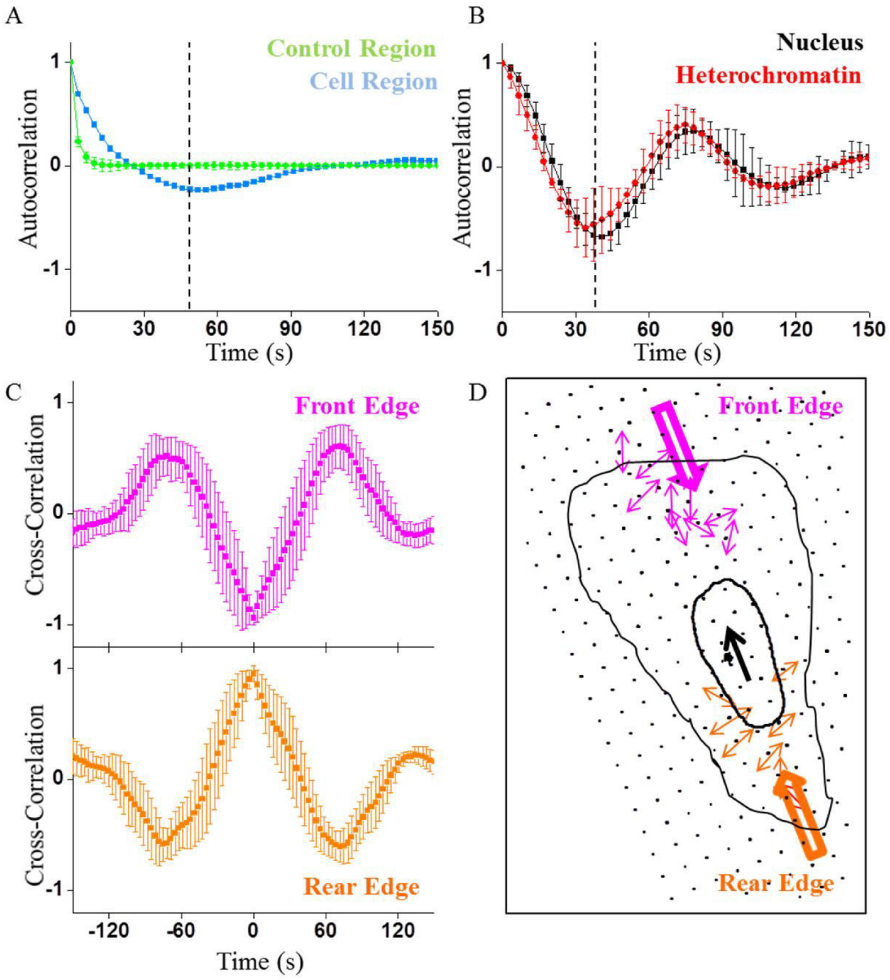

Figure 2.5: Autocorrelation and Cross-Correlation of Micropillars and Nucleus. **(A)** Typical autocorrelation curve for pillars in control and cell regions calculated from pillar displacement time series. **(B)** Typical autocorrelation curve for nucleus centroid and heterochromatin centroid calculated from nucleus and heterochromatin displacement time series. **(C)** Cross-correlation between nucleus and pillars on the front edge vs rear edge of the cell. **(D)** A map of trajectories for all pillars under the cell shows that pillars on the front edge move rearward while those at the rear move forward. The front and rear directions are defined by the nucleus movement.

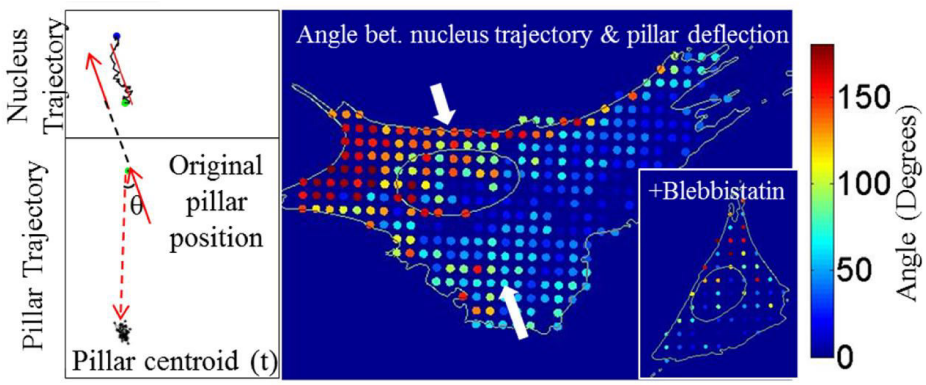

Figure 2.6: Angle between Nucleus Trajectory and Pillar Deflection. The direction of nucleus trajectory is defined from its initial to final observed position. The direction of pillar deflection is defined from its original position (fitting ideal lattice using MATLAB) to mean observed position. The color-coded image on the right represents the angle between nucleus trajectory and pillar deflection for all pillars under the cell in control and blebbistatin treated condition.

2.3 Force Transduction from Apical Stress Fibers to Heterochromatin Foci. Next, we probed whether the actomyosin coupling between focal adhesions and nucleus could transmit forces to chromatin. For this, fibroblasts expressing lifeact-mRFP and H2B-EGFP were cultured on LP patterns. These cells exhibit apical actin stress fibers, which are connected to focal adhesion complex at cell boundary, and apply active compressive load on the nucleus forming indents on its apical surface (Figure 2.7A). Actin stabilization using jasplakinolide enhanced these apical nuclear indents (Figure 2.7B). We investigated the role of these apical stress fibers (ASFs) in chromatin remodeling by performing simultaneous time lapse imaging of lifeact RFP and H2B-EGFP in these cells. H2B labelled fibroblasts show prominent heterochromatin foci providing an appropriate system to visualize the coupling between ASFs and chromatin assembly (Figure 2.7A). Time lapse imaging experiments revealed that ASFs show transverse movement over the nucleus with a speed of ~0.3 μm/min, which is similar to that observed previously.

More importantly, ASFs were found to press and slide over the nucleus resulting in the displacement (Figure 2.7C) or deformation (Figure 2.7D) of the heterochromatin foci. To quantify ASFs and heterochromatin foci movements, regions showing their co-translation were cropped and their centroid positions were tracked manually in *ImageJ*. Distance vs time plot (Figure 2.7F), line kymograph across the nucleus passing through the heterochromatin foci (Figure 2.7G) showed similar trajectories of ASFs and heterochromatin foci centroids for the duration of contact between the two. Interestingly, as the ASFs moved further, the heterochromatin foci showed recoil suggesting a direct transduction of force to these foci by ASFs. A comparison of speeds of ASF and heterochromatin foci showed similar speeds (~0.3 μm/min), confirming their co-translation.

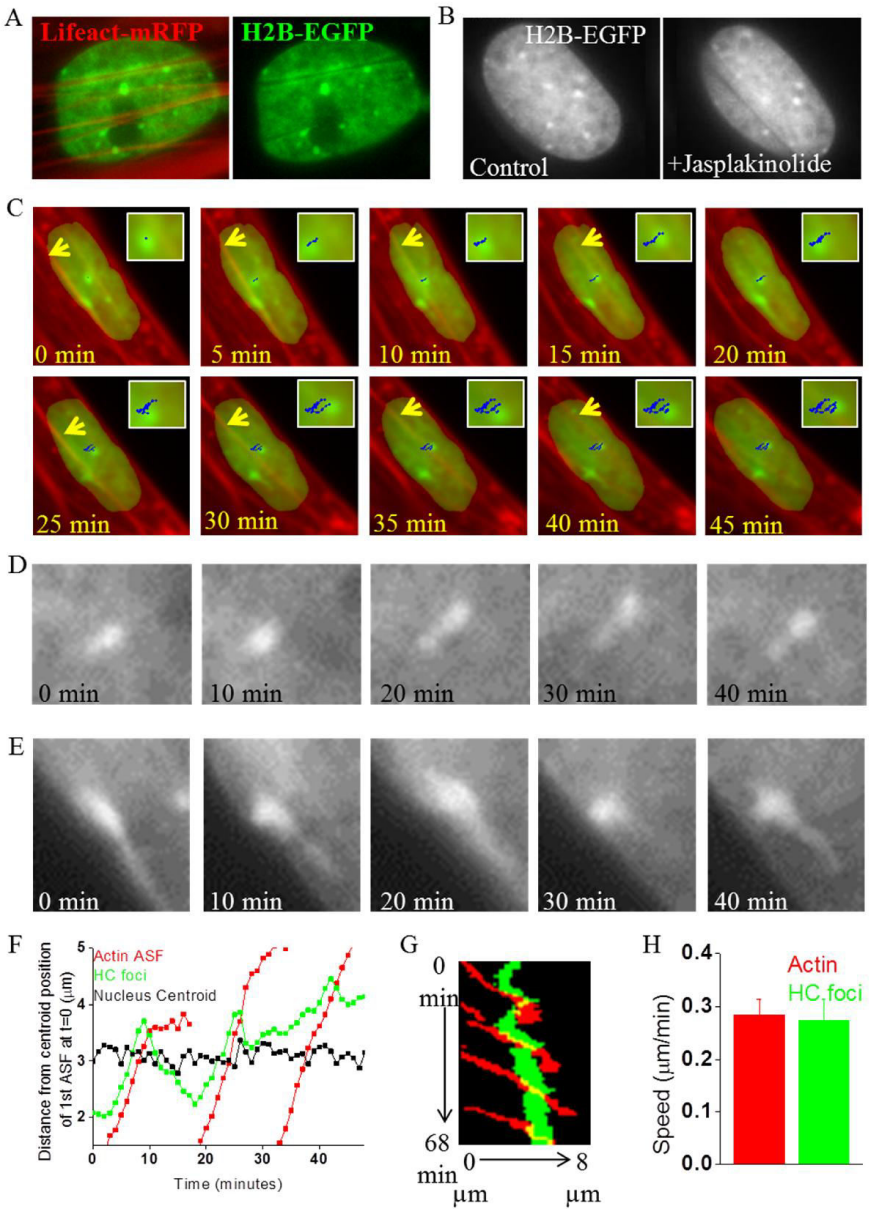

Figure 2.7: Direct Transduction of Forces to Heterochromatin by ASF. (A) Representative images of PMEFs labeled with Lifeact-mRFP and H2B-EGFP showing indentation by ASFs on the nucleus. **(B)** Typical H2B-EGFP nucleus before and after treatment with Jasplakinolide showing indents after drug treatment. **(C)** Time lapse images of actin (red) and nucleus (green) showing co-translation of ASFs and *heterochromatin* foci. Insets show zoomed in view of the heterochromatin foci centroid. **(D,E)** Time lapse images of heterochromatin foci showing their displacement (D) and deformation (E) as an ASF passes over the nucleus. **(F)** Distance vs time curve for actin, heterochromatin foci and nucleus centroid for the cell shown in (C) above. All distances were calculated from the origin, which was fixed at the initial centroid position of the 1st ASF. **(G)** Line kymograph across the nucleus showing heterochromatin foci (green) moving along with the ASFs (red). **(H)** Average speed of ASFs and heterochromatin foci centroids. N = 9, 15 measured over 9 cells.

DISCUSSION

This project studies the time scales of intrinsic coupling between focal adhesions and nucleus in cells cultured on micropillar arrays. We carried out simultaneous imaging of pillar deflections and nucleus and heterochromatin foci dynamics and then performed autocorrelation and cross-correlation analysis for these displacements. The autocorrelation time scales were similar (~40 s) for both pillar and nuclear displacements. This time scale is close to the time scale of fibroblast cell contraction, i.e. 1 min, suggesting that the coupling between pillar and nucleus is mediated by cytoskeletal contraction. Secondly, the maximum cross-correlation between pillar and nuclear displacements was observed at lag time less than 1 s. The response time for a purely elastic system, calculated by dividing the distance from cell edge to nucleus (~10 μm) with the speed of mechanical stress wave propagation along tensed cytoskeletal filaments (~30 m/s) is less than a microsecond. For a viscoelastic system, the response time as calculated by the ratio of cytoplasmic viscosity (~15 Poise) to cytoplasmic elastic modulus (~150 dyn/cm^2) is one-tenth of a second. However, for a purely viscous system, the response time calculated by dividing the distance from cell edge to nucleus (~10 μm) with the speed of wave propagation (~speed of pillar displacement, i.e. 0.1 μm/25s = 4 nm/s, neglecting the cytoplasmic viscous drag) is much longer and of the order of ~40 min. In the presence of a retrograde flow (10 nm/s), this response time decreases to ~10 min. Comparing these numbers with the lag time of pillar-nucleus cross-correlation, we conclude that the mechanical links between focal adhesions and nucleus in living cells must have a strong elastic component. A recent report also revealed that the cytoplasm behaves as an

elastic gel by analyzing motion of injected particles inside the cell. Further, the spatial maps of pillar displacements and their correlations showed distribution of active forces exerted by cells on the substrate. The spatial heterogeneity in pillar displacements with respect to nuclear movements possibly suggests a highly coordinated contractile process to test local microenvironment during cell migration. As a result, myosin inhibition using blebbistatin inhibited such spatial correlation. Our observed force transduction time scales suggest that chromatin structure could respond rapidly to local microenvironment signals thus facilitating better integration of biochemical pathways to the nucleus. Our observation that apical actin fibers can physically displace the heterochromatin foci, provide a strong evidence for the direct transduction of forces to internal chromatin structure. The dynamic links between the extracellular matrix to internal nuclear architecture via the active stresses generated by ASFs could be one of the major components in nuclear mechanotransduction. These links may be vital for maintaining the 3D organization of functional nuclear architecture and impinge on mechano-regulation of gene expression. Collectively, our studies reveal that cells are constantly testing the local microenvironment using actomyosin contractility and instantaneously transmit such mechanical signals to the nucleus to possibly maintain cellular homeostasis.

PUBLICATIONS FROM THIS WORK

- ***The regulation of dynamic mechanical coupling between actin cytoskeleton and nucleus by matrix geometry***
  Li Q, Kumar A, **Ekta Makhija** and G. V. Shivashankar
  Biomaterials, 2014. 35(3): p. 961-9.

- ***Micropillar displacements by cell traction forces are mechanically correlated with nuclear dynamics***
  Li Q*, **Makhija E***, Hameed FM and Shivashankar GV
  Biochem Biophys Res Commun, 2015. 461(2): p. 372-7.
  * Equal Contributors

CHAPTER 3: ACTOMYOSIN CONTRACTILITY REGULATES NUCLEAR AND CHROMATIN PLASTICITY

INTRODUCTION

Physical properties of the nucleus, such as its morphology and plasticity have been associated with important cellular functions like gene expression, genome integrity and cell behavior [61-65]. The major cellular components that regulate these physical properties are the cytoskeleton to nuclear links and the nuclear lamina [34, 35, 66-69]. Lineage specific physical properties of the nucleus emerge during cellular differentiation; while stem cell nuclei are highly deformable [47, 70] and have a plastic chromatin [71] with hyperdynamic chromatin proteins [44], with differentiation, nuclei lose their plasticity and become less deformable [43, 72]. The nucleus in a differentiated cell is physically coupled to the cytoskeleton via lamins and the linker of nucleoskeleton and cytoskeleton (LINC) complex, which comprises of transmembrane SUN and KASH domain proteins [30, 33, 56, 58, 73-78]. Any perturbation to these components is linked to changes in nuclear morphology and plasticity [79]. Therefore, the meshwork of actin stress fibers and lamin A/C serves as a critical physical intermediate in the maintenance of nuclear functional homeostasis. The physical properties of the nucleus govern the spatio-temporal packaging of chromatin, which regulates lineage specific gene expression programs [53, 80-83]. In addition, modulations in cytoskeletal to nuclear links have been implicated in DNA damage and genome integrity [84, 85]. The maintenance of nuclear physical properties is also essential in cell migration during developmental programs [86, 87] as well as in wound healing [88, 89]. Defects in nuclear morphology and its plasticity have also been shown to be important in metastatic potential and cancer cell invasion [90, 91]. Further, a number of diseases have been associated with loss of the

mechanical integrity of the nuclear lamina [92-97]. However, the regulation of the mechanical integrity of the cell nucleus by the active cytoskeletal network is not well understood.

Recent studies have revealed that cytoskeletal organization and nuclear morphology are regulated by EMS, such as substrate stiffness and geometry [8, 10, 16, 19, 54, 98-102]. With the cytoskeleton physically linked to the nucleoskeleton, these EMS can therefore be used to mediate changes in chromatin structure. Active cytoskeletal forces can mediate the mechanotransduction to the nucleus, to remodel 3D chromosome organization as well as permissivity to chromatin structure by regulatory molecules [21, 42]. Cytoskeletal to nuclear links are also essential to the maintenance of poised euchromatin and more repressive condensed chromatin, i.e. heterochromatin assembly [103]. Heterochromatin is anchored to the lamin envelope, and stabilized by links between the actin cytoskeleton and the nuclear membrane [39, 40, 104]. In this context, the dynamic control of nuclear plasticity by actomyosin contractility and its impact on heterochromatin plasticity are still unclear.

To understand the mechanism underlying the cytoskeleton mediated alterations in nuclear and chromatin plasticity, we modulated cytoskeletal organization using cell geometric constraints and measured nuclear deformability and heterochromatin dynamics. We found that in cells with CI geometry, the nucleus is more deformable than cells with elongated and polarized geometry. We further showed that this can be attributed to differential force generating actomyosin structures and differential lamin A/C

expression levels in the two geometries. Interestingly, these active cytoskeletal forces were also found to regulate the dynamics of sub-nuclear heterochromatin structures. Our observations suggest that active forces from the cytoskeleton regulate nuclear and chromatin plasticity, which could in turn affect the spatio-temporal regulation of genomic processes and thus cell behavior.

MATERIALS AND METHODS

Cell Culture, Pharmacological Perturbations and Plasmid Transfections:
Wild type NIH3T3 fibroblasts and NIH3T3 fibroblasts stably expressing H2B-EGFP were cultured in low glucose Dulbecco's Modified Eagle Medium (Gibco, Life Technologies) supplemented with 10% Fetal Bovine Serum (Gibco, Life Technologies) and 1% penicillin-streptomycin (Gibco, Life Technologies) at 37°C and 5% CO_2 in humid conditions. Cells were trypsinized (Gibco, Life Technologies) and seeded on fibronectin (Sigma) micropatterned dishes for 3 hours before imaging.

Cytochalasin-D (Sigma) was used at 500 nM working concentration and cells were imaged either immediately or 30 minutes after treatment. Jasplakinolide (Gene Ethics) was used at concentration of 200 nM and cells were imaged 20 minutes after treatment. Blebbistatin (Merck) was used at concentration of 25 μM and cells were imaged 30 minutes after treatment. Small molecule inhibitor of formin homology 2 domains (SMIFH2, ChemBridge Corporation) was used at a concentration of 20 μM and cells were imaged an hour after treatment. Nocodazole (Sigma) was used at a concentration of 10 μg/ml and cells were imaged an hour after treatment.

All transfections were carried out using jetPRIME (Polyplus transfection).

Preparation of PDMS stamps, Microcontact printing and Cell seeding on patterns: To make stamps, PDMS (Sylgard 184, Dow Corning) precursor and curing agent were mixed homogeneously in 10:1 ratio and poured over the silicon wafer which had LP or CI micropatterned wells. After degassing in the desiccator for 30 minutes to remove air bubbles from the PDMS mixture, the silicon wafer with the PDMS mixture was cured in the oven at 80°C for 2 hours. Solidified PDMS was then peeled from the wafer and cut into ~ 1cm by 1cm stamps. These stamps were oxidized using plasma for 4 minutes and then 15ul of 100 ug/ml fibronectin solution (mixed with Alexa Fluor 647 dye, Sigma) was poured over each stamp. Extra solution was wiped with a tissue and the stamp was allowed to dry for 10 minutes. The stamp was then checked under the microscope for complete drying between the micropatterned structures, after which it was inverted carefully onto the surface of an uncoated hydrophobic 35 mm dish (Ibidi). The stamp was gently removed after 2 minutes and the stamping on the dish was checked by visualizing Alexa 647 fluorescence in the far-red channel in the epifluorescence microscope. To passivate the non-patterned surface of the dish, it was then treated with 2 mg/ml pluronic F-127 for 5 minutes, and washed twice with PBS and cell culture medium before seeding 40,000 single cells.

Imaging, Image Processing and 3D Rendering: All imaging was carried out using a 100X objective on a NikonA1R Confocal microscope. Time lapse imaging was done in either widefield or confocal mode with 30 s, 60 s or 90 s

time intervals for up to 60 minutes in each condition. The z-depth for confocal imaging was 0.5 μm.

H2B-EGFP images were thresholded, projected nuclear area was calculated and time lapse images of the nuclear periphery were generated using custom written code in MATLAB. Merged images of the nuclear periphery at different time points were generated in ImageJ. Area fluctuation time series were plotted and fitted with third order polynomial or exponential curves in ORIGIN. The residual values were divided by the value of the polynomial at each time point to obtain the normalized residual area fluctuations. Such normalized residual area fluctuations for multiple cells were plotted as a histogram, which were then fitted with Gaussian curves. Full width at half maximum of the gaussian fitting indicates the amplitude (in percentage) of area fluctuations. Edge kymographs were generated from the nuclear periphery images using IMARIS. 3D rendering of actin, microtubules and the nucleus was also done using IMARIS. Line kymographs across the nucleus for visualizing heterochromatin foci dynamics were generated in ImageJ.

Heterochromatin Foci Trajectory Correlation Analysis: Time lapse confocal stacks of H2B-EGFP nuclei were opened in IMARIS. Nucleus trajectory was corrected for translation and rotation shift. Bright spots corresponding to heterochromatin foci were picked using surface thresholding and their centroid xyz trajectories were obtained. Vector correlation coefficient between heterochromatin foci with trajectories $\vec{A}(t)$ and $\vec{B}(t)$ was calculated as $\frac{\sum(\vec{A}(t)-\vec{A}_{mean})\,.\,(\vec{B}(t)-\vec{B}_{mean})}{\sqrt{(\vec{A}(t)-\vec{A}_{mean})^2}\sqrt{(\vec{B}(t)-\vec{B}_{mean})^2}}$ and the correlation matrices were generated using a custom written code in MATLAB.

RESULTS

3.1 Reduced Matrix Constraints Enhance Nuclear Plasticity. Various studies have shown that the geometry of the cell regulates cytoskeletal organization. Hence, to probe the effect of cytoskeletal organization on nuclear dynamics, NIH3T3 fibroblast cells were cultured on fibronectin micropatterns of two extreme geometries; namely – LP or CI. Cells cultured on these geometries exhibited distinct cytoskeletal organization and nuclear morphologies. Consistent with previous studies [19], LP cells were flat, their actin was organized as long apical stress fibers and the nucleus was also flat and elongated. On the other hand, CI cells were taller, their actin was organized as short filaments or patches and the nucleus was rounded (Figure 3.1A-D). Despite the nuclear height being greater in CI cells, the projected nuclear area, surface area and volume were less compared to LP cells (Figure 3.1E).

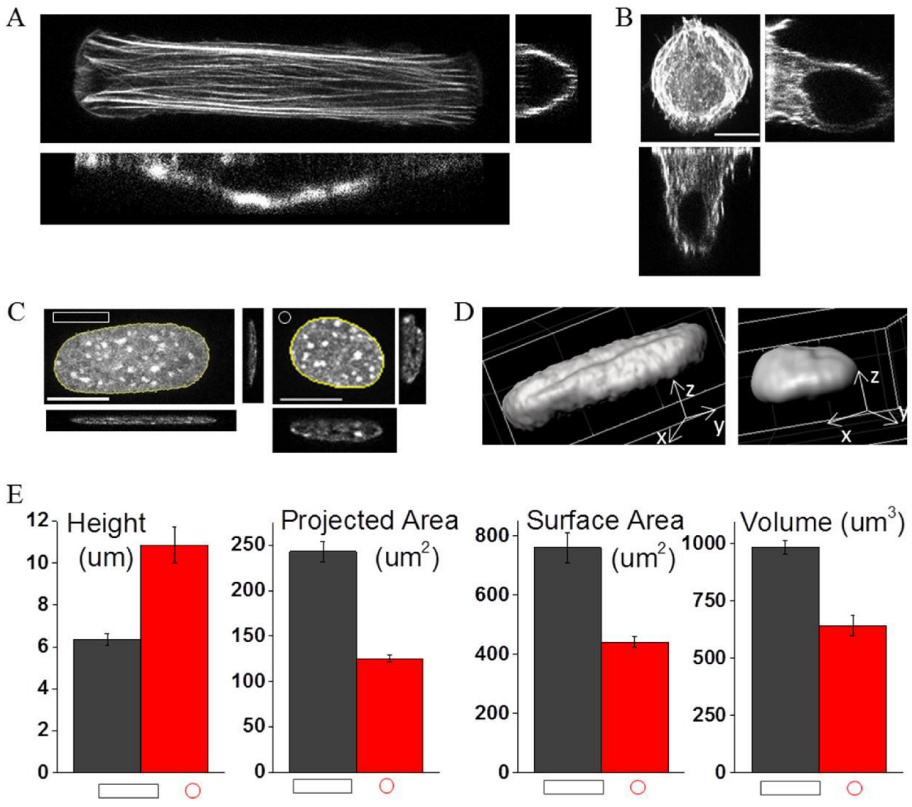

Figure 3.1: Effect of Cell Geometry on Nuclear Morphology. (A,B) Orthogonal views of actin labelling (Phalloidin) for typical LP (A) and CI (B) cells. **(C)** Orthogonal views of nucleus labelling (Hoechst) for typical LP and CI. **(D)** 3D rendering of nucleus in LP and CI cells. **(E)** Comparison of nuclear height, projected area, surface area and volume for BR (n = 10) and SC cells (n = 10).

Next, to study the dynamics of nuclear morphology as a function of the two extreme cytoskeletal organizations, time lapse imaging was performed using fibroblasts stably expressing H2B-EGFP and cultured on LP or CI fibronectin micropatterns. The time lapse images were thresholded to obtain the nuclear periphery before the time series was converted to a z stack and reconstructed in Imaris to form a surface (Figure 3.2B). These kymographs revealed increased nuclear periphery fluctuations in CI cells. Also, superimposition of nuclear peripheries at different time points (Figure 3.2A) revealed that in LP cells, the nuclear periphery does not undergo a significant alteration with time

as opposed to CI cells, which show significant fluctuations of the nuclear periphery within 10 minutes. To further quantify these fluctuations, the projected nuclear area vs time was fitted with a third order polynomial and the residuals were normalized by the value of the polynomial fit at each time point. These normalized residual fluctuations were then plotted as a function of time. Typical time traces (Figure 3.2C) revealed a relatively constant projected nuclear area in LP cells over a period of 20 minutes and up to 10% fluctuations in CI cells. This increased nuclear plasticity of CI cells was consistently different than LP cells, as observed over multiple cells (Figure 3.2F). However, the nuclear surface area and volume in CI cells did not show such large fluctuations (Figure 3.2F). To quantify the mean amplitude of fluctuations, a histogram of projected nuclear area was plotted that incorporated data from all time points and all cells (Figure 3.2D). Such histograms were then fitted with a Gaussian distribution and the full width at half maximum (FWHM) was used to compare the amplitude of area fluctuations. The FWHM of PNAF was 10% in CI cells, compared to only 4% in LP cells (Figure 3.2D inset). Typical time period of these PNAFs was ~5 to 10 minutes (Figure 3.2E).To understand this cell geometry-mediated change in nuclear plasticity, we next probed the role of cytoskeletal forces and nuclear stiffness.

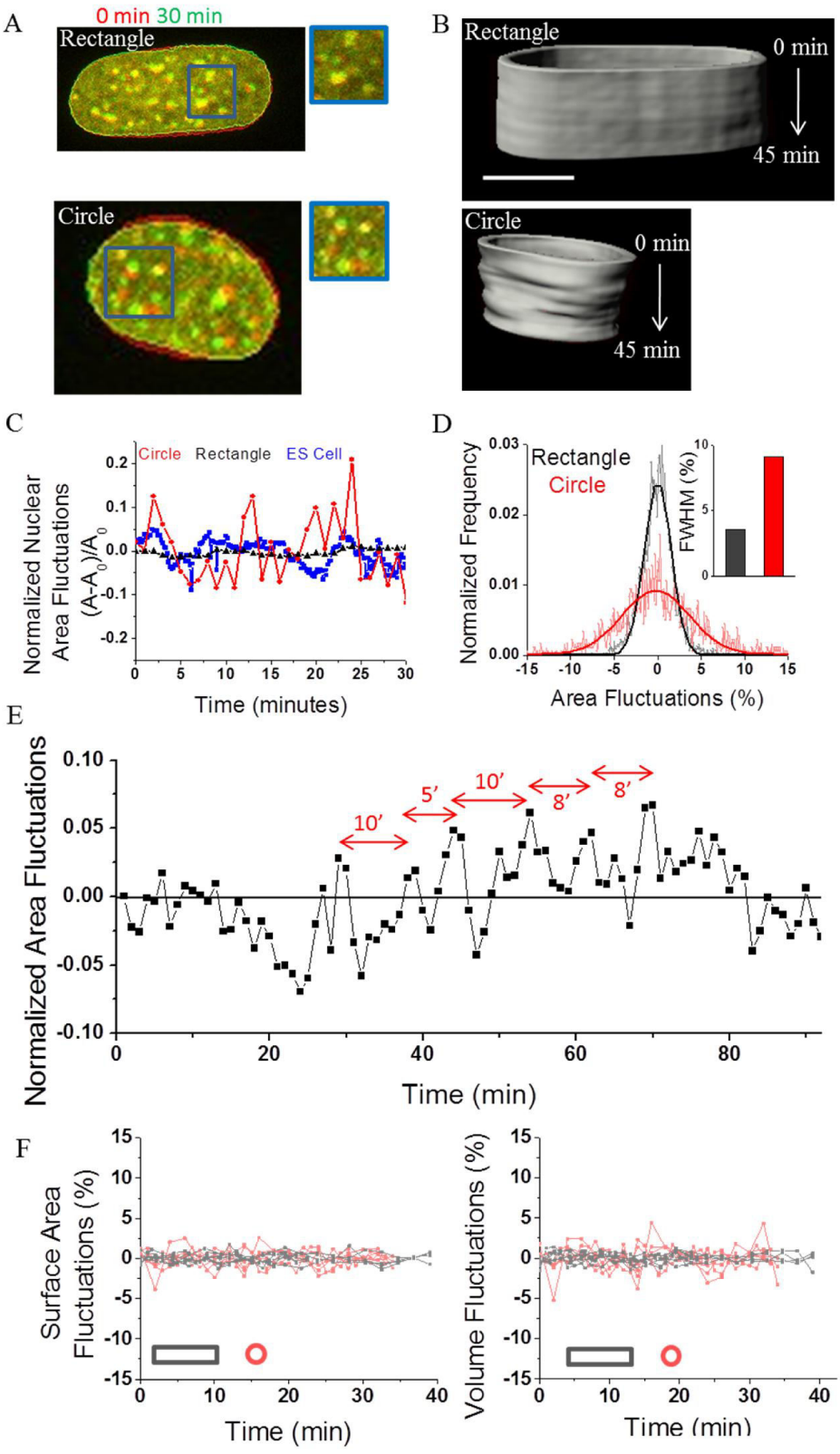

Figure 3.2: Effect of Cell Geometry on Nuclear Plasticity. (A) A merge of 0 min and 30 min images of H2B-EGFP labelled nuclei in LP and CI cells. **(B)** Nuclear periphery kymograph of typical LP and CI cells. **(C)** Normalized nuclear area

fluctuations for NIH3T3 cells on LP and CI patterns and ES cells (on unpatterned substrate). **(D)** Normalized histogram for nuclear area fluctuations in multiple LP and CI cells. **(E)** Long time series of area fluctuations in a typical CI cell nucleus to measure its periodicity. **(F)** Nuclear surface area and volume fluctuations as a function of time for BR (n = 8) and SC (n = 6) cells.

3.2 Actin, Myosin and Formin Regulate Matrix Assisted Nuclear Plasticity. To study the role of cytoskeletal forces in PNAF, actin organization was perturbed in both LP and CI cells by treating them with actin depolymerizing and actin stabilizing agents cytochalasin-D and jasplakinolide, respectively. In each case, time lapse imaging was first performed on control cells (n>15). These same cells were then treated with pharmacological agents and reimaged. Periphery kymographs for all treatments are shown in Figure 3.3D. Here, the PNAF showed a non-monotonic dependence on the state of actin polymerization. Depolymerization of F-actin in LP cells using cytochalasin-D decreased the projected nuclear area exponentially with time. In this case, the PNAF was calculated by normalizing the residuals of an exponential fit with the value of the fit at each time point. Cytochalasin-D treatment in LP cells enhanced PNAF from 4% to 8% (Figure 3.3A) and actin stabilization (using jasplakinolide) in CI cells reduced PNAF from 10% to 2% (Figure 3.3B). Surprisingly, further actin depolymerization in CI cells using cytochalasin-D also reduced the PNAF from 10% to 5% (Figure 3.3C). Consistent PNAF were obtained upon actin perturbation in multiple cells. Such non-monotonic dependence of PNAF on actin polymerization suggests that only cells with intermediate state of actin polymerization exhibit fluctuations in the projected nuclear area.

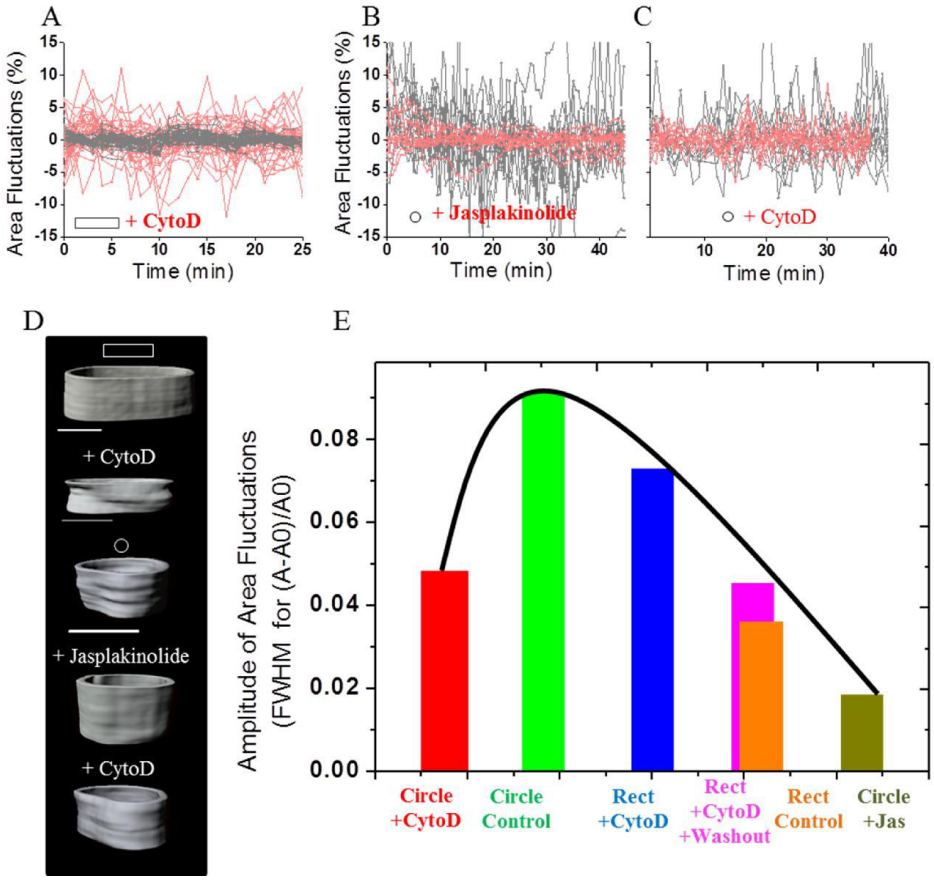

Figure 3.3: Role of Actin in Cell Geometry Mediated Nuclear Plasticity. (A-C) Nuclear area fluctuation time series for multiple control and cytochalasin-D treated LP cells (A), control and jasplakinolide treated CI cells (B) and control and cytochalasin-D treated CI cells (C). **(D)** Nuclear periphery kymographs for control and cytochalasin-D treated LP cells and control, jasplakinolide and cytochalasin-D treated CI cells. **(E)** FWHM of Gaussian fitting of histograms of PNAF of multiple control and treated LP and CI cells. Left to right represents increasing actin polymerization. CI + cytochalasin-D (n = 16), CI (n = 27), LP + cytochalasin-D (n = 43), LP + cytochalasin-D + washoff (n = 22), LP (n = 83), CI + jasplakinolide (n = 13).

To further explore the origin of such nuclear fluctuations mediated by intermediate state of actin polymerization, the myosin activity was perturbed using blebbistatin in cells with enhanced PNAF, i.e. LP cells treated with cytochalasin-D and CI cells. In each case the PNAF decreased to less than 5% (Figure 3.4), suggesting that along with small polymerized units of actin,

myosin is also necessary to induce the observed nuclear fluctuations. The blebbistatin mediated decrease in PNAF was highly reproducible.

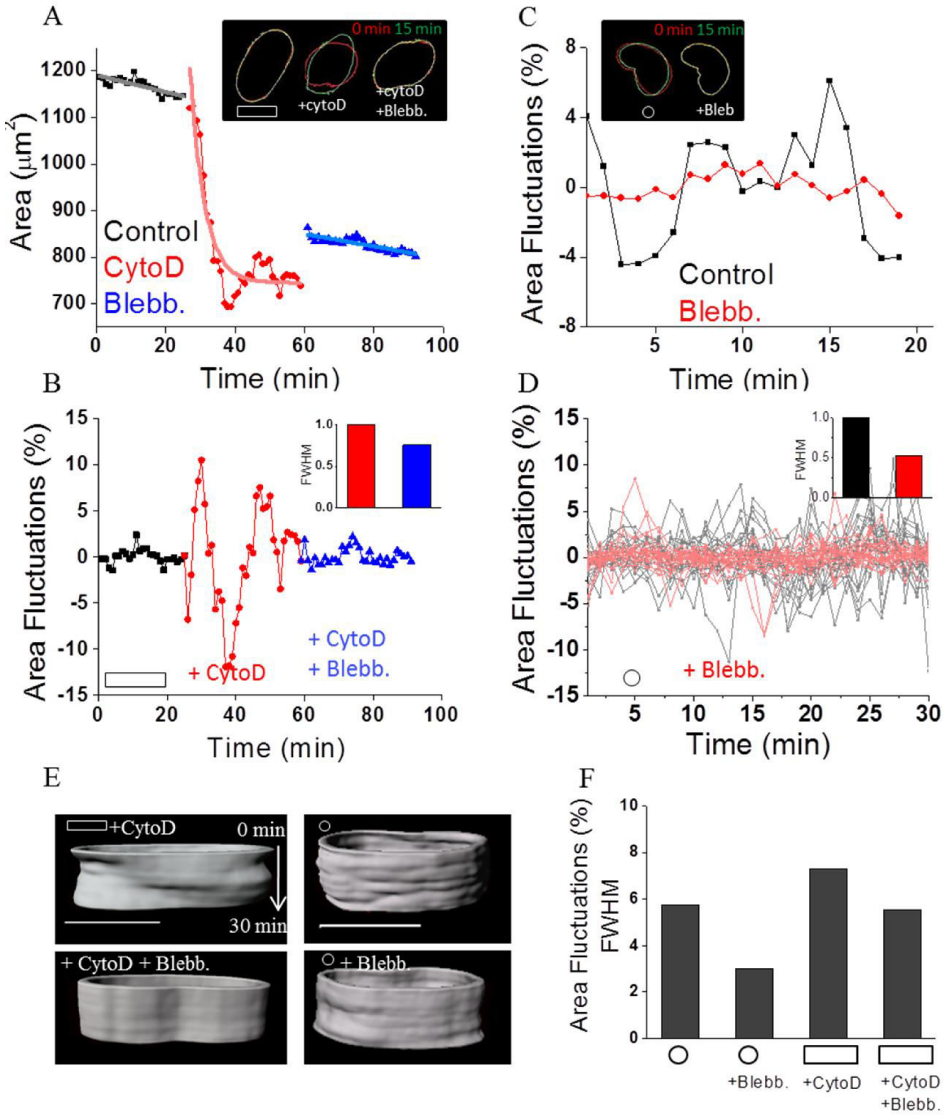

Figure 3.4: Role of Myosin in Cell Geometry Mediated Nuclear Plasticity. (A) Area vs time plot for a typical control BR cell and upon sequential treatment with cytochalasin-D and blebbistatin. Gray and blue curves represent third order polynomial fit. Light red curve represents exponential decay fit ($\tau \sim 4.2$ minutes). Inset shows merge of nuclear periphery outlines at 15 min interval for a typical LP cell in untreated, cytochalasin-D and blebbistatin conditions. **(B)** Typical PNAF trace for a LP cell sequentially treated with cytochalasin-D and blebbistatin. Inset represents the FWHM of Gaussian fitting of histograms of combined PNAFs of multiple cells (n = 5). **(C)** Typical PNAF trace for a control and blebbistatin treated CI cell. Inset shows merge of nuclear periphery outlines at 15 min interval for a typical CI cell in control and blebbistatin conditions. **(D)** PNAF vs time plot for multiple control and blebbistatin treated CI cells (n = 25). Inset represents the FWHM of Gaussian fitting of histograms of combined PNAFs for all cells. **(E)** Nuclear

periphery kymograph of control and blebbistatin treated CI cells, cytochalasin-D and blebbistatin treated cells. **(F)** FWHM of Gaussian fitting of histograms of PNAF of multiple control and treated LP and CI cells.

To assess if nucleators of actin polymerization, such as formin, could be generating these active forces, we inhibited formin activity using SMIFH2 in cells with enhanced PNAF, i.e. CI cells and cytochalasin-D treated LP cells. The PNAF in both cases were reduced by half in all cells (Figure 3.5), confirming that formin indeed plays a role in nuclear fluctuations. Next, we assessed if the physical links between force generating actin-myosin-formin nodes and the cell nucleus are required to generate the observed projected area fluctuations (Figure 3.6).

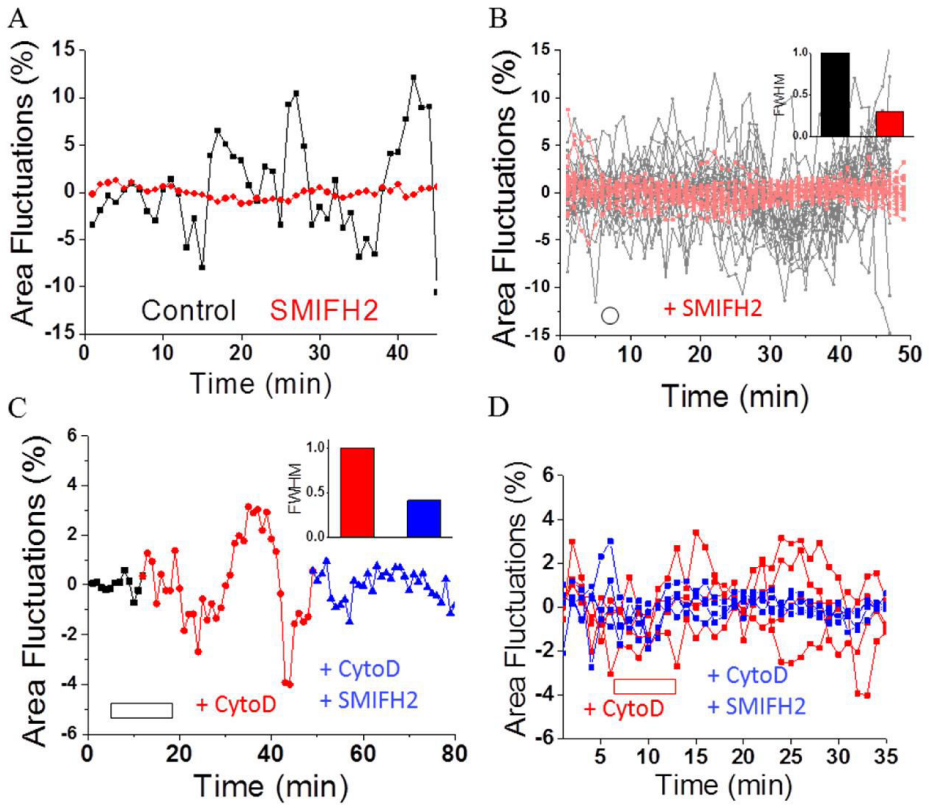

Figure 3.5: Role of Formin in Cell Geometry Mediated Nuclear Plasticity. (A-D) Nuclear area fluctuation time series for multiple control and SMIFH2 treated CI cells (A,B) and cytochalasin-D and SMIFH2 treated LP cells (C,D). Insets represent the FWHM of Gaussian fitting of histograms of combined PNAFs for all cells (n=26,4)

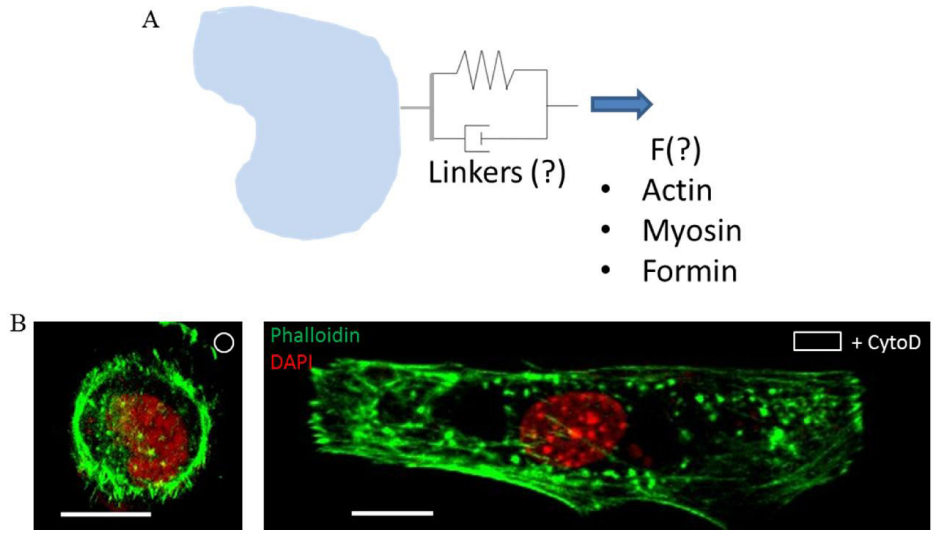

Figure 3.6: Actin-Myosin-Formin Asters Apply Force on the Nucleus. (A) A cartoon summarizing the experimental observations: myosin and formin along with intermediate polymerization states of actin are necessary for causing nuclear fluctuations. Forces from actin-myosin-formin may be applied directly or via linkers to the nucleus. **(B)** Phalloidin staining in CI and cytochalasin-D treated LP cells shows actin asters.

3.3 Nesprin and Microtubules Affect Amplitude of Nuclear Area Fluctuations. Actin is physically linked to the nucleus via Nesprin2, which is a component of the LINC Complex [105]. To understand whether this physical link is necessary for actin-myosin-formin regulated nuclear plasticity, cells were transfected with DN-KASH fused with mRFP, which displaces the endogenous nesprin from the nuclear envelope to the endoplasmic reticulum [60]. These cells were then cultured on CI fibronectin micropatterns and time lapse imaging of H2B-EGFP labelled nuclei was performed in cells expressing DN-KASH mRFP (Figure 3.7A). Periphery kymographs of these nuclei (Figure 3.7C) showed similar fluctuations as control CI cells. Typical time traces of the normalized PNAF (Figure 3.7B) and the FWHM of their Gaussian distribution (Figure 3.7B inset) revealed that although nesprin perturbed cells still exhibit nuclear fluctuations, the fluctuation amplitude is

reduced from 10% to 7.5% compared to control CI cells. Since this amplitude is still higher than control LP cells (which show 4% area fluctuations), it is likely that other components linking actin-myosin-formin network to the nucleus are also involved in these fluctuations. The PNAFs were also seen to be present in DN-KASH cells on LP patterns upon cytochalasin-D treatment (Figure 3.7D).

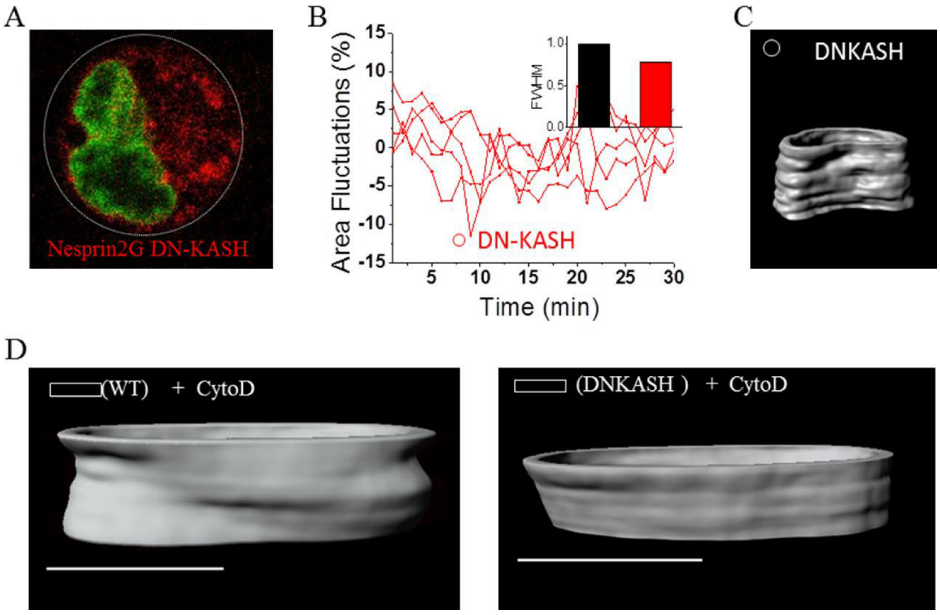

Figure 3.7: Role of Nesprin in Cell Geometry Mediated Nuclear Plasticity. (A) Widefield epifluorescence image of a typical CI cell co-expressing H2B-mRFP (green) and Nesprin2G DN-KASH EGFP (red). **(B)** PNAF vs time plot for multiple DN-KASH CI cells (n = 5). Inset represents the FWHM of Gaussian fitting of histograms of combined PNAFs for all cells. **(C,D)** Surface rendering of nuclear periphery kymographs for typical DN-KASH CI cell (C) and cytochalasin-D treated WT and DN-KASH cells (D).

We next explored whether microtubules serve as additional force transducers between the actin-myosin-formin network and the nuclear periphery. Microtubules are physically coupled to the nucleus via Nesprin4 [106] and to actin via microtubule-actin crosslinking factors (MACFs) [107]. In CI cells, the microtubules surround the nucleus closely and the microtubule organizing

centre (MTOC) indents on the nucleus (Figure 3.8A). A similar indent on the nucleus is also visible in LP cells treated with cytochalasin-D (Figure 3.8B). To probe whether the microtubule network that surround the nucleus could transmit force for nuclear fluctuations, microtubules were depolymerized using nocodazole in CI cells and cytochalasin-D treated LP cells. Typical time traces of the normalized PNAF (Figure 3.8D) and the FWHM of their Gaussian distribution (Figure 3.8D inset) revealed 25% increase compared to control CI cells. This suggests acto-myosin contractile forces are increased following depolymerization of microtubules [108]. Surprisingly, nocodazole treatment in cytochalasin-D treated LP cells caused nuclear buckling (Figure 3.8C), because of which the exact area fluctuations could not be measured. Microtubule stabilization using taxol also did not significantly alter the PNAF (Figure 3.8E). However, dynein inhibition using ciliobrevin-D decreased the PNAF by 50% (Figure 3.8F). Taken together, these results show that perturbations of the physical links only partially affect the amplitude of PNAF, suggesting that there are additional mechanisms that drive nuclear fluctuations.

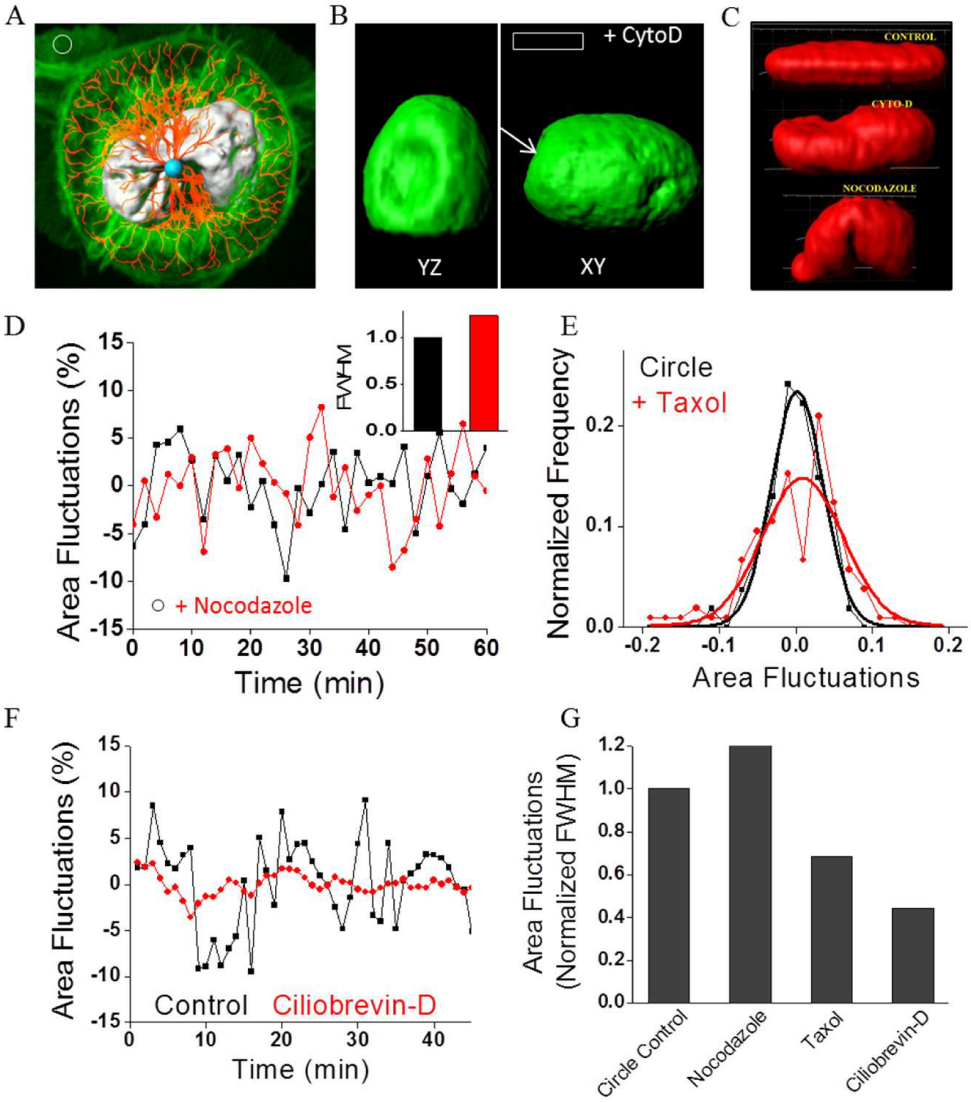

Figure 3.8: Role of Microtubules in Cell Geometry Mediated Nuclear Plasticity. **(A)** Top view of a 3D rendering of Phalloidin intensity (green), filament rendering of tubulin immunofluorescence (red) and a surface rendering of Hoechst intensity (gray) in a typical CI cell. **(B)** Side view (YZ) and top view (XY) of surface rendering of a H2B-EGFP nucleus in cytochalasin-D treated LP cell shows the indent in the nucleus. **(C)** Side view of surface rendering of H2B-EGFP nucleus before and after cytochalasin-D and cytochalasin-D + nocodazole treatments. **(D)** Typical PNAF trace for a CI cell treated with nocodazole. Inset represents the FWHM of Gaussian fitting of histograms of combined PNAFs of multiple cells (n = 26). **(E)** Normalized histogram for control and taxol treated CI cells. **(F)** Typical PNAF trace for a CI cell treated with Ciliobrevin-D. **(G)** FWHM of Gaussian fitting of histograms of PNAF of multiple control and treated CI cells. Nocodazole (n=26), Taxol (n=3), Ciliobrevin-D (n=5)

3.4 LaminA/C Levels Inversely Regulate Nuclear Plasticity. Structural lamin proteins in the nuclear envelope regulate nuclear stiffness - while laminA/C confers rigidity to the nucleus, its absence increases nuclear plasticity [109-111]. To understand the relation between lamin mediated nuclear stiffness and cytoskeletal mediated nuclear fluctuations we overexpressed laminA/C using transient transfection in fibroblasts before culturing them on CI patterns. Time lapse imaging was then performed for cells expressing both laminA/C-RFP and H2B-EGFP (Figure 3.9A). Typical time traces of normalized PNAF in these cells (Figure 3.9B) showed significantly lower amplitude than in control CI cells. The FWHM of Gaussian distribution of the area fluctuations was reduced by half compared to control CI cells (Figure 3.9B inset). The nuclear periphery kymograph (Figure 3.9D) also showed a significant decrease in periphery fluctuations compared to control CI cells.

This result suggested that geometric constraints placed on a cell might regulate laminA/C expression and thus alter PNAF. We therefore checked whether the endogenous laminA/C levels were altered in wild type cells on CI compared to LP patterns. To achieve this laminA/C mRNA levels were measured using RT-qPCR in both geometries. Interestingly, CI cells showed 80% reduction in laminA/C mRNA levels compared to LP cells (Figure 3.9C).

To further investigate the role of laminA/C in the inhibition of PNAF, laminA/C knock-out and control (stably transfected with empty vector) mouse embryonic fibroblasts (MEFs) [112] transfected with H2B-EGFP were cultured on LP micropatterns (Figure 3.9E, G). Time lapse imaging of the

nuclei in these cells revealed increased PNAF in the knock-out cells (Figure 3.9F, H). The FWHM of Gaussian distribution of area fluctuations showed 3 fold increase in the knockout cells compared to control MEFs (Figure 3.9H inset). The nuclear periphery kymograph (Figure 3.9D) also showed increased fluctuations in knock-out MEFs. Taken together, these results suggest that laminA/C mediated nuclear stiffness inversely regulates the cytoskeletal mediated nuclear plasticity. To summarize, nuclear fluctuations in CI cells are caused by (1) forces arising from actin-myosin-formin units and (2) decreased nuclear plasticity because of laminA/C downregulation. The forces from actin-myosin-formin units are applied directly on the nucleus or via microtubule-dynein links (Figure 3.10).

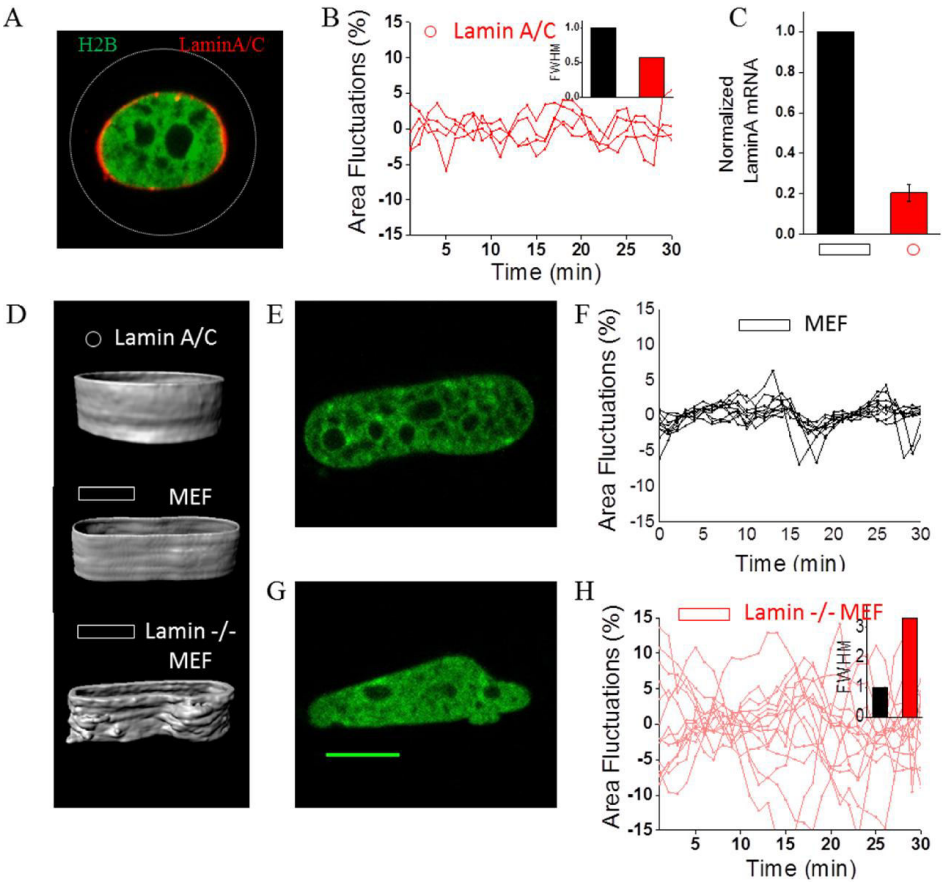

Figure 3.9: Role of LaminA/C in Cell Geometry Mediated Nuclear Plasticity. (A) Widefield epifluorescence image of a typical CI cell co-expressing H2B-EGFP (green) and LaminA/C-mRFP (red). **(B)** PNAF vs time plot for multiple laminA/C overexpressing CI cells (n = 4). Inset represents the FWHM of Gaussian fitting of histograms of combined PNAFs for all cells. **(C)** mRNA levels obtained by qRT-PCR for CI cells normalized with respect to LP cells (n=3 samples). **(D)** Surface rendering of a nuclear periphery kymograph for typical LaminA/C overexpressing CI cell, control MEF cell and Lamin$^{-/-}$ MEF cell. **(E)** Widefield epifluorescence image of a typical MEF cell expressing H2B-EGFP. **(F)** PNAF vs time plot for multiple MEF cells cultured on LP patterns (n = 10). **(G)** Widefield epifluorescence image of a typical lamin$^{-/-}$ MEF cell expressing H2B-EGFP. **(H)** PNAF vs time plot for multiple lamin$^{-/-}$ MEF cells cultured on LP patterns (n = 15). Inset represents the FWHM of Gaussian fitting of histograms of combined PNAFs for all MEFs and lamin$^{-/-}$ MEFS.

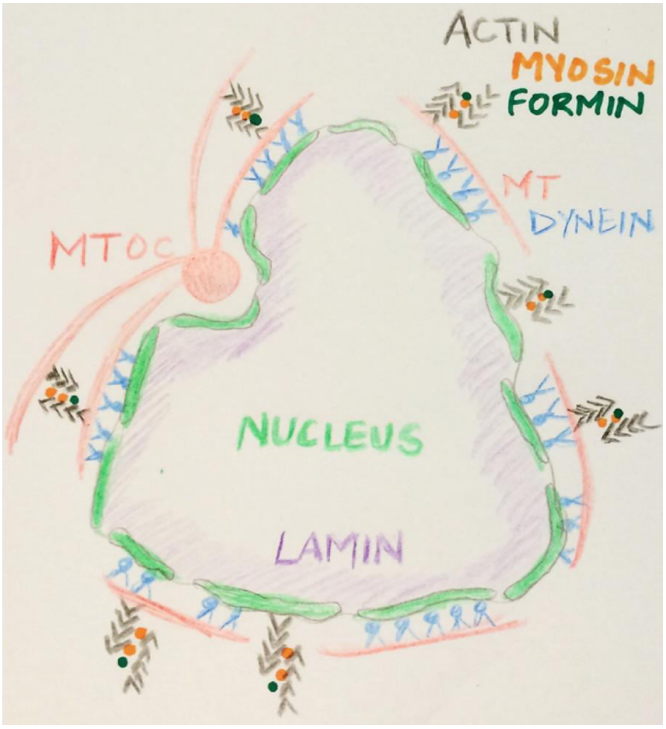

Figure 3.10: Model for Cytoskeletal and Nucleoskeletal Regulation of Nuclear Plasticity. A cartoon showing the nucleus in a CI cell (or cytochalasin-D treated LP cell). The MTOC presses and forms indent on the nucleus. LaminA/C expression levels are lower. Actin-myosin-formin units apply force on the nucleus either directly or via microtubule and dynein links.

3.5 Plastic Nuclei have Increased Chromatin Dynamics. To understand whether PNAF have an effect on chromatin dynamics, we measured chromatin dynamics in LP and CI cells using anisotropy PCC (Figure 3.11A. See Chapter 4 for details on the FAI technique for quantifying chromatin dynamics). We observed higher drop and drop rate in CI cells (Figure 3.11B), which implies a faster chromatin dynamics. The chromatin dynamics in LP cells were observed to increase upon actin depolymerization using latrunculin-A (Figure 3.12A-C) while the dynamics of CI cells was observed to decrease upon actin stabilization with jasplakinolide (Figure 3.12D-F).

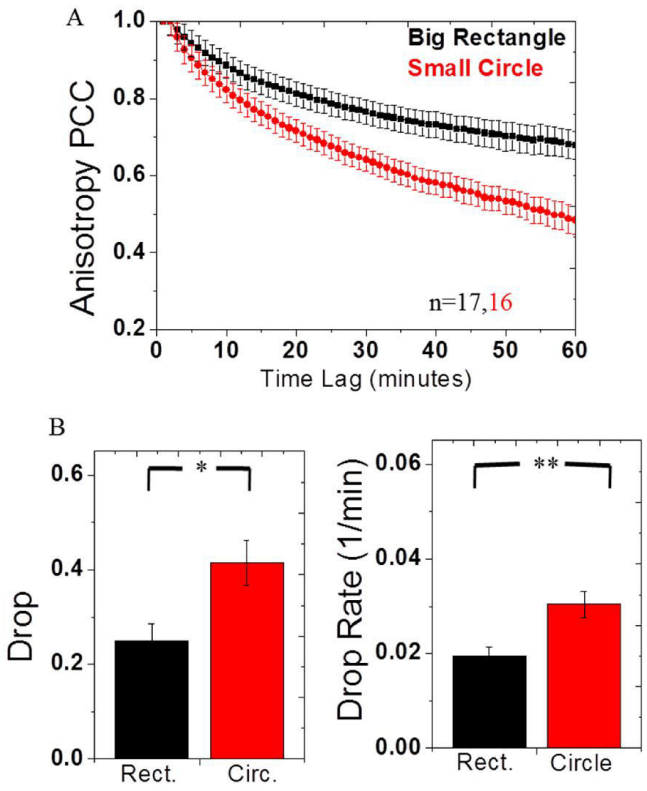

Figure 3.11: Effect of Cell Geometry on Chromatin Dynamics. (A) Comparison of anisotropy PCC curves for LP and CI cells. **(B)** Drop and drop rates for the two curves. Error bars show standard error.

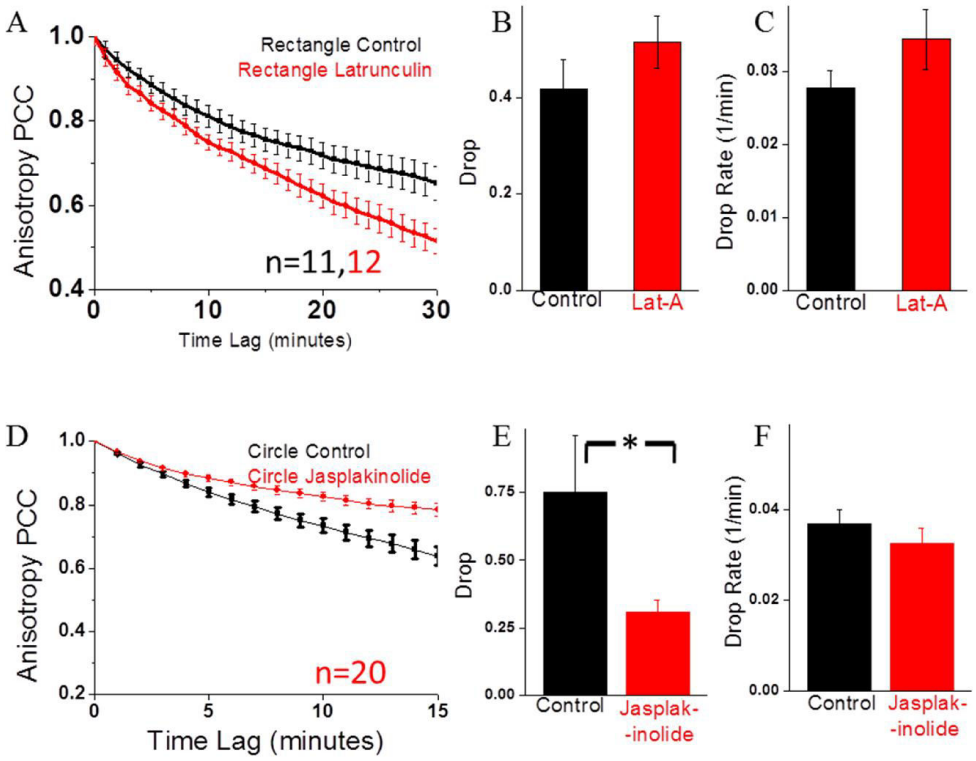

Figure 3.12: Role of Actin Polymerization in Chromatin Dynamics. (A) Comparison of anisotropy PCC vs time curves for control and latrunculin-A treated LP cells. **(B,C)** Drop and drop rates for the two curves. **(D)** Comparison of anisotropy PCC vs time curves for control and jasplakinolide treated CI cells. **(E,F)** Drop and drop rates for the two curves.

To study the local changes in chromatin dynamics, we followed the trajectories of heterochromatin foci, visible as bright spots in H2B-EGFP labelled nuclei (Figure 3.13A). To achieve this, line kymographs spanning the nucleus were plotted for z-projected time series of cells on CI and LP micropatterns. These kymographs showed an increase in heterochromatin dynamics in CI compared to LP cells (Figure 3.13A). Such dynamics in CI cells were abolished by blebbistatin treatment. In contrast, heterochromatin foci became more dynamic in LP cells following cytochalasin-D treatment. Typical XY trajectories of heterochromatin foci in CI (control and blebbistatin treated) and LP (control and cytochalasin-D treated) cells also followed a

similar dynamic behavior (Figure 3.13B). Mean squared displacement vs time curves suggest that while the foci are usually confined in LP cells, they become more diffusive in CI cells (Figure 3.13C).

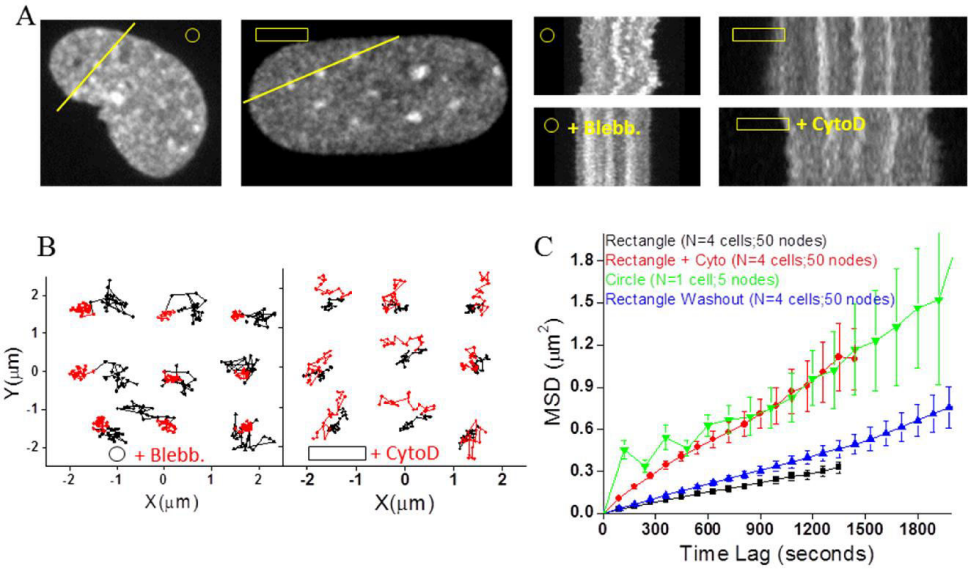

Figure 3.13: Effect of Cell Geometry Mediated Actomyosin Forces on Chromatin Dynamics. (A) Line kymographs across H2B-EGFP labelled nucleus in typical CI, CI+blebbistatin, LP and LP+cytochalasin-D cells. Bright spots represent heterochromatin foci. **(B)** XY trajectories of heterochromatin foci in typical CI, CI+blebbistatin, LP and LP+cytochalasin-D cells. **(C)** MSD vs time plots for CI, LP, LP+cytochalasin-D and washout LP cells.

We then sought to answer whether the correlation between heterochromatin foci trajectories changes as a function of PNAF. For this, 3D trajectories of individual foci were obtained using Imaris and their pairwise vector Pearson correlation coefficient was calculated (see *Experimental Procedure*, Figure 3.14A,B). In a typical CI cell, most pairs of foci trajectories were uncorrelated (Figure 3.14C,D). On the other hand, in a typical LP cell, the foci trajectories were highly correlated (Figure 3.14E-H). Additionally, the foci pairs in LP cells could be distinguished into two groups, based on their z-position. The foci in the apical region were correlated with other foci in apical region, while

those in the basal region were correlated with other foci in basal region, but apical and basal foci were uncorrelated with each other. Interestingly, the foci trajectory correlations increased drastically in CI cells following blebbistatin treatment (Figure 3.14D) while they were reduced for most foci pairs in LP cells upon cytochalasin-D treatment (Figure 3.14F,H). These results suggest that active cytoskeletal forces modulate correlated dynamics of chromatin domains.

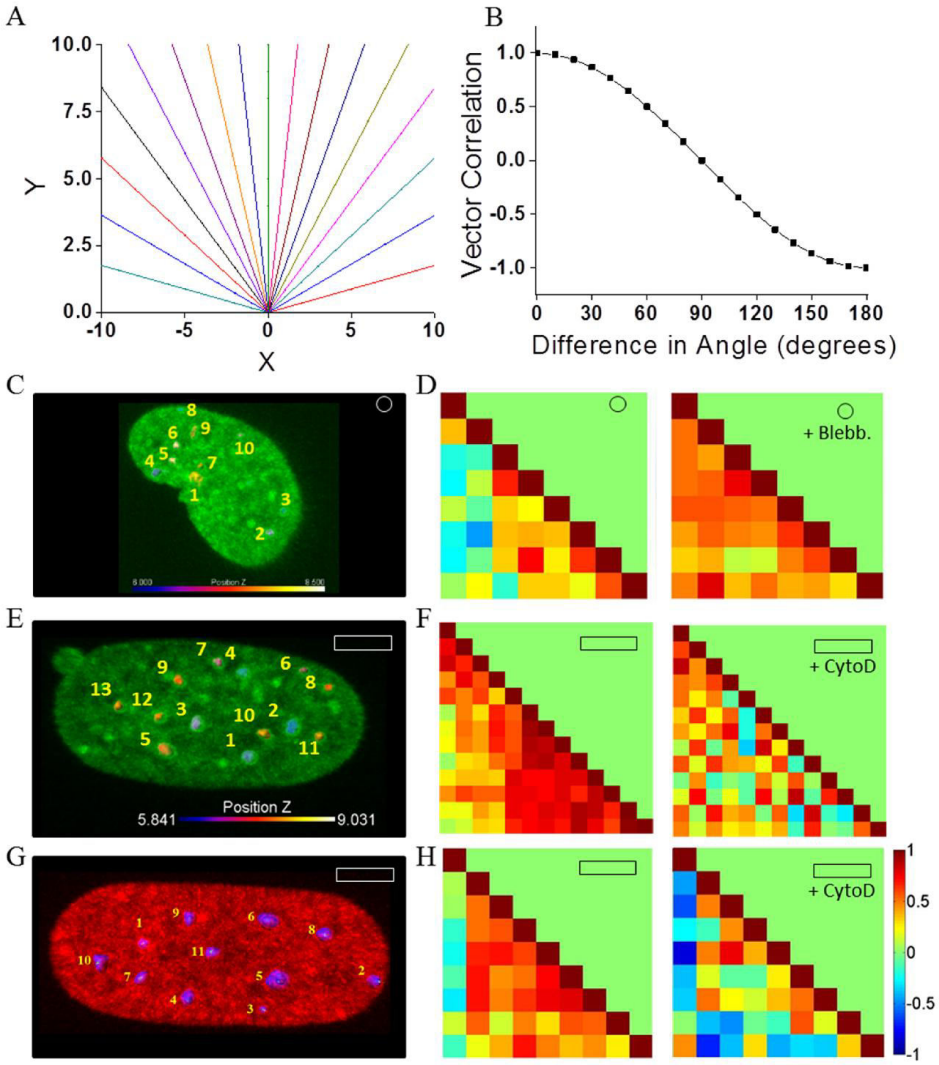

Figure 3.14: Effect of Cell Geometry Mediated Actomyosin Forces on Correlation Between Heterochromatin Foci. (A) Simulated XY tracks at angles varying from 0 to 180 degrees in 10 degree intervals. **(B)** Vector Pearson correlation coefficient calculated as a function of difference in angle between the simulated

tracks. **(C,E,G)** Maximum intensity z-projected images of H2B-EGFP nucleus in typical CI (C) and LP cells (E,G). Heterochromatin foci have been numbered and color-coded based on their z-position (in C,E). Blue color represents basal plane and yellow color represents apical plane. **(D,F,H)** Pearson correlation coefficient calculated between 3D trajectories of all heterochromatin foci pairs labelled in (C,E,G) in control and blebbistatin / cytochalasin-D perturbed conditions.

To understand whether such cytoskeletal mediated chromatin perturbation was reversible, LP cells treated with cytochalasin-D for 30 minutes were washed and time lapse imaging was performed using the same cells. Surprisingly, the spatial map of the chromatin images, which was altered upon cytochalasin-D treatment, was fully restored after the agent was washed off (Figure 3.15A). Photobleached regions in the nucleus were also restored after the drug was washed off in LP cells while in CI cells the bleach patterns were lost even before the drug treatment (Figure 3.15A). The correlation between H2B-EGFP intensity histograms (Figure 3.15B) and fluorescence anisotropy histograms (Figure 3.15C) of drug-perturbed and washed nuclei with control nuclei, revealed that an hour after the drug was washed off, the nuclei had almost returned to their initial configuration. Typical PNAF time traces (Figure 3.15D) and nuclear periphery kymographs (Figure 3.15E) also revealed loss of fluctuations after cytochalasin-D was washed off. Additionally, the pairwise foci trajectory correlations were completely restored an hour after the drug was washed off and apical and basal groupings similar to control nuclei was established (Figure 3.15F). The XYZ trajectories of some heterochromatin foci during the nuclear deformation phase immediately upon cytochalasin-D treatment also overlapped with their trajectory during the restoration phase immediately following the washout (Figure 3.15G). These results indicate the reversible nature of cytoskeletal mediated chromatin plasticity.

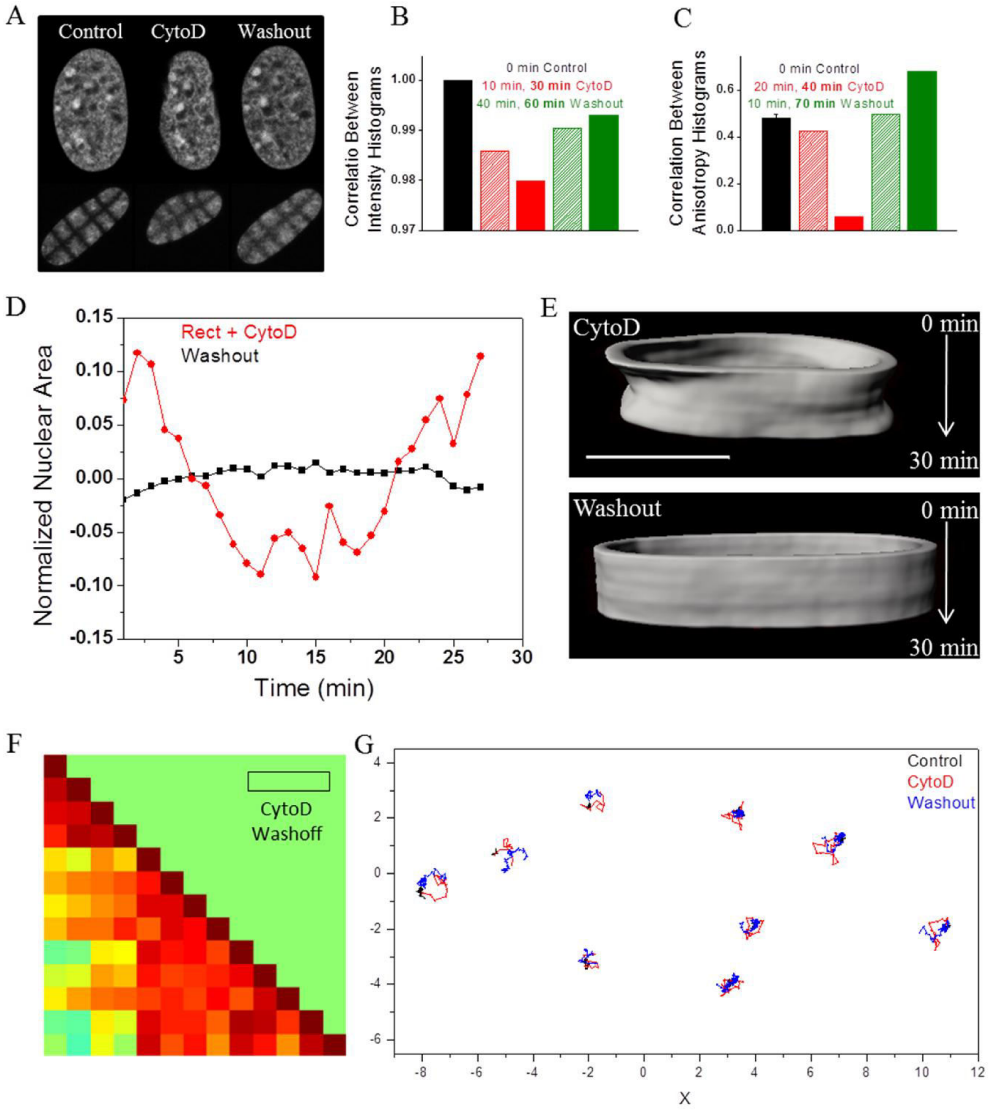

Figure 3.15: Reversible Nature of Actomyosin Mediated Nuclear and Chromatin Plasticity. (A) Widefield epifluorescence images of H2B-EGFP nucleus in typical LP cell in untreated, cytochalasin-D and washoff conditions. Dark lines in the lower panel represent photobleached regions. **(B)** Pearson correlation coefficient for H2B-EGFP intensity histograms in control, cytochalasin-D treated and washoff conditions. **(C)** Pearson correlation coefficient for H2B-EGFP fluorescence anisotropy histograms in control, cytochalasin-D treated and washoff conditions. **(D)** Typical PNAF trace for a LP cell treated with cytochalasin-D and after washout. **(E)** Surface rendering of nuclear periphery kymographs for typical cytochalasin-D treated and washed off LP cells. Scale Bar 10 µm. **(F)** Pearson correlation coefficient calculated between 3D trajectories of same heterochromatin foci pairs (as in Figure 11C) upon washoff of cytochalaisn-D. **(G)** XY trajectories of heterochromatin foci in a typical LP cell in control (black), cytochalasin-D (red) and wash off (blue) conditions.

DISCUSSION

A critical step in the alteration of genome function is the regulation of nuclear and chromatin plasticity, which can result from matrix remodeling. Cells possess an elaborate network of filamentous proteins that bridge the extracellular matrix with the nucleus. These include actin filaments, microtubules and intermediate filaments. In this paper, we have described an unusual non-monotonic dependence of actomyosin contractility in the regulation of nuclear dynamics. By altering cell geometric constraints and introducing pharmacological reagents, both actomyosin contractility and microtubule organization could be modulated to investigate this phenomenon. The non-monotonic dependence of nuclear fluctuations on actomyosin contractility supports recent findings that indicated the presence of small actin networks sequestering myosin and formin [113] and directly shows that these dynamic clusters, which were also visualized in our experiments (Figure 3.6), are the key intermediates in the mechanotransduction pathway driving nuclear dynamics. In order to assess whether forces generated by actomyosin contractility were applied directly on the nucleus, we overexpressed a dominant negative KASH plasmid of nesprin2, since nesprin2 is known to link actin to the nuclear envelope via its KASH domain. However, nesprin perturbed cells on CI pattern did not show significant change in PNAF compared to control CI cells. Since major changes in microtubule organization were observed when cell geometry was constrained, we induced microtubule depolymerization to assess whether these filaments were involved in the mechanotransduction of force to the nucleus. However, depolymerization of microtubules did not abolish nuclear plasticity, suggesting that the small actin

networks were exerting forces on the nucleus directly. Since the actin cytoskeleton is physically linked to the lamin meshwork via the LINC complex, we tested whether nuclear stiffness was modulated by altered cell geometry and whether this enhanced the nuclear dynamics. Surprisingly, we found that laminA/C was down-regulated as matrix constraints were reduced. This finding prompted us to transiently transfect cells with laminA/C. Indeed, overexpression of laminA/C abolished the nuclear fluctuations and this was in contrast to laminA/C knockdown, which increased nuclear fluctuations. Taken together, these experiments highlighted an important transcription dependent mechanoregulatory pathway involving actomyosin contractility that couples matrix properties to nuclear dynamics.

Next, we wanted to test whether the dynamics of chromatin remodeling were affected by the enhanced nuclear plasticity. Heterochromatin structures have been shown to be stabilized in cells that are strongly adhered to the extracellular matrix [114]. We hypothesized that a reduction in the number of physical links to the extracellular matrix may disrupt heterochromatin integrity, thus making chromatin more permissive. Consistent with this, heterochromatin dynamics increased and correlation between heterochromatin foci trajectories decreased in cells on CI geometry, suggesting that an elaborate structural network may be modulated by changes in actomyosin contractility. The dynamic correlations of heterochromatin in cells of elongated polarized geometry were position dependent. Here, the apical and basal foci were highly correlated with other apical and basal foci respectively. Interestingly, the pharmacological inhibitor washout experiments revealed that dynamic correlation in heterochromatin organization and its apical-basal

grouping, which was reduced upon actin depolymerization, was restored after the actin depolymerizing agent was washed out. This suggests that a 'structural memory' in the spatial organization of heterochromatin exists, and highlights the importance of mechanical homeostatic balance for higher order chromatin organization in living cells. In conclusion, our data systematically reveals an important link between cytoskeletal components and nuclear and chromatin dynamics. We suggest that mechanical changes within the extracellular matrix tune the epigenetic states of chromatin plasticity via actomyosin contractility to regulate cellular functions including transcription, genome integrity, migration and cellular homeostasis.

PUBLICATION FROM THIS WORK

- ***Nuclear Plasticity and Telomere Dynamics are Regulated by Extracellular Matrix Constraints***
  Ekta Makhija, D. S. Jokhun and G. V. Shivashankar
  (Under Review in PNAS)

CHAPTER 4: CELL GEOMETRIC CONSTRAINTS MODULATE CHROMATIN COMPACTION STATES

INTRODUCTION

Chromatin of eukaryotic cells is packaged in the nucleus with the help of various histone and non-histone proteins to create heterogeneously compacted regions, which provides spatial regulation of gene expression[80, 115]. The relative chromatin packaging provides an insight into the state of the nucleus i.e. its transcriptional activity[116], the phase of cell cycle[117, 118] and lineage commitment[72]. The chromatin organization in interphase cells has been shown to be dynamic, thus facilitating temporal regulation of gene expression[119-121]. This dynamics is regulated by various processes; binding/unbinding of core and linker histones, turnover of histone tail modifications, interaction with chromatin remodelling complexes and Brownian motion of chromosomes[122]. These different processes contribute to chromatin remodelling at different length and time scales; from few milliseconds for nucleosomal arrays[123], seconds for heterochromatin binding proteins[124, 125], minutes for linker histones[126] and RNA Polymerase II[127], to hours for core histones[128] and lamin proteins[129].

Various imaging techniques have been used to study chromatin structure and dynamics[130]. The most commonly used techniques are electron microscopy[131], immunostaining of various chromatin binding proteins and fluorescent labelling of the DNA in fixed cells. While these methods account for the chromatin compaction state, they lack information about its dynamics. In such fixed samples, biochemical methods like chromosome conformation capture and its variants have also been used to generate 3D maps of intergenomic distances[129]. Confocal microscopy combined with FRAP to

measure translational diffusion[43, 132] of fluorescently tagged proteins is commonly used to study chromatin dynamics. Further, the higher order packaging of chromatin has also been studied using Forster resonance energy transfer (FRET) [133, 134]. However, techniques to measure the local DNA compaction as well as spatial heterogeneities and dynamics associated with packaging chromatin in living cells are limited.

In this work, we first developed a technique to measure chromatin dynamics using FAI and applied it to study the effect of cell geometry on dynamics of chromatin compaction. FAI is based on the principle that when a fluorescent sample is excited with a linearly polarized light, the depolarization of the emission is proportional to the rotational mobility of the fluorophor molecules (Figure 4.1A). The effect of rotational diffusion of fluorophores on anisotropy *r*, is given by Perrin equation,

$\frac{r_0}{r} = 1 + \frac{\tau}{\theta}$,

where r_0 is the fundamental anisotropy of randomly oriented fluorophores in fixed configuration, τ is the fluorescence life time and θ is the rotational correlation time [135]. Fluorescence anisotropy (r) is calculated as

$$r = \frac{I_{II} - I_{\perp}}{I_{II} + 2I_{\perp}},$$

which is a measure of the emission depolarization owing to the rotational diffusion of the fluorophore (Figure 4.1A).Previous work from our lab has shown that FAI of core histones tagged to EGFP (H2B-EGFP) represents local chromatin compaction [43, 136-142]. Local chromatin compaction would arise from strong DNA-nucleosome interactions and tight packaging of

nucleosomes, both of which would decrease the rotational mobility of core histones. Thus, a higher anisotropy value (lower depolarization) would represent tightly packed chromatin and vice versa. Further in this chapter, we describe a quantitative analysis of FAI to explore the dynamics of chromatin compaction upon application of geometric constraints. We also extended the FAI technique for visualizing the binding of the transcription cofacmetry.tor MKLas a function of cell geometry.

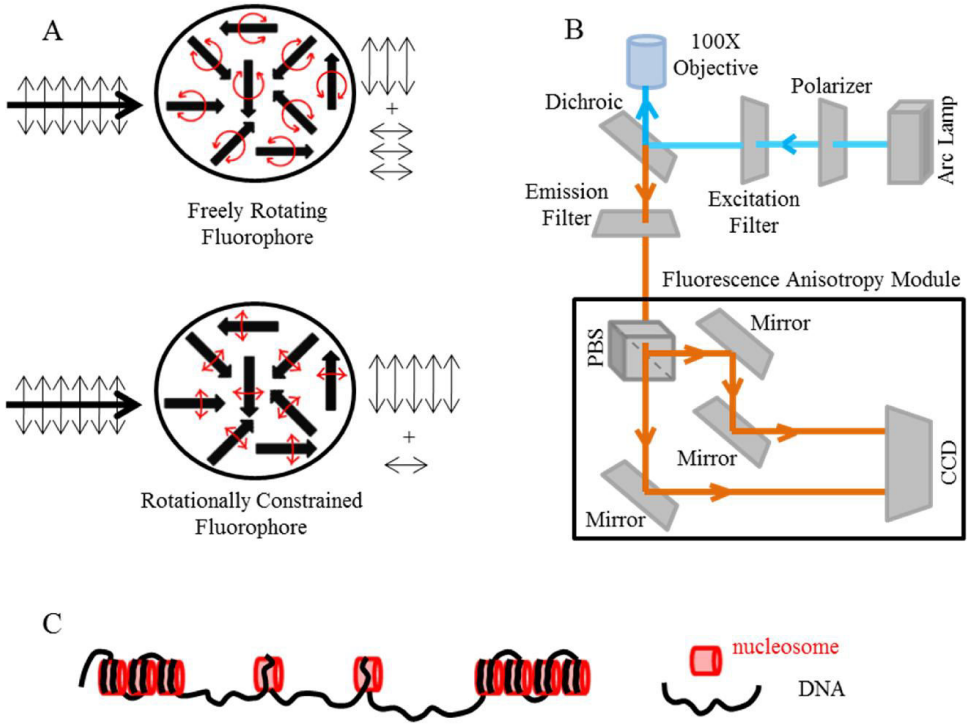

Figure 4.1: Principle of Fluorescence Anisotropy. (A) A cartoon summarizing the principle of fluorescence anisotropy. When linearly polarized light is incident on a fluorescent sample, the depolarization of the emission is proportional to the rotational mobility of the fluorophores. **(B)** Schematic of the experimental setup for fluorescence anisotropy. **(C)** A cartoon suggesting how chromatin compaction can regulate rotational mobility of histones.

MATERIALS AND METHODS

Cell culture: Stable transfections were carried out in NIH3T3 cells with H2B-EGFP plasmid. ES cells and PMEFs were obtained from H2B-EGFP transgenic mice. NIH3T3 and PMEF cells were cultured in DMEM

supplemented with 10% fetal bovine serum and 1% penicillin-streptomycin. ES cells were cultured in K/O DMEM supplemented with 15% knockout fetal bovine serum, 1mM sodium pyruvate (Sigma), 0.1 mM nonessential amino acids, 2mM L-Glutamine, 0.1 mM β-mercaptoethanol (Sigma) and 500 U/ml leukemia inhibitory factor (LIF) (Chemicon) and penicillin-streptomycin. All cell culture reagents were from GIBCO Invitrogen unless mentioned otherwise.

Fluorescence Anisotropy Imaging (FAI): Fluorescence anisotropy images were generated from intensity images acquired in parallel and perpendicular polarization on an inverted microscope (NikonA1R, 100X, 1.4NA objective). Linearly polarized light was generated by passing the arc lamp beam through a sheet polarizer. Excitation and emission filters corresponding to GFP were used. The emission was split into parallel and perpendicular polarizations and acquired on two halves of an Andor camera. Time lapse images were captured using NIS Elements software (Nikon). Schematic of the setup is shown in Figure 4.1B. A custom written program in MATLAB was used to compute anisotropy from the split image on a pixel by pixel basis after performing background subtraction and 3×3 smoothing of the original image. For each pixel, anisotropy was calculated as $r = \frac{I_{II} - g*I_{\perp}}{I_{II} + 2g*I_{\perp}}$, where g (g-factor) is the ratio of the sensitivity of the experimental setup for parallel and perpendicular channels [26]. To calculate the g-factor, anisotropy of fluorescein isothiocyanate (FITC) solution in water (r=0.02) was used in the above formula.

Image Analysis: The parallel and perpendicular images were aligned for translational and rotational shifts between the two channels using MATLAB.

The perpendicular emission intensity image was translated by Δx and Δy upto ± 5 pixels and rotated by $\Delta\theta$ upto ± 5 degrees. Correlation was calculated in each case with the parallel image. The Δx, Δy and $\Delta\theta$ values which gave maximum correlation were used to translate the original perpendicular images to obtain best alignment. The complete temporal sequence was corrected for any translation and rotation with respect to the first time frame. PCC was calculated using the "corr" function in MATLAB and then averaged over all image frames with time lag ranging from 1 min to 30 min. Before calculating the PCC between anisotropy images a 5 pixel border was removed from the nucleus periphery to avoid the artifacts that may arise from edge effects.

Preparation of PDMS stamps, Microcontact printing and Cell seeding on patterns: To make stamps, PDMS (Sylgard 184, Dow Corning) precursor and curing agent were mixed homogeneously in 10:1 ratio and poured over the silicon wafer which had 1800 μm^2 triangle and circular micropatterned wells. After degassing in the desiccator for 30 minutes to remove air bubbles from the PDMS mixture, the silicon wafer with the PDMS mixture was cured in the oven at 80°C for 2 hours. Solidified PDMS was then peeled from the wafer and cut into ~ 1cm by 1cm stamps. These stamps were oxidized using plasma for 4 minutes and then 15ul of 100 ug/ml fibronectin solution (mixed with Alexa Fluor 647 dye, Sigma) was poured over each stamp. Extra solution was wiped with a tissue and the stamp was allowed to dry for 10 minutes. The stamp was then checked under the microscope for complete drying between the micropatterned structures, after which it was inverted carefully onto the surface of an uncoated hydrophobic 35 mm dish (Ibidi). The stamp was gently removed after 2 minutes and the stamping on the dish was checked by

visualizing Alexa 647 fluorescence in the far-red channel in the epifluorescence microscope. To passivate the non-patterned surface of the dish, it was then treated with 2 mg/ml pluronic F-127 for 5 minutes, and washed twice with PBS and cell culture medium before seeding 40,000 single cells.

RESULTS

4.1 Core Histone Anisotropy Measures Chromatin Compaction.

Chromatin is known to be organized into highly compact heterochromatin forming distinct nodes and relatively decompact euchromatin regions in fibroblasts. FAI of core histone H2B in PMEFs was characterized as a measure of chromatin compaction by comparing H2B-EGFP intensity at heterochromatin and euchromatin regions (Figure 4.2A). The heterochromatin nodes, observed as the bright regions in the H2B-EGFP intensity image, were observed to correspond to high anisotropy, while euchromatin regions corresponded to lower anisotropy. However, anisotropy is not directly proportional to intensity, as seen in the scatter plot of anisotropy vs intensity (Figure 4.2B). In the next section we developed methods to visualize dynamics of chromatin in live cells.

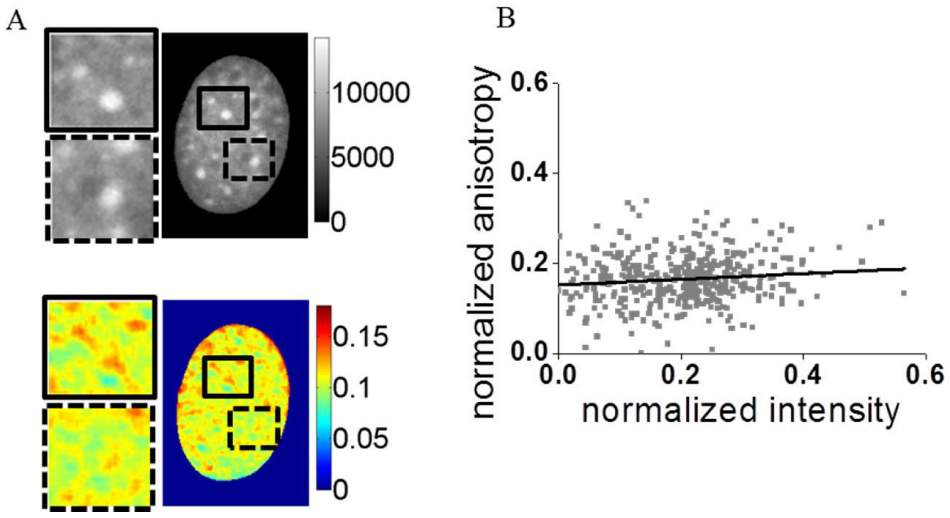

Figure 4.2: Relation between intensity and anisotropy. (A) The grayscale image represents a typical widefield image of nucleus of NIH3T3 cell labelled with H2B-EGFP. Bright spots represent hetereochromatin regions and dark spots represent nucleoli. The colorcoded image in the lower panel is the anisotropy image obtained from custom written code in MATLAB. **(B)** A scatter plot of normalized intensity vs anisotropy for all pixels in the nucleus.

4.2 Time Lapse FAI to Study Chromatin Dynamics. To study the dynamics of chromatin compaction, time lapse FAI of cells expressing H2B-EGFP was carried out. To quantify the temporal change in anisotropy pattern, we first developed a numerical approach for probing image correlation using a simulated image (Figure 4.3A). A series of decorrelated images was generated from this image by exchanging a pair of randomly chosen pixels in each iteration (Figure 4.3A). To quantify the magnitude of decorrelation for this image sequence, PCC of each image with respect to the first image was calculated and plotted as a function of time. It was observed that the PCC curve is sensitive to the rate of change (no. of pixel pairs exchanged per iteration) and addition of random noise (Figure 4.3B). Typical PCC vs time lag plot for an anisotropy image sequence is shown in Figure 4.3C. Such a curve can be fitted with a single exponential decay equation with 3 parameters - noise(η), time constant(τ) and drop(α). The drop in correlation at time lag

t=1, which is a measure of decorrelation between consecutive anisotropy images, was termed as the noise(η). It was observed that the PCC does not drop to zero at long time scales, but stabilizes after some time. This stable PCC value ($PCC_{t=\infty}$) is a measure of the fraction of anisotropy image that remains unchanged. It was used to define the parameter drop(α) = 1 - $PCC_{t=\infty}$ - noise(η). The time constant(τ) is obtained by fitting a single exponential decay equation to the PCC curve after removing the noise(η). τ is a measure of time taken for the anisotropy image to decorrelate to $PCC_{t=\infty}$. Simulated exponential curves with varying η, τ and α are shown in Figure 4.3D-F respectively. In further experiments, the parameter drop rate = α/τ was used to quantify chromatin dynamics.

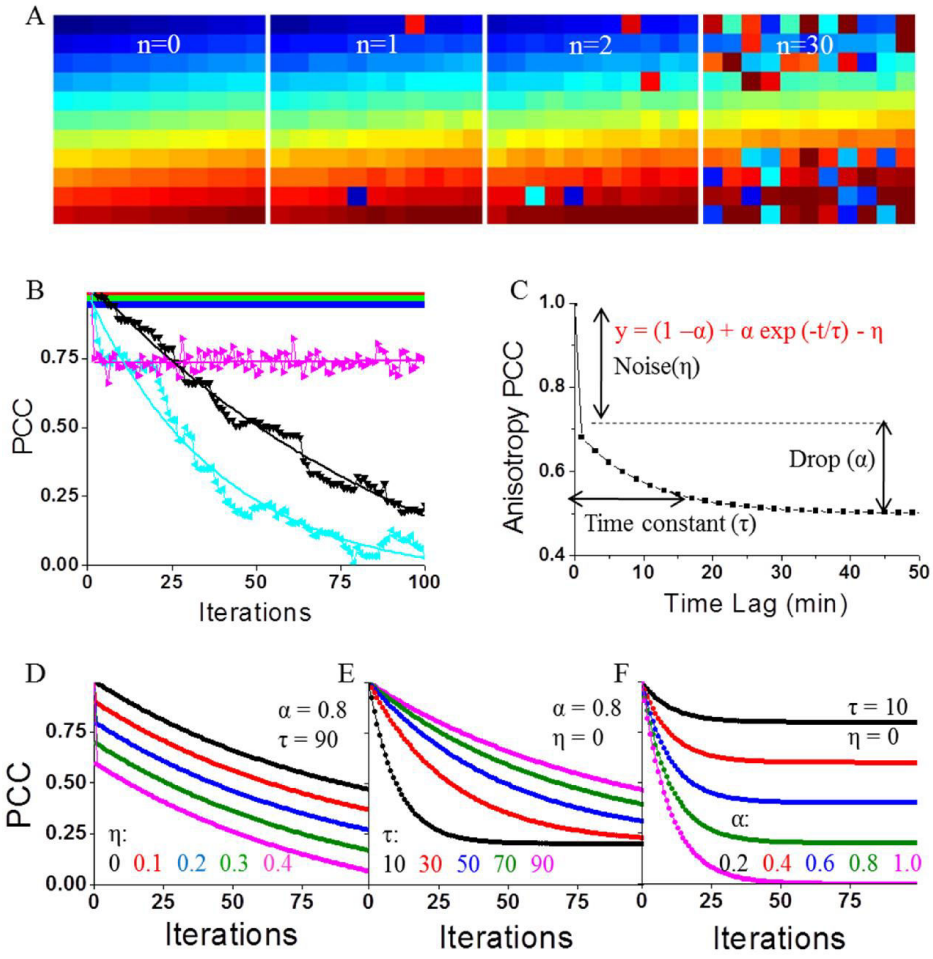

Figure 4.3: Image PCC to measure dynamics. (A) Simulation of dynamics in a 11x11 increasing numbered matrix. Each iteration exchanges a pair of pixels. The pixels in the center three rows are not allowed to be exchanged. **(B)** Pearson correlation coefficient of each iteration image calculated with initial image for the following cases: 1 pair of pixel exchange (black), 2 pairs of pixel exchange (cyan), addition of random noise (magenta), no change (red), multiplication by a constant number (green), subtraction of a constant number (blue). **(C)** PCC vs time curve for a typical H2B-EGFP anisotropy image time series fitted with the equation $y = (1 - \alpha) + \alpha \exp(-t/\tau) - \eta$. **(D-F)** Exponential decay curves with varying noise η (D), time constant τ (E) and drop α (F)

Next, the above parameters were used to understand the PCC curves obtained from anisotropy images of the nucleus at different time points, and compared with those obtained by simulation. Top panel in Figure 4.4A is a time series of a region of 11x11 pixels from nucleus anisotropy image. Using the experimental image at t=0, simulations were carried out either by varying the

number of randomly chosen pairs of pixels to be exchanged or fraction of image accessible for pixel exchange (bottom panel, Figure 4.4A). These simulation parameters affect the time constant (τ) and the drop (α) of the PCC curve, respectively. By comparing the original and simulated PCC curves (Figure 4.4B, black and green curves, respectively), it is estimated that 88% of total area is dynamic with 3% area changing per min.

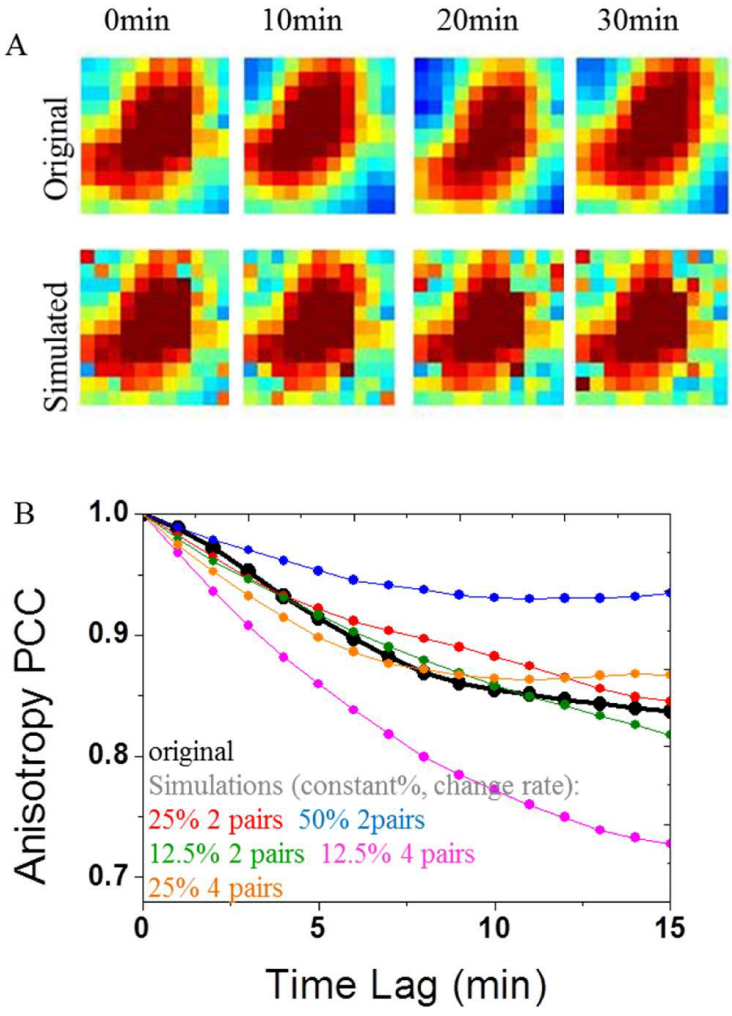

Figure 4.4: Interpretation of anisotropy PCC. (A) Simulation of dynamics in a ROI cropped from H2B-EGFP anisotropy image. **(B)** PCC curves for the actual dynamics of the ROI (black curve) compared with a few simulated dynamics generated by varying the percentage of pixels that remain constant and the rate of change. Comparison with various simulations shows that ~12.5 % pixels remain constant and the rate of change is ~2 pixels per minute.

As a next step in characterizing anisotropy PCC, the exposure time was varied from 100ms to 400ms for time lapse imaging (Figure 4.5A). Anisotropy PCC curves revealed higher noise for shorter exposure times (Figure 4.5B,C). The exposure time was kept constant at 300ms for all further experiments.

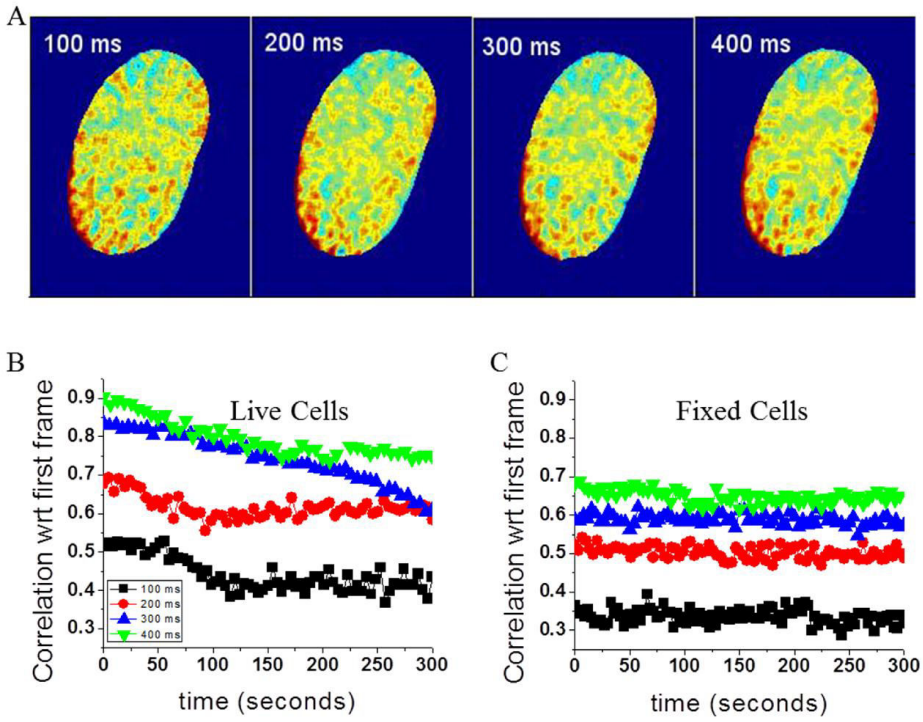

Figure 4.5: Anisotropy PCC depends on imaging conditions. (A) Anisotropy images for a typical H2B-EGFP nucleus captured at different exposure times. **(B,C)** PCC vs time curves for live (B) and fix cell (C) anisotropy images series captured at different exposure times.

To measure the sensitivity of FAI technique, anisotropy PCC curves of PFA fixed cells were compared with that of live cells (Figure 4.6A). As expected, drop rate for fixed cells (0.01) was significantly lower than for live cells (0.04) indicating reduced dynamics in chromatin compaction (Figure 4.6B). It was observed that the intensity PCC curves are much less sensitive than the anisotropy PCC curves (Figure 4.6A) suggesting that FAI captures subtle changes in chromatin dynamics that cannot be observed by intensity profile. In

subsequent sections, we show the utility of anisotropy PCC to probe chromatin remodelling in different functional context.

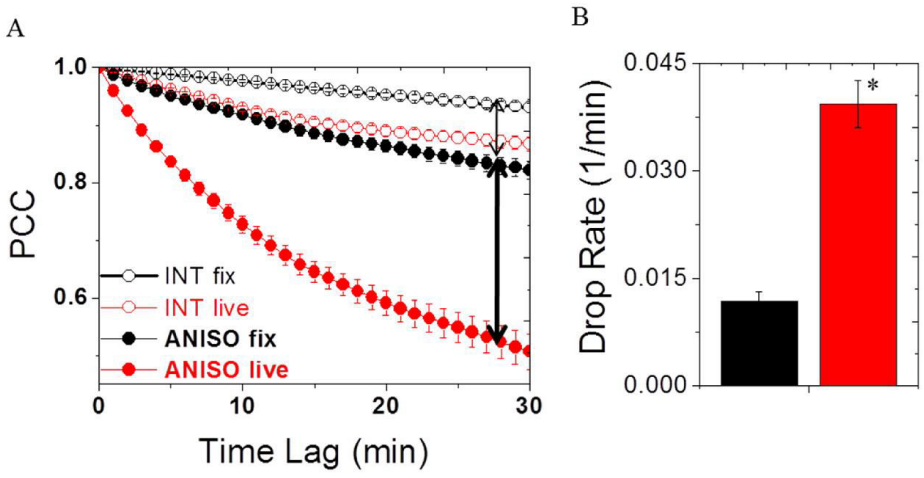

Figure 4.6: Anisotropy PCC measures chromatin dynamics. (A) Intensity and Anisotropy PCC vs time curves for multiple fix and live cells. **(B)** Drop rate (α/τ) obtained by fitting the fix and live anisotropy PCC curves to the equation $y = (1 - \alpha) + \alpha \exp(-t/\tau) - \eta$.

4.3 Time Lapse FAI Reveals Distinct Dynamics between Heterochromatin and Euchromatin Assembly. The local variations in chromatin dynamics were probed in either heterochromatin or euchromatin (21 x 21 pixels) regions (Figure 4.7A) and anisotropy PCC curves were plotted. It was observed that euchromatin regions have significantly higher noise (η=0.5) than heterochromatin (η=0.2, Fig 7B inset1) which implies rapid loss of structural information in loosely packaged euchromatin region. Consistent with this, the drop rate (a measure of the time to reach steady state during polymer relaxation) is slightly higher in euchromatin region (0.035) when compared to heterochromatin (0.025, Figure 4.7B inset2).

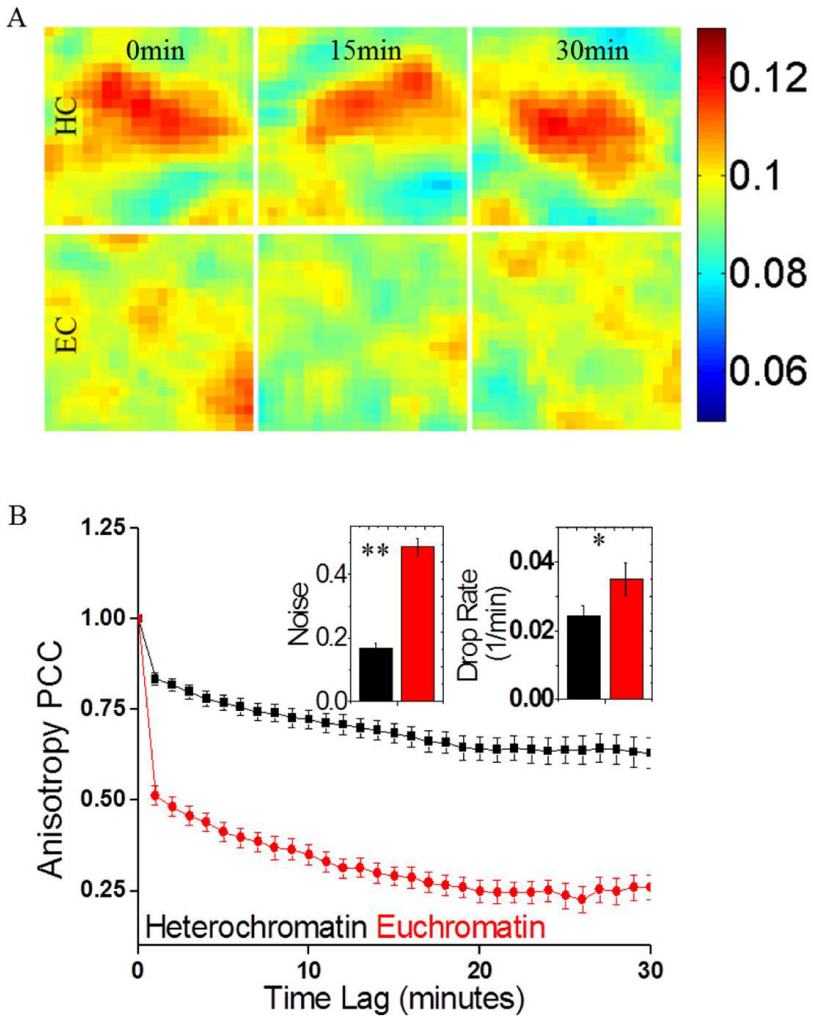

Figure 4.7: Anisotropy PCC shows that euchromatin is more dynamic than heterochromatin. (A) Time lapse images of anisotropy in 3.5x3.5μm^2 ROI in heterochromatin and euchromatin regions. **(B)** Anisotropy PCC vs time curves in heterochromatin and euchromatin regions. Insets show noise (η) and drop rate (α/τ) obtained by fitting these curves to the equation $y = (1 - \alpha) + \alpha \exp(-t/\tau) - \eta$.

4.4 FAI Captures Changes in Chromatin Dynamics in Distinct Cellular Differentiation States. FRAP studies of chromatin binding proteins reveal a hyperdynamic nuclear structure in stem cells [43, 44, 142]. We therefore applied FAI to quantitatively measure the differences in chromatin compaction dynamics between ES and PMEF cells. Time lapse anisotropy images were recorded for 1 hour and anisotropy PCC was plotted (Figure 4.8A,B). Stem

cells exhibit a significantly dynamic chromatin structure (drop rate = 0.12) as compared to PMEFs (drop rate = 0.06) (Figure 4.8B inset). Further, to assess local variations in chromatin dynamics, anisotropy PCC curves were plotted by dividing the nucleus into 11x11 pixel regions and region-wise drop rates were measured (Figure 4.8C). The region with lower drop rate is less dynamic and vice versa as seen in the colour coded images (Figure 4.8C). The region-wise drop rates in ES cells were on an average higher compared to PMEFs, suggesting that chromatin structure in stem cells undergoes rapid conformational changes.

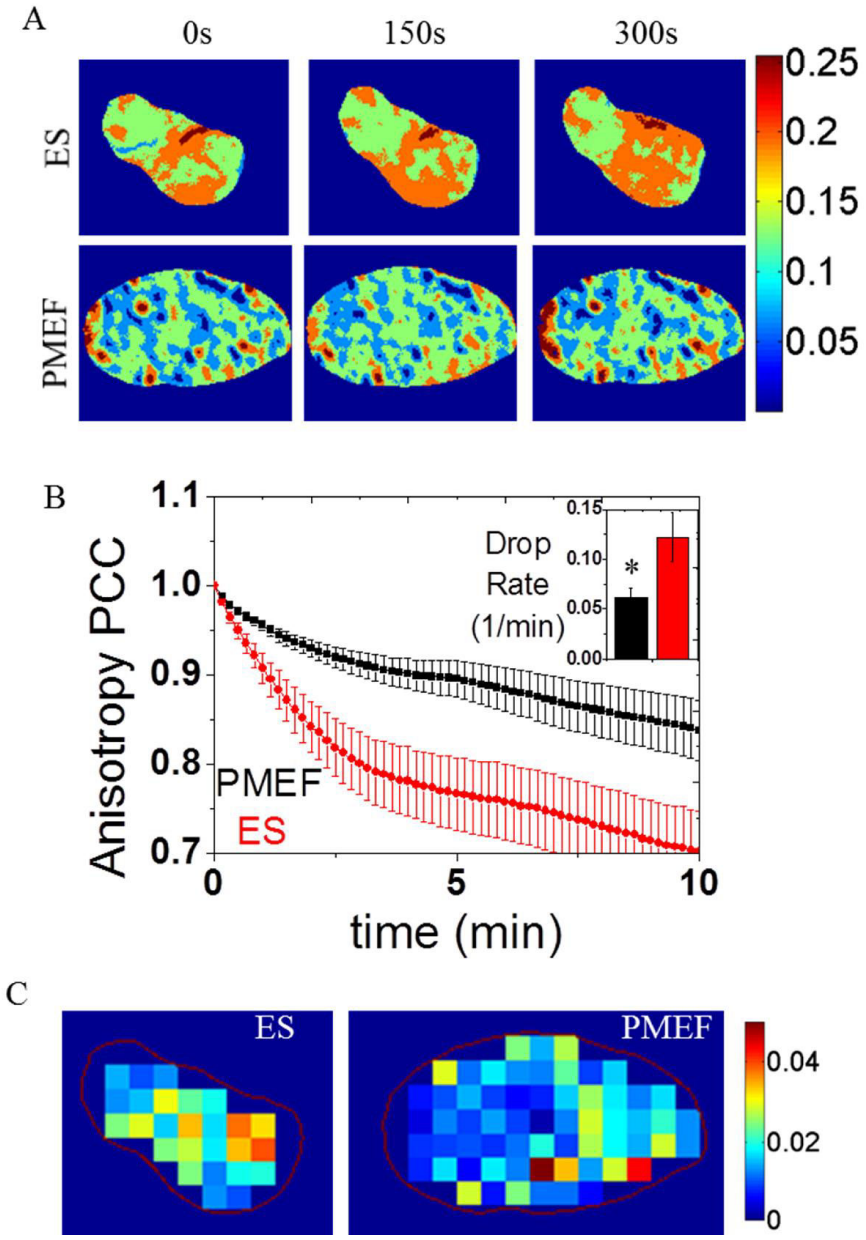

Figure 4.8: Chromatin dynamics of stem cells vs differentiated cells. (A) Typical H2B-EGFP anisotropy images of ES and PMEF cells. **(B)** Comparison of anisotropy PCC curves for ES and PMEF cells. Inset shows the drop rates for the two curves. Error bars show standard error. **(C)** Comparison of local anisotropy drop rates in ES and PMEF cells. Box size is 10 x 10 pixels. *p=0.03

4.5 Cell Geometric Constraints Affect Chromatin Dynamics. Previous reports indicate that the cellular geometry impinges on cytoskeletal and chromatin architecture resulting in altered genetic programs [10]. To quantitatively analyse the change in chromatin dynamics arising due to cell

geometric constraints, we mapped anisotropy PCC curves in cells plated on micropatterned triangle and circle shapes of 1800μm^2 area. Figure 4.9A shows representative image of single cells labelled with actin (lifeact RFP) and H2B-EGFP plated on triangular and circular micropatterns and Figure 4.9B shows time lapse anisotropy images. The anisotropy PCC curves were plotted (Figure 4.9C) and it was observed that the circular cells have a significantly higher drop rate (0.04) than triangular ones (0.02), which implies faster chromatin remodelling (Figure 4.9C inset). Normalized difference images (5min-0min) of anisotropy for the two geometries shows a higher difference in case of circle cells (Figure 4.9D), also confirming the faster chromatin dynamics in cells on circular geometry.

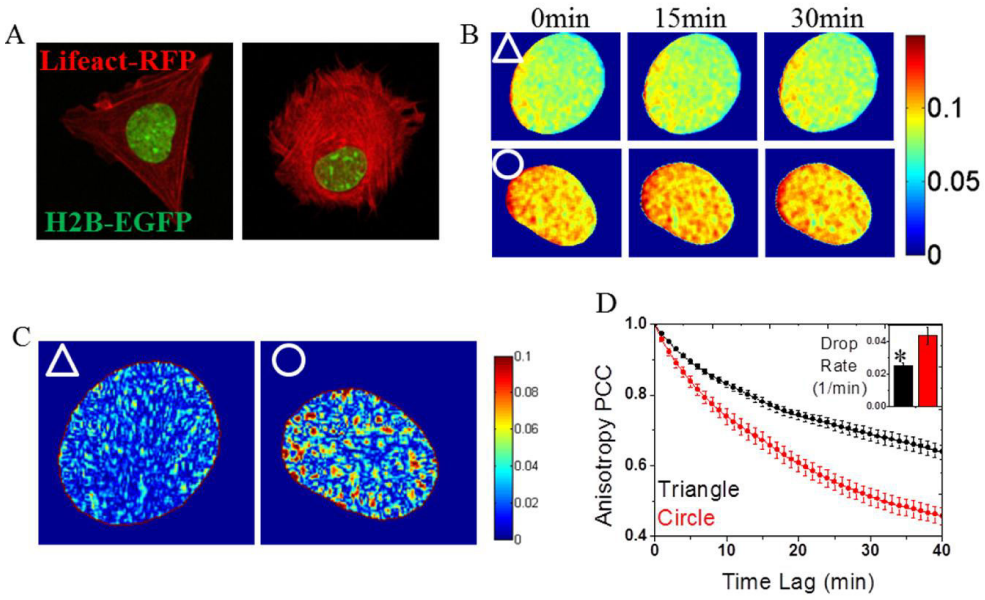

Figure 4.9: Effect of cell shape on chromatin dynamics. (A) Images of NIH3T3 cells stably transfected with H2B-EGFP, transiently transfected with lifeact-RFP and cultured on 1800μm^2 triangular and circular fibronectin micropatterns. **(B)** Typical H2B-EGFP anisotropy image series for triangular and circular cells **(C)** Difference image of anisotropy |5min-0min| for triangular and circular cells **(D)** Comparison of anisotropy PCC curves for triangular and circular cells. Inset shows the drop rates for the two curves. Error bars show standard error. *p=2.4E-4

4.6 Simultaneous Anisotropy of Transcription Cofactor and Core Histone.

Next, we measured simultaneous anisotropy of transcription cofactor MKL and histone H2B to understand the correlation between TF binding and chromatin compaction. MKL is associated with transcription factor serum response factor (SRF) and helps in the co-regulation of serum responsive genes. MKL, which has a nuclear localization signal (NLS) sequence embedded in a G-actin binding site, is localized either in the cytoplasm or in the nucleus, depending on the state of actin polymerization (Figure 4.10A). In serum starved conditions, MKL is sequestered in the cytoplasm and upon stimulation with 15% FBS, it translocates to the nucleus at a time scale of about 10 minutes (Figure 4.10B, C). Similar MKL nuclear translocation occurs when serum starved cells are stimulated with cytochalasin-D (Figure 4.10D, E). In serum starved conditions, cells are in a quiescent state, whereas upon serum stimulation, a large number of genes get transcribed via the SRF-MKL pathway. We measured MKL and H2B anisotropy simultaneously inside the nucleus for cells expressing both MKL-mRFP and H2B-EGFP. Zoom in of the anisotropy maps revealed that regions with high MKL anisotropy correspond to low H2B anisotropy, i.e. MKL binds in regions of decondensed chromatin (Figure 4.11A). Additionally, zoom in at regions with high H2B anisotropy revealed low MKL anisotropy, suggesting lower MKL binding at heterochromatin regions. Scatter plot of normalized MKL anisotropy vs normalized H2B anisotropy for such regions showed a negative slope in the linear fit (Figure 4.11B). Further, we tracked the regions of high MKL anisotropy or high H2B anisotropy in cells of two extreme geometries: LP and CI. We observed that MKL binding foci are more dynamic in LP cells than CI

cells (Figure 4.12), possibly suggesting higher transcriptional activity at MKL bound regions in LP cells. This is in confirmation with previous work that shows higher MKL activity in polarized cells [12]. The dynamics of high H2B anisotropy foci, on the other hand, was lower in LP cells (Figure 4.12), which supports our observation that chromatin dynamics is lower in polarized cells, compared to CI cells. Further detailed studies on the effect of cell geometry on chromatin dynamics is done in the next project.

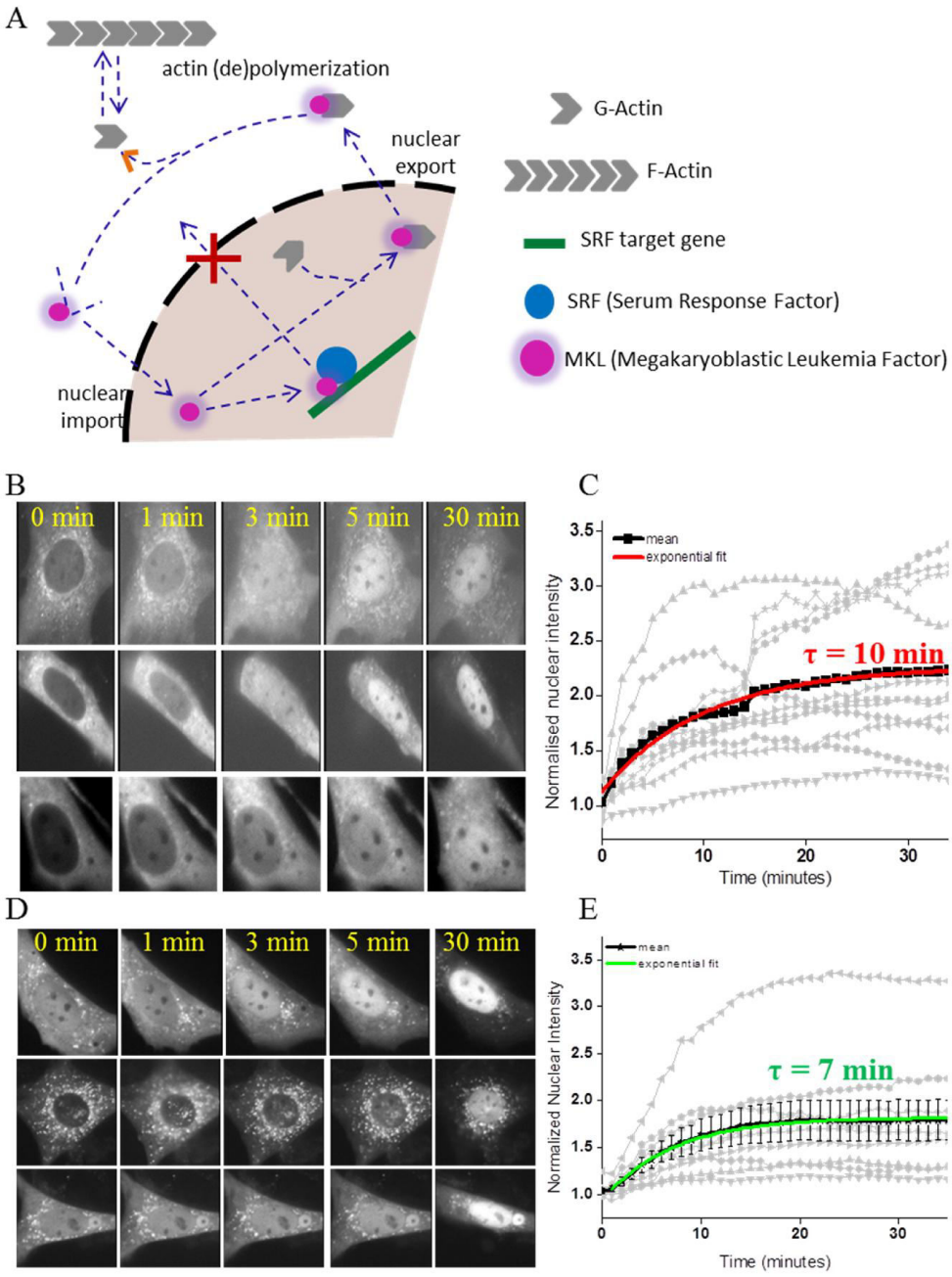

Figure 4.10: MKL translocation to the nucleus. (A) A cartoon summarizing the MKL-SRF pathway. MKL shuttles to the nucleus upon serum or cyto-D stimultion. **(B,D)** MKL-mRFP image time series upon serum (B) and cyto-D (D) stimulation. Serum/Cyto-D added at time 0 min. Image at 0 min corresponds to 24h serum starvation. **(C,E)** Normalized nuclear MKL intensity as a function of time. Bold curve represent the mean curve fitted with exponential function.

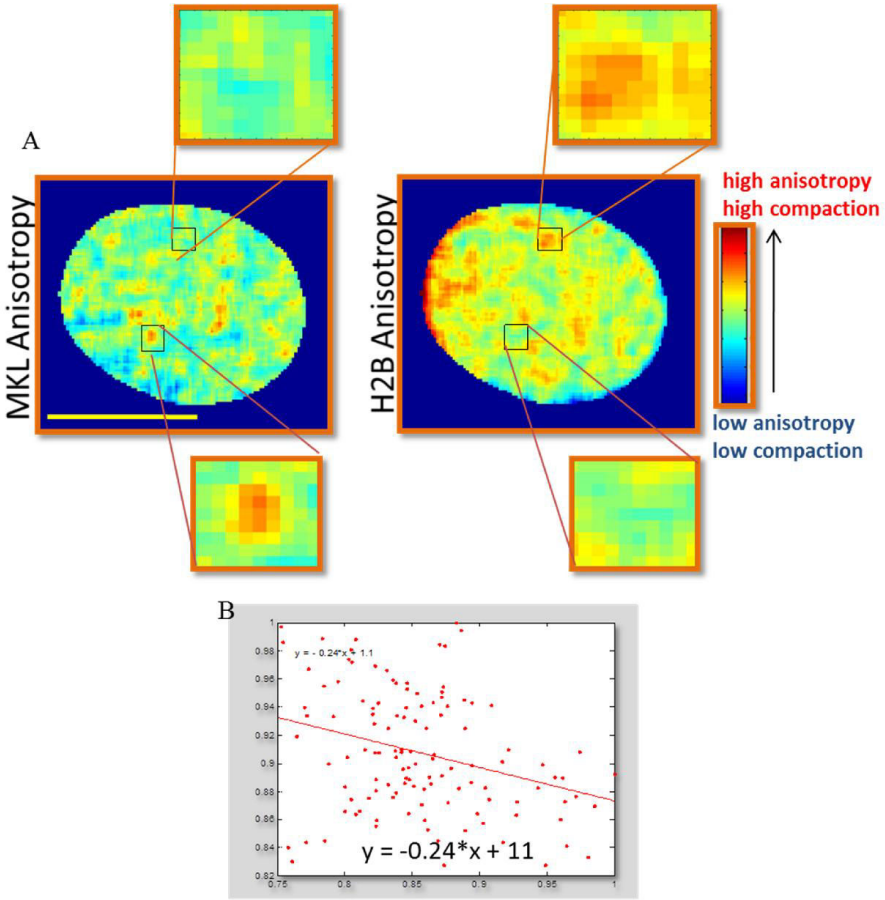

Figure 4.11: Relation between MKL binding and chromatin compaction. (A) MKL-mRFP and H2B-EGFP anisotropy images for the same nucleus. Upper zoomed region corresponds to compact chromatin while lower region corresponds to MKL binding. **(B)** Scatter plot for MKL vs H2B anisotropy in regions corresponding to high MKL anisotropy (MKL binding).

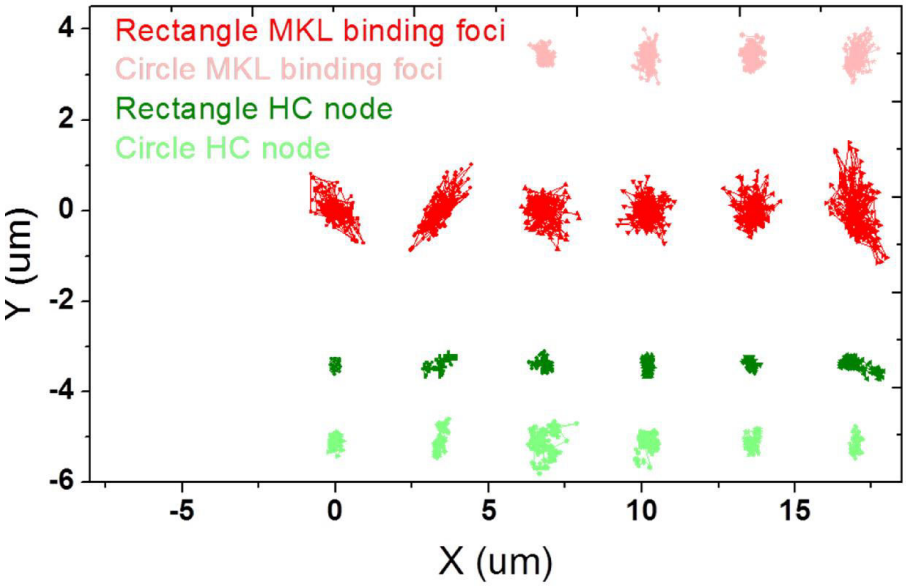

Figure 4.12: Effect of cell geometry on dynamics of MKL binding foci. XY trajectories of MKL binding foci (high MKL anisotropy punctae) and heterochromatin foci (high H2B anisotropy punctae) in LP and CI cells.

DISCUSSION

In this chapter we have established FAI as a method to measure differential chromatin compaction in living cells. The compaction maps obtained by FAI were correlated with heterochromatin and euchromatin regions visualized by intensity profile. Using PCC curves derived from time lapse FAI, we demonstrated the dependence of rate and extent of chromatin remodelling on the structural variation in packaging. Further, using FAI we quantify changes in chromatin dynamics in distinct cellular geometries or differentiation states. Using simultaneous anisotropy measurement of transcription cofactor MKL and of histone H2B, we observed that MKL binds in regions of decondensed chromatin. MKL binding foci are more dynamic in polarized cells, supporting previous data that suggests higher activity of serum responsive pathway in polarized cells. Taken together, time lapse FAI provides a sensitive measure to

capture subtle chromatin dynamics and transcription factor binding in various cellular functional states.

PUBLICATIONS FROM THIS WORK

- ***Probing Chromatin Structure and Dynamics Using Fluorescence Anisotropy Imaging***
  Ekta Makhija, K. Venkatesan Iyer, Shefali Talwar and G. V. Shivashankar
  Handbook of Imaging in Biological Mechanics (Edited by Corey P. Neu, Guy M. Genin, 10/2014: chapter 31: pages 391-400; CRC Press., ISBN: 9781466588134)

- ***Role of Cell Geometry on Nuclear Mechanics, Chromosome Reorganization, and Gene Expression***
  Yejun Wang*, **Ekta Makhija***, Karthik Damodaran and G. V. Shivashankar
  Molecular and Cellular Mechanobiology (Edited by Shu Chien, Adam Engler, and Peter Wang) (In preparation 2015)
  * Equal Contributors

CHAPTER 5: CONCLUSION AND DISCUSSION

EMS alter nuclear morphology and important nuclear functions like transcription and differentiation. The physical transmission of such signals from focal adhesions to chromatin happens via the mechanical link formed by cytoskeleton, LINC complex proteins and the nuclear lamina. Perturbations of any component in this mechanical link have been shown to affect the physical properties of the nucleus as well as the subsequent transcriptional response of the nucleus. In the ***first project***, we measured the time lag between traction forces at the focal adhesions and nuclear and heterochromatin displacements. To achieve this, fibroblasts were cultured on fibronectin coated micropillar substrates and simultaneous imaging of pillars and nucleus was performed. Pillars at the leading cell periphery exhibited higher displacements than those in the cell interior. Myosin inhibition resulted in decreased pillar displacements, confirming that the pillar displacements at cell periphery in control cells arise from traction forces generated by actomyosin contractility. Autocorrelation analysis of pillar, nucleus and heterochromatin displacements revealed similar decorrelation time scale of ~40 s, which closely matches the time scale of fibroblast cell contraction [46]. Separate cross-correlation analysis of displacements of front and rear edge pillars with the nuclear displacement revealed instantaneous (less than a second) negative and positive correlations respectively, which were abolished upon myosin inhibition. Our results suggest that forces generated at focal adhesions by sensing the local microenvironment are mediated to the nucleus and chromatin by a coordinated contractile transmission via elastic cytoskeletal links.

Previous work in the lab has demonstrated the apical organization of parallel actin stress fibers in cells cultured on LP geometric fibronectin micropatterns,

which press on the nucleus and generate indents on its apical surface. We observed that when these stress fibers move transversely over the nucleus, the heterochromatin nodes also move along with them. To further explore the force transmission from focal adhesions to nucleus and chromatin via the cytoskeletal links, in the ***second project*** we compared the nuclear and chromatin dynamics in cells cultured on fibronectin micropatterns of different geometries; LP and CI. While the LP cells display long actin stress fibers and a flat and elongated nucleus, the CI cells exhibit small filamentous or punctated form of actin and a rounded nucleus. The nucleus in CI cells displays envelope oscillations whose amplitude was measured to be 10% of the normalized projected nuclear area, compared to only 4% fluctuations of LP cell nucleus. Systematic perturbations of actin, myosin and formin in both LP and CI geometries revealed that the enhanced nuclear fluctuations arise from active forces by actin-myosin-formin structures that correspond to intermediate state of actin polymerization. Perturbations of KASH domain and microtubules revealed only slight effect on these fluctuations, while dynein inhibition with ciliobrevin-D significantly decreased PNAFs, suggesting that the active forces from actin-myosin-formin either act directly on the nucleus or via dynein links. Further, laminA/C overexpressing cells cultured on CI patterns did not display enhanced PNAF and laminA/C knockout cells on LP patterns exhibited enhanced PNAF. RT-PCR experiments revealed 80% lower levels of laminA/C expression in CI cells compared to LP cells. These results suggest that nuclear envelope oscillations are regulated by a balance between active cytoskeletal forces and laminA/C conferred nuclear rigidity.

To probe whether the PNAFs also correspond to enhanced chromatin dynamics, we tracked heterochromatin foci which are visible as bright spots in H2B-EGFP images. 3D trajectories of these foci revealed enhanced dynamics in CI cells compared to LP cells. The heterochromatin dynamics were also observed to be similarly regulated by a balance between active cytoskeletal forces and laminA/C expression. Additionally the correlation between trajectories of different heterochromatin nodes in the same nucleus were also associated with nuclear fluctuations, with nodes in LP cells highly correlated compared to CI cells. These results suggest that active cytoskeletal forces could possibly regulate the spatial organization and interaction of certain chromosome domains via nuclear envelope fluctuations.

In the ***third project***, we aimed to probe chromatin dynamics at a resolution higher than just 3D tracking of heterochromatin foci. For this, we generated time series of chromatin compaction maps of the whole nucleus using FAI of H2B-EGFP labelled cell nucleus. It is based on the principle that rotational mobility of fluorescently tagged core histones corresponds to the local chromatin compaction and regulates the magnitude of depolarization of emission, when excited with a polarized light. Quantitative image correlation analysis of time series of the chromatin compaction maps was used to extract quantities like noise in anisotropy image time series (η), total fraction of chromatin that is subject to change (α) and time scale of compaction dynamics (τ). The quantity α/τ, i.e. fractional change in compaction map per minute was significantly higher in live cells compared to fixed cells, at euchromatin regions compared to heterochromatin regions and in ES cells compared to PMEFs. As a next step, this technique was used to compare the difference in

chromatin dynamics in cells cultured on different geometric micropatterns. The chromatin compaction structure was observed to be more dynamic in CI cells compared to LP cells. Similar to the PNAFs and heterochromatin dynamics, the dynamics of chromatin compaction maps was enhanced in polarized cells upon actin perturbation and reduced in CI cells upon actin stabilization, supporting our conclusion that extracellular geometric signals alter active cytoskeletal forces to regulate nuclear and chromatin dynamics.

As a next step, we examined the cytoplasmic to nuclear shuttling of MKL, which is an actin polymerization dependent mechanoresponsive transcription regulator. MKL, which is known to bind to G-actin in the cytoplasm, was observed to translocate to the nucleus upon serum induced actin polymerization or competitive binding of cytochalasin-D to G-actin. Simultaneous FAI of MKL mCherry and H2B-EGFP revealed that MKL preferentially binds in regions of open chromatin. Time tracking of MKL binding foci revealed higher dynamics in LP cells, possibly suggesting higher transcriptional activity of MKL dependent genes.

Taken together, this thesis shows that EMS, in the form of cell geometric constraints, affect nuclear and chromatin dynamics by regulating cytoskeletal organization and laminA/C expression. Such mechanical regulation of chromatin dynamics could be the first step in tuning the epigenetic state of cells to achieve mechanical reprogramming of cells. Various ongoing experiments in the lab are aimed at understanding the relation of such nuclear and chromatin dynamics to genomic integrity and short and long term transcriptional changes.

BIBLIOGRAPHY

1. Lodish, H.F., *Molecular cell biology*. 6th ed. 2008, New York: W.H. Freeman.

2. Lo, C.M., et al., *Cell movement is guided by the rigidity of the substrate.* Biophys J, 2000. **79**(1): p. 144-52.

3. Sheetz, M.P., D.P. Felsenfeld, and C.G. Galbraith, *Cell migration: regulation of force on extracellular-matrix-integrin complexes.* Trends Cell Biol, 1998. **8**(2): p. 51-4.

4. Pelham, R.J., Jr. and Y. Wang, *Cell locomotion and focal adhesions are regulated by substrate flexibility.* Proc Natl Acad Sci U S A, 1997. **94**(25): p. 13661-5.

5. Choquet, D., D.P. Felsenfeld, and M.P. Sheetz, *Extracellular matrix rigidity causes strengthening of integrin-cytoskeleton linkages.* Cell, 1997. **88**(1): p. 39-48.

6. Wang, N., J.P. Butler, and D.E. Ingber, *Mechanotransduction across the cell surface and through the cytoskeleton.* Science, 1993. **260**(5111): p. 1124-7.

7. Schwarzbauer, J.E. and J.L. Sechler, *Fibronectin fibrillogenesis: a paradigm for extracellular matrix assembly.* Curr Opin Cell Biol, 1999. **11**(5): p. 622-7.

8. Engler, A.J., et al., *Matrix elasticity directs stem cell lineage specification.* Cell, 2006. **126**(4): p. 677-89.

9. Iskratsch, T., H. Wolfenson, and M.P. Sheetz, *Appreciating force and shape-the rise of mechanotransduction in cell biology.* Nat Rev Mol Cell Biol, 2014. **15**(12): p. 825-33.

10. Kilian, K.A., et al., *Geometric cues for directing the differentiation of mesenchymal stem cells.* Proc Natl Acad Sci U S A, 2010. **107**(11): p. 4872-7.

11. Yourek, G., et al., *Shear stress induces osteogenic differentiation of human mesenchymal stem cells.* Regen Med, 2010. **5**(5): p. 713-24.

12. Jain, N., et al., *Cell geometric constraints induce modular gene-expression patterns via redistribution of HDAC3 regulated by actomyosin contractility.* Proc Natl Acad Sci U S A, 2013. **110**(28): p. 11349-54.

13. Remuzzi, A., et al., *Orientation of endothelial cells in shear fields in vitro.* Biorheology, 1984. **21**(4): p. 617-30.

14. Malek, A.M. and S. Izumo, *Mechanism of endothelial cell shape change and cytoskeletal remodeling in response to fluid shear stress.* J Cell Sci, 1996. **109 (Pt 4)**: p. 713-26.

15. Gupta, M., et al., *Adaptive rheology and ordering of cell cytoskeleton govern matrix rigidity sensing.* Nat Commun, 2015. **6**: p. 7525.

16. Zemel, A., et al., *Optimal matrix rigidity for stress fiber polarization in stem cells.* Nat Phys, 2010. **6**(6): p. 468-473.

17. Belmont, A.S., F.M. Kendall, and C.A. Nicolini, *Coupling of nuclear morphometry to cell geometry and growth in human fibroblasts.* Cell Biophys, 1980. **2**(2): p. 165-75.

18. Lovett, D.B., et al., *Modulation of Nuclear Shape by Substrate Rigidity.* Cell Mol Bioeng, 2013. **6**(2): p. 230-238.

19. Li, Q., et al., *The regulation of dynamic mechanical coupling between actin cytoskeleton and nucleus by matrix geometry.* Biomaterials, 2014. **35**(3): p. 961-9.

20. Farge, E., *Mechanical induction of Twist in the Drosophila foregut/stomodeal primordium.* Curr Biol, 2003. **13**(16): p. 1365-77.

21. Iyer, K.V., et al., *Mechanical activation of cells induces chromatin remodeling preceding MKL nuclear transport.* Biophys J, 2012. **103**(7): p. 1416-28.

22. Hay, D.C., et al., *Activation of NF-kappaB nuclear transcription factor by flow in human endothelial cells.* Biochim Biophys Acta, 2003. **1642**(1-2): p. 33-44.

23. Dupont, S., et al., *Role of YAP/TAZ in mechanotransduction.* Nature, 2011. **474**(7350): p. 179-83.

24. Miralles, F., et al., *Actin dynamics control SRF activity by regulation of its coactivator MAL.* Cell, 2003. **113**(3): p. 329-342.

25. Pawlowski, R., et al., *An actin-regulated importin alpha/beta-dependent extended bipartite NLS directs nuclear import of MRTF-A.* EMBO J, 2010. **29**(20): p. 3448-58.

26. Zebda, N., O. Dubrovskyi, and K.G. Birukov, *Focal adhesion kinase regulation of mechanotransduction and its impact on endothelial cell functions.* Microvasc Res, 2012. **83**(1): p. 71-81.

27. Fletcher, D.A. and R.D. Mullins, *Cell mechanics and the cytoskeleton.* Nature, 2010. **463**(7280): p. 485-92.

28. Brangwynne, C.P., et al., *Microtubules can bear enhanced compressive loads in living cells because of lateral reinforcement.* J Cell Biol, 2006. **173**(5): p. 733-41.

29. Herrmann, H., et al., *Intermediate filaments: from cell architecture to nanomechanics.* Nat Rev Mol Cell Biol, 2007. **8**(7): p. 562-73.

30. Tzur, Y.B., K.L. Wilson, and Y. Gruenbaum, *SUN-domain proteins: 'Velcro' that links the nucleoskeleton to the cytoskeleton.* Nat Rev Mol Cell Biol, 2006. **7**(10): p. 782-8.

31. Yen, R.T., et al., *Speed of stress wave propagation in lung.* J Appl Physiol (1985), 1986. **61**(2): p. 701-5.

32. Hu, S. and N. Wang, *Control of stress propagation in the cytoplasm by prestress and loading frequency.* Mol Cell Biomech, 2006. **3**(2): p. 49-60.

33. Wang, N., J.D. Tytell, and D.E. Ingber, *Mechanotransduction at a distance: mechanically coupling the extracellular matrix with the nucleus.* Nat Rev Mol Cell Biol, 2009. **10**(1): p. 75-82.

34. Ramdas, N.M. and G.V. Shivashankar, *Cytoskeletal control of nuclear morphology and chromatin organization.* J Mol Biol, 2015. **427**(3): p. 695-706.

35. Mazumder, A. and G.V. Shivashankar, *Emergence of a prestressed eukaryotic nucleus during cellular differentiation and development.* J R Soc Interface, 2010. **7 Suppl 3**: p. S321-30.

36. Morgan, J.T., et al., *Nesprin-3 regulates endothelial cell morphology, perinuclear cytoskeletal architecture, and flow-induced polarization.* Mol Biol Cell, 2011. **22**(22): p. 4324-34.

37. Zhang, Q., et al., *Nesprin-2 is a multi-isomeric protein that binds lamin and emerin at the nuclear envelope and forms a subcellular network in skeletal muscle.* J Cell Sci, 2005. **118**(Pt 4): p. 673-87.

38. Solovei, I., et al., *LBR and lamin A/C sequentially tether peripheral heterochromatin and inversely regulate differentiation.* Cell, 2013. **152**(3): p. 584-98.

39. Makatsori, D., et al., *The inner nuclear membrane protein lamin B receptor forms distinct microdomains and links epigenetically marked chromatin to the nuclear envelope.* J Biol Chem, 2004. **279**(24): p. 25567-73.

40. Raz, V., et al., *Changes in lamina structure are followed by spatial reorganization of heterochromatic regions in caspase-8-activated human mesenchymal stem cells.* J Cell Sci, 2006. **119**(Pt 20): p. 4247-56.

41. Booth-Gauthier, E.A., et al., *Force-induced changes in subnuclear movement and rheology.* Biophys J, 2012. **103**(12): p. 2423-31.

42. Poh, Y.C., et al., *Dynamic force-induced direct dissociation of protein complexes in a nuclear body in living cells.* Nat Commun, 2012. **3**: p. 866.

43. Bhattacharya, D., et al., *Spatio-temporal plasticity in chromatin organization in mouse cell differentiation and during Drosophila embryogenesis.* Biophys J, 2009. **96**(9): p. 3832-9.

44. Meshorer, E., et al., *Hyperdynamic plasticity of chromatin proteins in pluripotent embryonic stem cells.* Dev Cell, 2006. **10**(1): p. 105-16.

45. Tan, J.L., et al., *Cells lying on a bed of microneedles: An approach to isolate mechanical force.* Proceedings of the National Academy of Sciences of the United States of America, 2003. **100**(4): p. 1484-1489.

46. Galbraith, C.G. and M.P. Sheetz, *A micromachined device provides a new bend on fibroblast traction forces.* Proceedings of the National Academy of Sciences of the United States of America, 1997. **94**(17): p. 9114-9118.

47. Pajerowski, J.D., et al., *Physical plasticity of the nucleus in stem cell differentiation.* Proc Natl Acad Sci U S A, 2007. **104**(40): p. 15619-24.

48. Lakowicz, J.R., *Principles of fluorescence spectroscopy*. 1983, New York: : Plenum Press. xiv, 496 p.

49. Banerjee, B., D. Bhattacharya, and G.V. Shivashankar, *Chromatin structure exhibits spatio-temporal heterogeneity within the cell nucleus.* Biophysical Journal, 2006. **91**(6): p. 2297-2303.

50. Vartiainen, M.K., et al., *Nuclear actin regulates dynamic subcellular localization and activity of the SRF cofactor MAL.* Science, 2007. **316**(5832): p. 1749-1752.

51. Desprat, N., et al., *Tissue deformation modulates twist expression to determine anterior midgut differentiation in Drosophila embryos.* Dev Cell, 2008. **15**(3): p. 470-7.

52. Vogel, V. and M. Sheetz, *Local force and geometry sensing regulate cell functions.* Nat Rev Mol Cell Biol, 2006. **7**(4): p. 265-75.

53. Shivashankar, G.V., *Mechanosignaling to the cell nucleus and gene regulation.* Annu Rev Biophys, 2011. **40**: p. 361-78.

54. Khatau, S.B., et al., *A perinuclear actin cap regulates nuclear shape.* Proc Natl Acad Sci U S A, 2009. **106**(45): p. 19017-22.

55. Luxton, G.W., et al., *Linear arrays of nuclear envelope proteins harness retrograde actin flow for nuclear movement.* Science, 2010. **329**(5994): p. 956-9.

56. Chambliss, A.B., et al., *The LINC-anchored actin cap connects the extracellular milieu to the nucleus for ultrafast mechanotransduction.* Sci Rep, 2013. **3**: p. 1087.

57. Burke, B. and C.L. Stewart, *The nuclear lamins: flexibility in function.* Nat Rev Mol Cell Biol, 2013. **14**(1): p. 13-24.

58. Maniotis, A.J., C.S. Chen, and D.E. Ingber, *Demonstration of mechanical connections between integrins, cytoskeletal filaments, and nucleoplasm that stabilize nuclear structure.* Proc Natl Acad Sci U S A, 1997. **94**(3): p. 849-54.

59. Na, S., et al., *Rapid signal transduction in living cells is a unique feature of mechanotransduction.* Proc Natl Acad Sci U S A, 2008. **105**(18): p. 6626-31.

60. Lombardi, M.L., et al., *The interaction between nesprins and sun proteins at the nuclear envelope is critical for force transmission between the nucleus and cytoskeleton.* J Biol Chem, 2011. **286**(30): p. 26743-53.

61. Isermann, P. and J. Lammerding, *Nuclear mechanics and mechanotransduction in health and disease.* Curr Biol, 2013. **23**(24): p. R1113-21.

62. Martins, R.P., et al., *Mechanical regulation of nuclear structure and function.* Annu Rev Biomed Eng, 2012. **14**: p. 431-55.

63. Woringer, M., X. Darzacq, and I. Izeddin, *Geometry of the nucleus: a perspective on gene expression regulation.* Curr Opin Chem Biol, 2014. **20**: p. 112-9.

64. Burke, B. and C.L. Stewart, *Functional architecture of the cell's nucleus in development, aging, and disease.* Curr Top Dev Biol, 2014. **109**: p. 1-52.

65. Guilluy, C. and K. Burridge, *Nuclear mechanotransduction: Forcing the nucleus to respond.* Nucleus, 2015. **6**(1): p. 19-22.

66. Webster, M., K.L. Witkin, and O. Cohen-Fix, *Sizing up the nucleus: nuclear shape, size and nuclear-envelope assembly.* J Cell Sci, 2009. **122**(Pt 10): p. 1477-86.

67. Broers, J.L., et al., *Decreased mechanical stiffness in LMNA-/- cells is caused by defective nucleo-cytoskeletal integrity: implications for the development of laminopathies.* Hum Mol Genet, 2004. **13**(21): p. 2567-80.

68. Shumaker, D.K., E.R. Kuczmarski, and R.D. Goldman, *The nucleoskeleton: lamins and actin are major players in essential nuclear functions.* Curr Opin Cell Biol, 2003. **15**(3): p. 358-66.

69. Guilluy, C., et al., *Isolated nuclei adapt to force and reveal a mechanotransduction pathway in the nucleus.* Nat Cell Biol, 2014. **16**(4): p. 376-81.

70. Talwar, S., et al., *Correlated spatio-temporal fluctuations in chromatin compaction states characterize stem cells.* Biophys J, 2013. **104**(3): p. 553-64.

71. Mattout, A. and E. Meshorer, *Chromatin plasticity and genome organization in pluripotent embryonic stem cells.* Curr Opin Cell Biol, 2010. **22**(3): p. 334-41.

72. Meshorer, E. and T. Misteli, *Chromatin in pluripotent embryonic stem cells and differentiation.* Nat Rev Mol Cell Biol, 2006. **7**(7): p. 540-6.

73. Crisp, M., et al., *Coupling of the nucleus and cytoplasm: role of the LINC complex.* J Cell Biol, 2006. **172**(1): p. 41-53.

74. Versaevel, M., et al., *Super-resolution microscopy reveals LINC complex recruitment at nuclear indentation sites.* Sci Rep, 2014. **4**: p. 7362.

75. Tapley, E.C. and D.A. Starr, *Connecting the nucleus to the cytoskeleton by SUN-KASH bridges across the nuclear envelope.* Curr Opin Cell Biol, 2013. **25**(1): p. 57-62.

76. Starr, D.A. and H.N. Fridolfsson, *Interactions between nuclei and the cytoskeleton are mediated by SUN-KASH nuclear-envelope bridges.* Annu Rev Cell Dev Biol, 2010. **26**: p. 421-44.

77. Osmanagic-Myers, S., T. Dechat, and R. Foisner, *Lamins at the crossroads of mechanosignaling.* Genes Dev, 2015. **29**(3): p. 225-37.

78. Swift, J. and D.E. Discher, *The nuclear lamina is mechano-responsive to ECM elasticity in mature tissue.* J Cell Sci, 2014. **127**(Pt 14): p. 3005-15.

79. Sims, J.R., S. Karp, and D.E. Ingber, *Altering the cellular mechanical force balance results in integrated changes in cell, cytoskeletal and nuclear shape.* J Cell Sci, 1992. **103 (Pt 4)**: p. 1215-22.

80. Lanctot, C., et al., *Dynamic genome architecture in the nuclear space: regulation of gene expression in three dimensions.* Nat Rev Genet, 2007. **8**(2): p. 104-15.

81. Schneider, R. and R. Grosschedl, *Dynamics and interplay of nuclear architecture, genome organization, and gene expression.* Genes Dev, 2007. **21**(23): p. 3027-43.

82. Talwar, S., N. Jain, and G.V. Shivashankar, *The regulation of gene expression during onset of differentiation by nuclear mechanical heterogeneity.* Biomaterials, 2014. **35**(8): p. 2411-9.

83. Fedorchak, G.R., A. Kaminski, and J. Lammerding, *Cellular mechanosensing: getting to the nucleus of it all.* Prog Biophys Mol Biol, 2014. **115**(2-3): p. 76-92.

84. Wang, L., et al., *Actin polymerization negatively regulates p53 function by impairing its nuclear import in response to DNA damage.* PLoS One, 2013. **8**(4): p. e60179.

85. Zuchero, J.B., B. Belin, and R.D. Mullins, *Actin binding to WH2 domains regulates nuclear import of the multifunctional actin regulator JMY.* Mol Biol Cell, 2012. **23**(5): p. 853-63.

86. Miller, C.J. and L.A. Davidson, *The interplay between cell signalling and mechanics in developmental processes.* Nat Rev Genet, 2013. **14**(10): p. 733-44.

87. Kumar, A. and G.V. Shivashankar, *Mechanical force alters morphogenetic movements and segmental gene expression patterns during Drosophila embryogenesis.* PLoS One, 2012. **7**(3): p. e33089.

88. Gundersen, G.G. and H.J. Worman, *Nuclear positioning.* Cell, 2013. **152**(6): p. 1376-89.

89. Harada, T., et al., *Nuclear lamin stiffness is a barrier to 3D migration, but softness can limit survival.* J Cell Biol, 2014. **204**(5): p. 669-82.

90. Rynearson, A.L. and C.R. Sussman, *Nuclear structure, organization, and oncogenesis.* J Gastrointest Cancer, 2011. **42**(2): p. 112-7.

91. Ribeiro, A.J., et al., *Nuclear stiffening inhibits migration of invasive melanoma cells.* Cell Mol Bioeng, 2014. **7**(4): p. 544-551.

92. Parnaik, V.K. and K. Manju, *Laminopathies: multiple disorders arising from defects in nuclear architecture.* J Biosci, 2006. **31**(3): p. 405-21.

93. Worman, H.J., C. Ostlund, and Y. Wang, *Diseases of the nuclear envelope.* Cold Spring Harb Perspect Biol, 2010. **2**(2): p. a000760.

94. Mattout, A., et al., *Nuclear lamins, diseases and aging.* Curr Opin Cell Biol, 2006. **18**(3): p. 335-41.

95. Folker, E.S., et al., *Lamin A variants that cause striated muscle disease are defective in anchoring transmembrane actin-associated nuclear lines for nuclear movement.* Proc Natl Acad Sci U S A, 2011. **108**(1): p. 131-6.

96. Lee, J.S., et al., *Nuclear lamin A/C deficiency induces defects in cell mechanics, polarization, and migration.* Biophys J, 2007. **93**(7): p. 2542-52.

97. Verstraeten, V.L., et al., *Increased mechanosensitivity and nuclear stiffness in Hutchinson-Gilford progeria cells: effects of farnesyltransferase inhibitors.* Aging Cell, 2008. **7**(3): p. 383-93.

98. Solon, J., et al., *Fibroblast adaptation and stiffness matching to soft elastic substrates.* Biophys J, 2007. **93**(12): p. 4453-61.

99. Chen, C.S., *Mechanotransduction - a field pulling together?* J Cell Sci, 2008. **121**(Pt 20): p. 3285-92.

100. Roca-Cusachs, P., et al., *Micropatterning of single endothelial cell shape reveals a tight coupling between nuclear volume in G1 and proliferation.* Biophys J, 2008. **94**(12): p. 4984-95.

101. Wang, D., et al., *Tissue-specific mechanical and geometrical control of cell viability and actin cytoskeleton alignment.* Sci Rep, 2014. **4**: p. 6160.

102. Kim, D.H. and D. Wirtz, *Cytoskeletal tension induces the polarized architecture of the nucleus.* Biomaterials, 2015. **48**: p. 161-72.

103. Mazumder, A. and G.V. Shivashankar, *Gold-nanoparticle-assisted laser perturbation of chromatin assembly reveals unusual aspects of nuclear architecture within living cells.* Biophys J, 2007. **93**(6): p. 2209-16.

104. Dahl, K.N., et al., *Power-law rheology of isolated nuclei with deformation mapping of nuclear substructures.* Biophys J, 2005. **89**(4): p. 2855-64.

105. Zhang, Q., et al., *The nesprins are giant actin-binding proteins, orthologous to Drosophila melanogaster muscle protein MSP-300.* Genomics, 2002. **80**(5): p. 473-81.

106. Roux, K.J., et al., *Nesprin 4 is an outer nuclear membrane protein that can induce kinesin-mediated cell polarization.* Proc Natl Acad Sci U S A, 2009. **106**(7): p. 2194-9.

107. Sun, D., C.L. Leung, and R.K. Liem, *Characterization of the microtubule binding domain of microtubule actin crosslinking factor (MACF): identification of a novel group of microtubule associated proteins.* J Cell Sci, 2001. **114**(Pt 1): p. 161-172.

108. Waterman-Storer, C., et al., *Microtubules remodel actomyosin networks in Xenopus egg extracts via two mechanisms of F-actin transport.* J Cell Biol, 2000. **150**(2): p. 361-76.

109. De Vos, W.H., et al., *Increased plasticity of the nuclear envelope and hypermobility of telomeres due to the loss of A-type lamins.* Biochim Biophys Acta, 2010. **1800**(4): p. 448-58.

110. Lammerding, J., et al., *Lamins A and C but not lamin B1 regulate nuclear mechanics.* J Biol Chem, 2006. **281**(35): p. 25768-80.

111. Dechat, T., et al., *Nuclear lamins: major factors in the structural organization and function of the nucleus and chromatin.* Genes Dev, 2008. **22**(7): p. 832-53.

112. Sullivan, T., et al., *Loss of A-type lamin expression compromises nuclear envelope integrity leading to muscular dystrophy.* J Cell Biol, 1999. **147**(5): p. 913-20.

113. Luo, W., et al., *Analysis of the local organization and dynamics of cellular actin networks.* J Cell Biol, 2013. **202**(7): p. 1057-73.

114. Brown, S.W., *Heterochromatin.* Science, 1966. **151**(3709): p. 417-25.

115. Moindrot, B., P. Bouvet, and F. Mongelard, *Chromatin structure and organization: the relation with gene expression during development and disease.* Subcell Biochem. **61**: p. 373-96.

116. Hubner, M.R., M.A. Eckersley-Maslin, and D.L. Spector, *Chromatin organization and transcriptional regulation.* Curr Opin Genet Dev, 2013. **23**(2): p. 89-95.

117. Pederson, T., *Chromatin structure and the cell cycle.* Proc Natl Acad Sci U S A, 1972. **69**(8): p. 2224-8.

118. Essers, J., et al., *Dynamics of relative chromosome position during the cell cycle.* Mol Biol Cell, 2005. **16**(2): p. 769-75.

119. Belmont, A., *Dynamics of chromatin, proteins, and bodies within the cell nucleus.* Curr Opin Cell Biol, 2003. **15**(3): p. 304-10.

120. Cheung, A.Y. and A.S. Reddy, *Nuclear architecture and dynamics: territories, nuclear bodies, and nucleocytoplasmic trafficking.* Plant Physiol. **158**(1): p. 23-5.

121. Hemmerich, P., L. Schmiedeberg, and S. Diekmann, *Dynamic as well as stable protein interactions contribute to genome function and maintenance.* Chromosome Res. **19**(1): p. 131-51.

122. Marshall, W.F., et al., *Interphase chromosomes undergo constrained diffusional motion in living cells.* Curr Biol, 1997. **7**(12): p. 930-9.

123. Poirier, M.G., et al., *Dynamics and function of compact nucleosome arrays.* Nat Struct Mol Biol, 2009. **16**(9): p. 938-44.

124. Festenstein, R., et al., *Modulation of heterochromatin protein 1 dynamics in primary Mammalian cells.* Science, 2003. **299**(5607): p. 719-21.

125. Cheutin, T., et al., *Maintenance of stable heterochromatin domains by dynamic HP1 binding.* Science, 2003. **299**(5607): p. 721-5.

126. Misteli, T., et al., *Dynamic binding of histone H1 to chromatin in living cells.* Nature, 2000. **408**(6814): p. 877-81.

127. Kimura, H., K. Sugaya, and P.R. Cook, *The transcription cycle of RNA polymerase II in living cells.* J Cell Biol, 2002. **159**(5): p. 777-82.

128. Kimura, H. and P.R. Cook, *Kinetics of core histones in living human cells: little exchange of H3 and H4 and some rapid exchange of H2B.* J Cell Biol, 2001. **153**(7): p. 1341-53.

129. van Steensel, B. and J. Dekker, *Genomics tools for unraveling chromosome architecture.* Nat Biotechnol, 2010. **28**(10): p. 1089-1095.

130. Sajan, S.A. and R.D. Hawkins, *Methods for identifying higher-order chromatin structure.* Annu Rev Genomics Hum Genet. **13**: p. 59-82.

131. Daban, J.R., *Electron microscopy and atomic force microscopy studies of chromatin and metaphase chromosome structure.* Micron. **42**(8): p. 733-50.

132. Mueller, F., et al., *Monitoring dynamic binding of chromatin proteins in vivo by fluorescence recovery after photobleaching.* Methods Mol Biol, 2012. **833**: p. 153-76.

133. Lleres, D., et al., *Quantitative analysis of chromatin compaction in living cells using FLIM-FRET.* J Cell Biol, 2009. **187**(4): p. 481-96.

134. Sasaki, K., et al., *Real-time imaging of histone H4 hyperacetylation in living cells.* Proc Natl Acad Sci U S A, 2009. **106**(38): p. 16257-62.

135. Lakowicz, *Principles of Fluorescence Spectroscopy.* Springer, 2006.

136. Banerjee, B., D. Bhattacharya, and G.V. Shivashankar, *Chromatin structure exhibits spatio-temporal heterogeneity within the cell nucleus.* Biophys J, 2006. **91**(6): p. 2297-303.

137. Hameed, F.M., M. Rao, and G.V. Shivashankar, *Dynamics of passive and active particles in the cell nucleus.* PLoS One. **7**(10): p. e45843.

138. Iyer, K.V., et al., *Mechanical activation of cells induces chromatin remodeling preceding MKL nuclear transport.* Biophys J. **103**(7): p. 1416-28.

139. Maharana, S., et al., *Dynamic organization of transcription compartments is dependent on functional nuclear architecture.* Biophys J. **103**(5): p. 851-9.

140. Rao, J., et al., *Trichostatin-A induces differential changes in histone protein dynamics and expression in HeLa cells.* Biochem Biophys Res Commun, 2007. **363**(2): p. 263-8.

141. Sinha, D.K., et al., *Probing the dynamic organization of transcription compartments and gene loci within the nucleus of living cells.* Biophys J, 2008. **95**(11): p. 5432-8.

142. Talwar, S., et al., *Correlated spatio-temporal fluctuations in chromatin compaction States characterize stem cells.* Biophys J. **104**(3): p. 553-64.